

KfK 2735
Februar 1979

Analysis of π N Charge- Exchange Scattering Data at Intermediate Energies

G. Höhler, H. P. Jakob, F. Kaiser, G. Brandenburger
Institut für Kernphysik

Kernforschungszentrum Karlsruhe

KERNFORSCHUNGSZENTRUM KARLSRUHE

Institut für Kernphysik

KfK 2735

Analysis of π N Charge-Exchange Scattering Data
at Intermediate Energies

von

G. Höhler^{x)}, H.P. Jakob⁺, F. Kaiser^{x)} and G. Brandenburger^{z)}

^{x)} Institut für Theoretische Kernphysik der Universität Karlsruhe

⁺ Supported by Bundesministerium für Forschung und Technologie

Kernforschungszentrum Karlsruhe GmbH, Karlsruhe

Als Manuskript vervielfältigt
Für diesen Bericht behalten wir uns alle Rechte vor

Kernforschungszentrum Karlsruhe GmbH
ISSN 0303-4003

Analysis of π N Charge-Exchange Scattering Data at Intermediate
Energies

Abstract:

Pion-Nucleon charge-exchange scattering data up to 6 GeV/c are analysed, using Legendre expansions of $d\sigma/d\Omega$ and $P(d\sigma/d\Omega)/\sin \theta$ and zero trajectories. In several cases there are large discrepancies between the Legendre coefficients derived directly from data and those calculated from phase shifts. The number of coefficients needed for a good fit is remarkably large already around 1 GeV/c and does not increase up to 2.2 GeV/c. In $A_{10}(k)$ a peak is found at 1.0 GeV/c which is difficult to accept.

Although the data cover a large angular range, extrapolations to $\cos \theta = \pm 1$ have fairly large uncertainties because of strong structures in the near-forward and near-backward directions. Further progress in phase shift analysis depends on a determination of these structures by suitable experiments, because they contain information on higher partial waves and resonances. These experiments would also help to exploit in a better way the knowledge of the absolute phase obtained from forward and backward dispersion relations.

The zero trajectories calculated directly from data have a simple and reasonable behaviour above 1.1 GeV/c, but they show unexpected complications in the range 0.6 - 1.1 GeV/c. These are possibly due to an unknown systematic experimental error which could also be responsible for the above mentioned large contributions from high partial waves. Zero trajectories calculated from phase shifts are also shown. Some local deviations from a smooth behaviour indicate at which energies the partial wave analysis is not yet satisfactory.

ANALYSE DER π N LADUNGSUSTAUSCH-DATEN BEI MITTLEREN ENERGIEN

Zusammenfassung

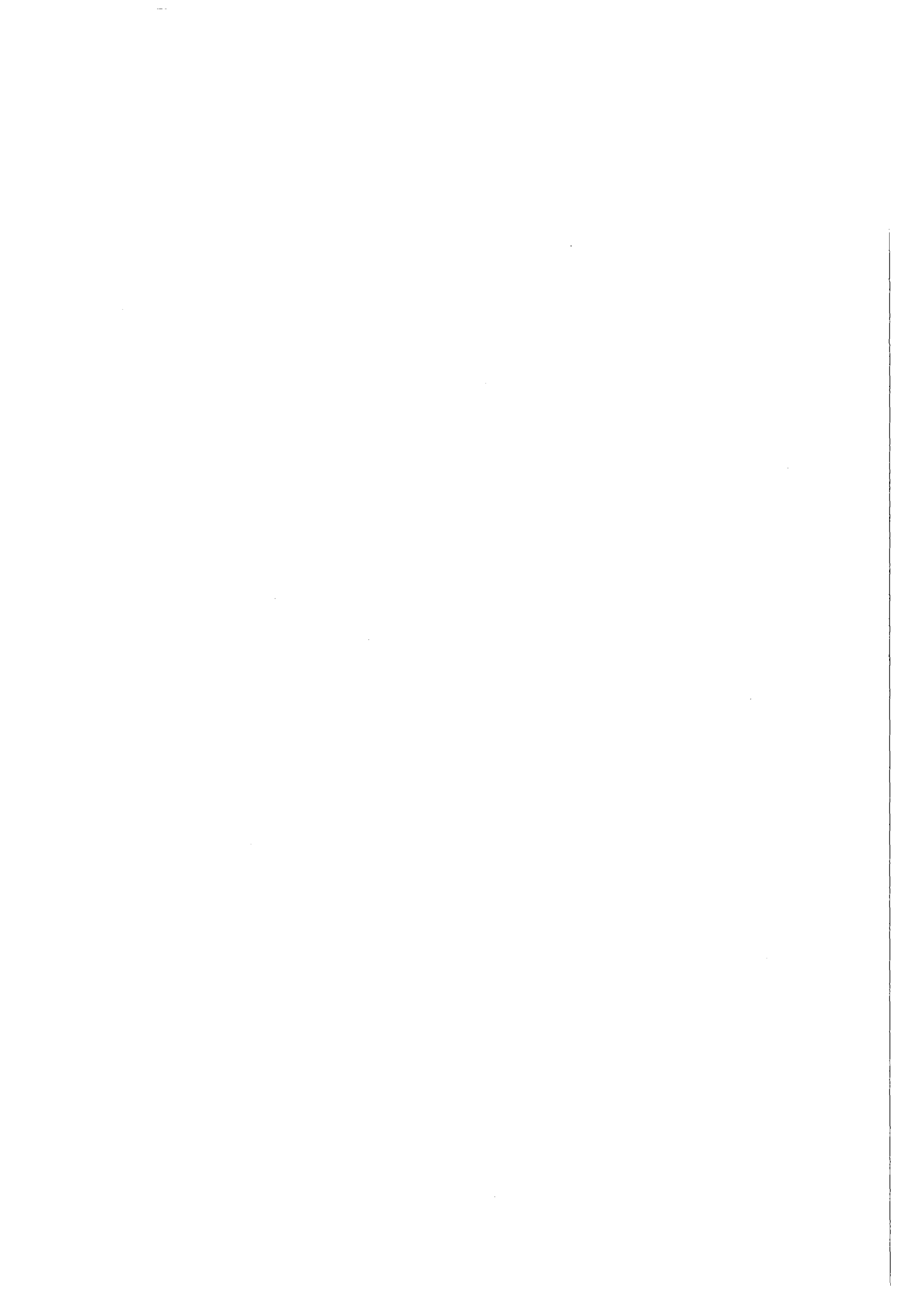
Es werden Pion-Nukleon Ladungsaustausch-Daten bis 6 GeV/c analysiert, wobei Legendre-Entwicklungen von $d\sigma/d\Omega$ und $P(d\sigma/d\Omega)/\sin \theta$ und Nullstellen-Trajektorien benutzt werden. In verschiedenen Fällen gibt es große Diskrepanzen zwischen den aus Daten und aus Streuphasen bestimmten Koeffizienten. Die Zahl der für einen guten Fit benötigten Koeffizienten ist schon bei 1 GeV/c bemerkenswert gross und steigt nicht bis 2.2 GeV/c. $A_{10}(k)$ hat bis 1.0 GeV/c ein deutliches Maximum, das schwer zu interpretieren ist.

Obwohl die Daten einen weiten Winkelbereich überdecken, haben Extrapolationen nach $\cos \theta = \pm 1$ ziemlich grosse Unsicherheiten, weil es nahe der Vorwärts- und Rückwärtsrichtung starke Strukturen gibt. Weiterer Fortschritt in der Phasenanalyse hängt von der experimentellen Bestimmung dieser Strukturen ab, weil diese Information über höhere Partialwellen und Resonanzen enthalten. Diese Experimente würden auch helfen, die aus Vorwärts- und Rückwärts-Dispersionsrelationen folgende Information über die absolute Phase der Amplitude besser auszunutzen.

Die aus Daten bestimmten Nullstellen-Trajektorien sind oberhalb von 1.1 GeV/c einfach, aber im Bereich 0.6-1.1 GeV/c kompliziert. Vermutlich kommt dies ebenso wie die oben erwähnten hohen Partialwellen von systematischen experimentellen Fehlern. Lokale Strukturen in den aus Streuphasen berechneten Trajektorien weisen auf Mängel der Phasenanalyse hin.

Table of Contents

	page
1. Introduction	1
2. Legendre fits to the differential cross sections	2
2.1 Choice of the cut-off value N	3
2.2 Legendre coefficients of $d\sigma/d\Omega$	4
3. Legendre fits to the polarization data	6
4. Legendre coefficients from fits to the data	7
5. Extrapolation to the forward and backward direction	9
5.1 Extrapolation to 0°	9
5.2 The slope at $\theta=0^\circ$	11
5.3 The backward cross section	12
5.4 The slope of the backward cross section	13
5.5 Extrapolation of polarization data to 0° and 180°	14
6. Zeros of transversity and invariant amplitudes	15
6.1 Introduction	15
6.2 Discussion of the results	17
6.3 Zeros of invariant amplitudes	22
7. Summary and conclusions	24
Appendix	26
References	28
Figure Captions	30



1. Introduction

Up to now πN phase shift analysis¹⁻⁴ was mainly based on experimental data for the elastic reactions $\pi^\pm p \rightarrow \pi^\pm p$, because data for the charge-exchange cross section were scarce and less accurate and polarization data existed in the latter case only at a few energies⁵.

Recently the situation has improved considerably, because the results of high statistics experiment in the range 0.6 ... 2.7 GeV/c became available where both $d\sigma_0/d\Omega$ and P_0 have been measured⁶.

One could think that phase shift analysis can easily be updated by adding these data to the input. Unfortunately the situation is more difficult, one of the reasons being that in some kinematical regions the new input is not quite consistent with isospin constraints⁷, presumably due to experimental errors, but there are other problems as well.

In order to support the effort made in phase shift analysis, we have performed a direct analysis of the charge-exchange data. Legendre fits to the differential cross sections and polarizations are treated in sects. 2 and 3. Fits of this type were used as a first step in the Saclay phase shift analysis². The energy dependence of the expansion coefficients shows whether different data sets are compatible with each other. The uncertainties of the coefficients can be used for an estimate of those of the dominant resonant partial waves. The necessary number of coefficients gives information on the number of relevant partial waves.

Furthermore Legendre expansions are the usual tool for extrapolations to $\theta = 0^\circ$ and 180° which are of interest in connection with evaluations of forward and backward dispersion relations.

Legendre coefficients are also needed for a comparison of experiments in which the π^0 in the final state is determined with others in which only the γ -distribution is measured.^{8,9}

In sect. 4 we discuss the results for Legendre coefficients determined by another method and from phase shifts. The comparison of the extrapolation of $d\sigma/d\Omega$ to $\theta = 0^\circ$ with the prediction from the optical theorem and the forward dispersion relation is treated in sect. 5. This point has already been briefly discussed by Brown et al.⁶, who came to the disturbing conclusion that, at some energies, there are large discrepancies between the extrapolation of their data and our prediction¹⁰. We shall also present results for the forward and backward slopes which are sensitive to contributions from high partial waves.

Finally, we have used our Legendre fits as well as phase shifts for a determination of zero trajectories of transversity amplitudes (sect. 6). Up to now only zero trajectories for elastic $\pi^\pm p$ amplitudes have been discussed in the literature^{11,12*}. The trajectories are important for the study of discrete ambiguities of phase shift analysis^{13,11,12} and in connection with dual models^{11,14}. Zero trajectories of invariant amplitudes have been treated elsewhere¹⁵. Our conclusions are summarized in sect. 7.

2. Legendre fits to the differential cross sections

The differential cross section data have been fitted to a Legendre expansion

$$\frac{d\sigma}{d\Omega} = \frac{1}{q} \sum_{n=0}^N A_n P_n(z), \quad (2.1)$$

where θ and q denote the scattering angle and the momentum in the c.m. frame ($z = \cos \theta$). The coefficients A_n are dimensionless parameters which are related to partial waves by

$$A_n = 2 \sum_{\substack{\ell, \ell' \\ J, J'}} a_n(\ell, \ell'; J, J') \operatorname{Re} [T_{\ell' J'}^- T_{\ell J}^{-*}]. \quad (2.2)$$

The determination of the coefficients is discussed in the Appendix, eq. (A.7). The $T_{\ell J}^-$ are the isospin odd combinations of partial wave amplitudes for isospin $I=1/2$ and $3/2$

$$T_{\ell J}^- = \frac{1}{3} (T_{\ell J}^{1/2} - T_{\ell J}^{3/2}), \quad (2.3)$$

$$T_{\ell J}^I = \frac{1}{2i} \{ \eta_{\ell J}^I \exp(2i\delta_{\ell J}^I) - 1 \}, \quad (2.4)$$

$\delta_{\ell J}^I$ being the real phase shift and $\eta_{\ell J}^I$ the absorption parameter.

* The completion of this manuscript has been delayed because we wanted to include the "1978" version (Ref.³⁵) of the phase shift analysis of Ref.³. Zero trajectories of charge-exchange amplitudes have recently been discussed by D. Chew (Ref.^{12a}). We are grateful to her for a correspondence.

The data of Brown et al.⁶ cover a large angular interval. In the forward direction the center of the first bin lies at $z=0.98$ or 0.95 at most energies and in the backward direction it lies at $z= -0.94$. One could think that the cross sections in the remaining small intervals are well determined by the fit. But unfortunately this is not true.

At most energies the cross section has a rapid variation in the range $0.95 \leq |\cos \theta| \leq 1$. If the structure is a near-forward or near-backward peak, the extrapolation frequently leads to negative forward or backward cross sections. In any case it depends sensitively on the number N of terms in the expansion (2.1).

For these reasons Legendre fits to the new Rutherford data⁶ alone are of little interest. In the following we shall consider fits which take into account our prediction from the forward dispersion relation, assuming our error estimate of Ref.¹⁰. Furthermore we have included the existing accurate backward data^{17,18}. In the range from 1.0 to 1.8 GeV/c, where the backward cross section has not yet been measured we have added the estimate from phase shift analysis,³⁵ assuming a fairly large error.

2.1 Choice of the cut-off value N

First we discuss the dependence of χ^2 per degree of freedom (χ_{DF}^2) on the number of coefficients in eq. (2.1). Fig. 1 shows that the decrease is not monotonic. There are steps in $\chi_{DF}^2(N)$ which follow from the fact that some of the higher coefficients are small for dynamical reasons. Because of this feature it is not appropriate to apply a formal determination of N which is based on the difference $\chi_{DF}^2(N) - \chi_{DF}^2(N+1)$ (Fisher test, see p. 200 in Ref.¹⁶).

Such a test was used by Brown et al.⁶, who chose $N = 6$ up to 1027 MeV/c, $N = 8$ up to 1767 MeV/c and $N = 10$ at higher momenta. Fig. 1 shows that a significant improvement of χ_{DF}^2 can be obtained if one goes up to $N = 8$ at 618 MeV/c and up to $N=10$ at and above 675 MeV/c.

It is certainly unexpected that A_{10} should give a significant contribution in the region around 1 GeV/c, where the resonances D15(1679) and F15(1684) are located. Therefore one has to check further conditions:

i) The diagonal error of A_{10} should be small in comparison with A_{10} . This is true in the range 776-1077 MeV/c, $\Delta A_{10}/A_{10}$ being 0.20 or smaller.

ii) A_{10} should remain approximately unchanged, if N increases. This is fulfilled

in the above momentum range for $N=10,11,12$. However, a large change occurs at some momenta for $N=13$.

iii) A_{10} should have a reasonable and smooth energy dependence. This is fulfilled (see Fig. 2).

The discussion will be continued in sects. 2.2 and 4.

It is surprising that the behaviour of $\chi_{DF}^2(N)$ does not suggest an increase of N between 1 and 2 GeV/c. Even at 2.7 GeV/c the fit to the Rutherford data is satisfactory already for $N=12$ (Fig. 1).

We have tried to use the same Legendre fit at 6 GeV/c, where data at all angles are available. However we have not been able to find a reasonable result. It is necessary to choose a large value of N because of the rapidly varying forward structure. Even with $N=20$ the fit in this region is not yet good. But in the central region it develops more oscillations than indicated by the data, leading to negative cross sections at most of the minima.

Since a similar difficulty occurs already at lower momenta, we have used the method described in sect. 4 for the determination of Legendre coefficients above 2.5 GeV/c.

2.2 Legendre Coefficients of $d\sigma/d\Omega$

Fig. 2 shows our results for $A_n(k)$ as derived from the data of Brown et al.⁶, Nelson et al.²¹ and Feltesse²² together with forward cross sections¹⁰ and backward cross sections from Refs.^{17,18}. Up to 2.2 GeV/c we have chosen $N=11$, but the lower coefficients are almost the same for $N=10$ and $N=9$.

In addition we have plotted $A_n(k)$ as determined with the method described in sect. 4 and coefficients obtained from experiments in which only the γ -distribution has been measured.^{8,9}

Finally we have plotted $A_n(k)$ -values from phase shift analyses. The points at different momenta are connected by straight lines. We have used the "1976 CMU-LBL" solution⁴ and the "Karlsruhe-Helsinki 78" solution^{3,35}.

Discussion

i) The coefficients derived from the data of Brown et al.⁶ show a well-defined momentum dependence up to $A_{10}(k)$. The higher coefficients have larger errors but, surprisingly, $A_{10}(k)$ has a pronounced peak in the mass region 1860 MeV ($k \approx 1.0$ GeV/c). The simplest interpretation would be an interference of the D_{15} and F_{15} -resonances with an imaginary $J=15/2$ background term.

ii) A comparison between the A_n -values obtained from our fit to the data and the values calculated from phase shifts shows several discrepancies, which are a consequence of the fact that the phase shift solution³⁵ does not give a good fit to some of the data of Brown et al.⁶. The main difficulties occur around 1.0 GeV/c in A_1 , A_4 , A_{10} and in a larger momentum range in A_8 , A_9 , A_{10} . If a better fit is enforced, the phase shift solution develops difficulties in other places.³⁵

Some of the discrepancies are due to the fact that the input of phase shift analysis contains also earlier data²¹⁻²⁵ which differ considerably from those of Brown et al.⁶ in some kinematic regions.

It is remarkable that our Legendre fit leads to a smooth momentum dependence of the coefficients $A_n(k)$ which can easily be interpolated by a spline fit.

The coefficients derived from the CMU-LBL phase shifts⁴ show larger fluctuations, because these authors have not imposed fixed- t analyticity. Large discrepancies with our result from the data of Brown et al.⁶ occur in A_0 at 1.84 GeV/c, in A_1 , A_4 , A_5 , A_8 around 1.0 GeV/c and in A_3 , A_4 , A_5 , A_8 above 1.5 GeV/c, where the result is not satisfactory because of large fluctuations in the energy dependence. One should notice that the data of Brown et al.⁶ have not yet been included in the CMU-LBL phase shift solution.

The fluctuations in the $A_n(k)$ derived from the CMU-LBL-phase shifts⁴ indicate that analyticity along only 4 hyperbolas is not sufficient for a smoothing of the momentum dependence.

iii) The normalization of different experiments can be compared in Fig. 2a, since A_0 is proportional to the total charge-exchange cross section

$$A_0 = \frac{q^2}{4\pi} \sigma_{ex}^{tot}. \quad (2.5)$$

Fig. 2a shows a good agreement between Brown et al.⁶ and Nelson et al.²¹. Some deviations from the values of Bulos et al.⁸ are probably due to the fact that the number of Legendre coefficients used by these authors is too small ($N=6$ up to 1027 MeV/c, cf. our Fig. 1). Except for a few points the agreement with the values of Kistiakowsky et al.⁹ is reasonable, since the diagonal errors should not be taken too seriously.

iv) The transition to the Regge region (6 GeV/c) shows the expected increase of A_n for higher n (sect. 4). More accurate data are necessary for a good resolution of the structures above 2.0 GeV/c which are important for the determination of the higher resonances.

Table I gives our result for $A_n(k)$ as obtained from the data of Brown et al.⁶ combined with backward cross sections and the forward points as discussed above. Legendre coefficients calculated from phase shifts are given in Table II ("Karlsruhe-Helsinki 78").

3. Legendre Fits to Polarization Data

In phase shift analysis³ and for the discussion of zeros of transversity amplitudes (see sect. 6) the data enter in the combination

$$\frac{d\sigma}{d\Omega} (1 \pm P). \quad (3.1)$$

One could consider fits to the plus and minus combinations separately, but then the average would not represent a good fit to $d\sigma/d\Omega$, which has been measured much more accurately than P . Therefore we prefer to fit $d\sigma/d\Omega$ and

$$\frac{P}{\sin \theta} \frac{d\sigma/d\Omega}{q} = \frac{1}{2} \sum_{n=1}^N B_n(k) P_n'(z). \quad (3.2)$$

The coefficients B_n are related to partial waves, eq. (2.3), by

$$B_n = 2 \sum_{\substack{\ell, \ell' \\ J, J'}} b_n(\ell, \ell', J, J') \text{Im}(T_{\ell, J}^-, T_{\ell, J}^{-*}). \quad (3.3)$$

The calculation of the Clebsch-Gordan coefficients is treated in the Appendix.

In most cases accurate $d\sigma/d\Omega$ -data⁶ are available at momenta very near those of the polarization data^{6,24}. Since interpolations in $\cos \theta$ are necessary

on the left hand side of eq. (3.2), we have inserted our Legendre fit to $d\sigma/d\Omega$ in all cases.

At two momenta (Shannon et al.²⁴: 1245 and 1790 MeV/c) the angular range of the polarization data is too small for a reasonable fit.

Fig. 3 shows the coefficients $B_n(k)$, eq. (3.2) obtained from polarization data and also the values calculated from phase shifts^{35,4}. It is seen that the coefficients have a well-determined momentum dependence up to $B_8(k)$. The dependence of $B_n(k)$ on N is fairly small as long as n lies somewhat below N .

At some energies $P d\sigma/d\Omega/\sin \theta$ has a rapid angular dependence near the forward and backward directions which is not well-determined experimentally because of the large bin width of the P-data. **Therefore it is of interest to check the smoothness of the extrapolation of $P d\sigma/d\Omega/\sin \theta$ to 0° and 180° as a function of momentum.** (See below, sect. 5).

In general the agreement between $B_n(k)$ from data and from phase shifts is reasonable, but there are fairly large discrepancies at some energies. In the case of the CMU-LBL 76 phase shifts one should remember that the data of Brown et al.⁶ are not part of the input.

The structures of $B_n(k)$ give information only on the interference between different resonances or between a resonance and the background, since a resonant amplitude alone does not contribute to the polarization parameter.

4. Legendre coefficients from fits to the data

As mentioned in sect. 2 the usual determination of Legendre coefficients leads to difficulties at high energies. One needs a large number of coefficients because of the narrow near-forward structure. But these coefficients cannot be determined in a reasonable way because the experimental information at larger angles is rather poor.

Therefore we have used another method. First we determine an interpolation of the cross section data by a spline fit, introducing no more structures than indicated by the data. Then we calculate the Legendre coefficients by an integration

$$A_n(k) = (n+\frac{1}{2}) q^2 \int_{-1}^{+1} \frac{d\sigma}{d\Omega} P_n(z) dz . \quad (4.1)$$

This method has been applied at several momenta above 2.5 GeV/c, where data at all angles are available (2.7, 3.7, 4.8, 6 GeV/c, Refs.^{6,25,26}).

In order to reproduce the structure of the experimental data at 6 GeV/c one has to go up to $n \approx 30$. The negative slope at $t=0$ leads to negative values of coefficients A_n for $n > 14$.

It is interesting to consider the k - and n -dependence of $A_n(k)$ as following from reggeized ρ -exchange (see for instance Ref.¹⁹), since the highest resonances are expected to be seen as structures superimposed on the ρ -exchange background.

The differential cross section following from a reggeized ρ -exchange model reads

$$\frac{d\sigma}{dt} = k^{2\alpha(t)-2} F(t) ; \quad \alpha(t) = \alpha(0) + \alpha' t. \quad (4.2)$$

One obtains for A_n (assuming $\alpha(0) = 0.5$)

$$A_n(k) = \frac{2n+1}{4\pi} \frac{q^2}{k} \int_{-4q^2}^0 e^{2\alpha' \ell_n k \cdot t} F(t) P_n(1+t/2q^2) dt. \quad (4.3)$$

The k -dependence of A_n is complicated. q^2/k has an appreciable increase, because it reaches its asymptotic value $m/2$ only slowly. The factor $P_n(1+t/2q^2)$ leads to an increase with increasing k which can have a structure although the Regge term has no s -channel poles. Finally the logarithmic shrinkage gives a slow decrease.

The n -dependence of $A_n(k)$ at fixed k shows an increase for small n and a decrease for large n , when the first zero of P_n reaches the forward peak. At least some higher coefficients must be negative because $d\sigma/dt$ has a negative slope at $t=0$.

Fig. 2 includes our result for the $A_n(k)$ as determined from eq. (4.1). It is in reasonable agreement with that of Kistiakowsky et al.¹⁸ who measured only the γ -distribution in the final state. Some discrepancies are probably due to the fact that it is difficult to resolve narrow structures with this method. Others are caused by discrepancies between different experiments (see for instance Fig. 4). Further charge-exchange experiments in the 2-6 GeV/c region would be of great interest for the study of the higher nucleon resonances.

Eq. (4.1) can also be applied for a discussion of the uncertainties of the higher A_n , for instance in the 1.0 GeV/c region, where our result shows a peak of A_{10} (Fig.2). In Fig. 5 we have plotted $\Delta\sigma P_n(z)$, $n=4$ and 10 , where $\Delta\sigma$ is $d\sigma/d\Omega$ from data or from the fit ($N=11$) minus the prediction from phase shift analysis³⁵. We notice that a number of data points at small angles and in the near backward peak do not lie on the abscissa, i.e. deviate from the phase shift fit at several energies. The area under the solid line is proportional to the discrepancies in A_{10} and A_4 . There are two possibilities:

*) Differential cross sections and polarizations at 1.8-3.0 GeV/c are being measured at the KEK accelerator by K.Miyake et al.

i) The effect is due to systematic experimental errors and the true value of A_{10} is small. Experimental errors in the near-backward direction are indicated by the poor connection between the data of Brown et al.⁶ and of Debenham et al.¹⁷ The rapid variation of the acceptance (Fig. 8 or Ref.⁶) shows that it is difficult to measure near $z = \pm 1$.

ii) The imaginary part of the $J= 15/2$ partial waves is larger than expected.

We think that the second possibility will only be considered seriously if the behaviour of A_{10} is confirmed by another experiment, since there is no indication for a similar interference effect with the strong F37 resonance $\Delta(1913)$.

5. Extrapolations to the forward and backward directions

5.1 Extrapolation to $\theta=0^\circ$

In the past the dispersion relation for forward scattering has been tested by comparing the prediction for charge-exchange forward scattering with the extrapolation of differential cross section data to $\theta=0^\circ$. Nowadays the data are much more accurate, but unfortunately, this does not lead to an improved test. The difficulties are seen if one considers the data of Brown et al.⁶ at $k = 1975$ MeV/c, where the authors concluded from their Fig. 11 that our prediction from the dispersion relation disagrees with the extrapolation of their cross sections.

Table III shows that the extrapolation depends so strongly on the cut-off in the Legendre expansion eq. (2.1) that a reliable test of the dispersion relation is not possible. (It happens that the agreement is good for the choice $N=10$ in Table 4 of Ref.⁶).

Rutherford data ⁶ only			Forward ¹⁰ and backward ¹⁸ points added	
N	χ^2_{DF}	$d\sigma(0^\circ)/d\Omega$	χ^2_{DF}	$d\sigma(0^\circ)/d\Omega$
6	3.09	0.64	2.97	0.64
7	2.10	0.43	2.87	0.59
8	2.15	0.46	2.94	0.57
9	0.89	0.82	0.92	0.70
10	0.80	0.67	0.88	0.68
11	0.81	0.59	0.81	0.66
12	0.77	0.39	0.84	0.66
13	0.79	0.34	0.86	0.65

Table V Fits to the data at 1975 MeV/c Dispersion relation: 0.67 ± 0.05 mb/sr

The reason for this difficulty is the strong variation of $d\sigma/d\Omega$ at $\cos \theta > 0.95$, which amounts to a factor of 1.8 in the present case. The situation is similar at some other energies and also in the backward direction. In the upper part of our energy range the strong variation is related to properties of the reggeized ρ -exchange amplitudes¹⁹: the invariant amplitude C^- decreases rapidly towards the "cross-over zero" and the flip amplitude B^- is so large that it causes a characteristic narrow structure near $t=0$ at momenta above the resonance region.

We conclude that it is desirable to perform special experiments at $\cos \theta$ -values very near ± 1 (like those of Refs.^{17,20}) in order to determine details of the near-forward and near-backward shapes of $d\sigma/d\Omega$. The results would be of interest for the determination of resonance parameters and of higher partial waves in phase shift analysis, since the uncertainty of the structures leads to large uncertainties in some of the higher Legendre coefficients which are related to partial waves by eq. (2.2). Furthermore they could be used for stringent tests of forward and backward dispersion relations or, assuming analyticity, for consistency checks between different sets of data including total cross sections, where unresolved discrepancies exist¹⁰.

In Fig. 6 we compare the forward cross section derived from Legendre fits with the prediction from the forward dispersion relation which is part of the input. The agreement is good at higher energies, but there is a systematic deviation below 1 GeV/c. This might be related to the fact that the data below and above 1 GeV/c were analysed in a somewhat different way⁶.

The extrapolation of the data of Nelson et al.²¹ is systematically lower than the dispersion prediction at and above 1590 MeV/c, but one should notice that the discrepancies are not larger than some discrepancies between the data of Nelson et al.²¹ and Brown et al.⁶, for instance at 1590 MeV/c.

The old data of Borgeaud et al.²⁷ are still of interest, because they are concentrated in a small t -region near $t=0$. The agreement with the dispersion prediction is reasonable above 1.2 GeV/c, but there are discrepancies around 1.0 GeV/c where the prediction comes mainly from the optical theorem.

Above 2.5 GeV/c we have plotted the extrapolation of the charge-exchange data of Guisan et al.^{25,29}. There are some discrepancies which need further attention.

Discrepancies with the result of Kistiakowsky et al.⁹ are not serious, because it is difficult to resolve the narrow near-forward structure with this method.

The Karlsruhe-Helsinki phase shift analysis³⁵ uses our table¹⁰ as part of the input. Therefore it is expected that the predicted forward cross section lies near the solid line. The forward cross sections calculated from the CMU-LBL analysis⁴ do not agree well with the prediction from the dispersion relation. We think that these authors should give a larger weight to the analyticity constraint at $t=0$.

5.2 The slope at $\theta = 0^\circ$

Because of the above mentioned difficulties it is of interest to check whether the different extrapolations to $\theta=0^\circ$ lead to a reasonable momentum dependence of the slope

$$B_0 = \left. \frac{d}{d\cos\theta} \frac{d\sigma}{d\Omega} \right|_0 = \frac{1}{2q^2} \sum_{n=0}^N n(n+1)A_n \quad (5.1)$$

At high energies it is more convenient to consider the logarithmic slope as used in elastic scattering

$$b_0 = \left. \frac{d}{dt} \ln \frac{d\sigma}{dt} \right|_{t=0} = \frac{B_0}{2q^2 \frac{d\sigma}{d\Omega}} = \frac{\pi}{2q^4} \frac{B_0}{\frac{d\sigma}{dt}} \quad (5.2)$$

The dominant term in the decomposition

$$\left. \frac{d}{dt} \frac{d\sigma}{dt} \right|_{t=0} = - \frac{1}{32\pi m^2} \left\{ |B^-|^2 + |C^-/k|^2 \right\}_{t=0} + \frac{|C^-|}{4\pi k^2} \left. \frac{\partial |C^-|}{\partial t} \right|_{t=0} \quad (5.3)$$

is the flip contribution ($\sim |B^-(0)|^2$) which is strongly reduced by the last term, the 2nd term being small already at 1 GeV/c. For instance at 6 GeV/c the 3 terms in (5.3) give the following contributions to b_0 according to the phase shift solution

$$b_0 = -34.9 - 0.3 + 21.5 = -13.7 \text{ GeV}^{-2}$$

corresponding to $B_0 = 58.5 \text{ mb}$.

According to a single Regge pole model $b_{0,\text{flip}}$ is constant in energy.

Fig. 7 shows that the slope is not yet well determined in the region of the resonance peak at 1.0 GeV/c, because our extrapolation of the Rutherford data⁶

deviates systematically from the direct measurement of the slope by Borgeaud et al.²⁰. The discrepancy with the CMU-LBL prediction⁴ is not serious, because in this solution the Rutherford data have not yet been taken into account. At higher energies the method of Kistiakowsky et al.⁹ is not suitable for the determination of details of the shape.

The structure of $B_0(k)$ comes mainly from the rapid momentum dependence of $\partial \bar{\sigma} / \partial t$ which has been studied in the dispersion approach by Jakob and Kroll²⁸. This quantity is sensitive to contributions from high spin resonances.

Our values for the slope of the Saclay measurements²⁵ have been taken from a fit by Grein and Kroll who used the method of Ref.²⁹.

5.3 The backward cross section

The charge-exchange backward cross section has been discussed in the literature because, with old data, it seemed that it saturates or even violates the lower isospin bound (σ_+ , σ_0 = backward cross sections)

$$(\sqrt{\sigma_+} - \sqrt{\sigma_0})^2 \leq 2\sigma_0 \leq (\sqrt{\sigma_+} + \sqrt{\sigma_0})^2 \quad (5.4)$$

in large energy intervals or possibly everywhere³⁰. However a more detailed study led to the result that a "phase degeneracy" of the $I=1/2, 3/2$ amplitudes is excluded and that one cannot draw conclusions on the phase from near-saturation of the bound³¹. The present situation is shown in Fig. 8. Our figure differs from that of Törnquist³⁰ insofar as we have ignored many old data which have a poor accuracy or have been extrapolated to 180° over a relatively large distance. At present there is no indication for a violation of the isospin bound and the saturation over a large energy range is excluded.

Since the data of Debenham et al.¹⁷ are consistent with the bounds even in the region where both bounds are close together (800 MeV/c) we conclude that a normalization error of these data is not the reason for the discrepancy with the data of Brown et al.⁶, which are lower by about 30%.

The isospin bounds at all angles will be discussed in Ref.⁷.

If backward cross sections are used for accurate tests of isospin bounds one should keep in mind that there are appreciable radiative corrections, in particular for

$\pi^- p$ scattering at high energies.³²

At higher energies the CMU-LBL-prediction⁴ is fluctuating strongly.

Starting from the backward amplitude reconstructed from phase shifts Pietarinen has recently used the backward dispersion relation in order to calculate a smoothed version of this amplitude³³.

5.4 The slope of the backward cross section

Fig. 9 shows our results for

$$B_{180} = \frac{d}{d\cos\theta} \frac{d\sigma}{d\Omega} \Big|_{180^\circ} = - \frac{1}{2q^2} \sum_{n=0}^N (-1)^n n(n+1) A_n. \quad (5.5)$$

The deviation of the phase shift prediction from the result of our fit around 1 GeV/c is due to the above mentioned discrepancy between the data of Brown et al.⁶ and Debenham et al.¹⁷. Around 980 MeV/c the latter ones alone give a slope of $B_0 \approx 18$ mb.

At higher momenta the slopes B_{180} are fairly small, but this is due to our definition. The data are usually fitted by

$$\frac{d\sigma}{du} = A \exp \{ b_{180} (u - u_{\max}) \}. \quad (5.6)$$

At 6 GeV/c the logarithmic slope b_{180} is $11.3 \pm 1.2 \text{ GeV}^{-2}$ (Boright et al.²⁶) which corresponds to $B_{180} = -0.45$ mb.

$$b_{180} = \frac{d}{du} \ln \frac{d\sigma}{du} \Big|_{180^\circ} = - \frac{1}{2q^2} \frac{B_{180}}{d\sigma/d\Omega} \Big|_{180^\circ}. \quad (5.7)$$

($B_{180} < 0$, $b_{180} > 0$ for a backward peak).

According to Regge models the flip contribution is small at high energies.

In the range 1.0 - 1.8 GeV/c the slope is not well-determined because accurate backward data have not yet been measured.

5.5 Extrapolation of polarization data to 0° and 180°

In sect. 3 we have discussed Legendre fits of polarisation data combined with differential cross sections, because this combination leads to a simple expression in terms of invariant amplitudes. At 0° and 180° we have

$$\left. \frac{P d\sigma/d\Omega}{\sin \theta} \right|_{0^\circ} = \frac{1}{2q^2} \sum_{n=1}^N n(n+1) B_n(k) = \frac{q^2}{8\pi^2 W} \text{Im} (C^* B^-) \Big|_{0^\circ}, \quad (5.8)$$

$$\left. \frac{P d\sigma/d\Omega}{\sin \theta} \right|_{180^\circ} = - \frac{1}{2q^2} \sum_{n=1}^N (-1)^n n(n+1) B_n(k) = \frac{q^2}{8\pi^2 W} \text{Im} (C^* B^-) \Big|_{180^\circ}, \quad (5.9)$$

At 0° the amplitude C^- is well-known from total cross sections and the dispersion relation. Therefore the extrapolation shows to what extent the component B_\perp^- orthogonal to C^- is determined by data alone.

Fig. 10 shows that our fit scatters considerably in regions of rapid variations beyond the last experimental point. We have indicated by arrows the direction of the correction expected from an eye-ball fit to the data.

At some momenta the phase shift prediction differs considerably from the data, the direction of the necessary correction is again indicated by arrows.

The solid line was obtained from the fixed- t solution³⁵ belonging to the new phase shift set.

If the data are correct, the component B_\perp^- is considerably too large (by a factor of the order of 2) in the range 614 - 776 MeV/c and $-B_\perp^-$ is too large in the range 974 - 1750 MeV/c i.e. the bump-dip structure in Fig. 10 is less pronounced.

Fig. 11 shows the same quantity at 180° . Again the Legendre fit is uncertain and the phase shift fit deviates systematically from the data in some regions in a direction indicated by the arrows.

Table VI gives results derived from the "Karlsruhe-Helsinki 78" solution for the values of the differential cross sections, their slopes and $P(d\sigma/d\Omega)/\sin \theta$ at 0° and 180° .

6. Zeros of Transversity and Invariant Amplitudes

6.1 Introduction

Transversity amplitudes are combinations of the usual spin no-flip and flip amplitudes

$$F(\pm) = G \pm i H. \quad (6.1)$$

They have the property that their modulus can be determined from data

$$|F(\pm)|^2 = \frac{d\sigma}{d\Omega} (1 \pm P) \equiv \Sigma(\pm). \quad (6.2)$$

In particular one can determine the zeros of $F(\pm)$ in the complex $z = \cos \theta$ or $w = \exp(i\theta)$ -plane at each momentum where data are available. Barrelet¹¹ has developed a special method for this purpose.

The zeros at real s and complex z are intersections of the surface $\text{Im } s=0$ with "zero trajectories" which are two-dimensional surfaces in the 4-dimensional space of the complex Mandelstam variables s and $t = -2q^2(1-z)$. In general the resulting curves in the $\text{Re } s, \text{Re } t, \text{Im } t$ -space are expected to be smooth except in regions where two trajectories "intersect" each other or near resonances which do not have a sufficient number of Legendre zeros. A general discussion of zero trajectories and their intersection has recently been given in Ref.³⁴.

In the following we present results for zero trajectories of charge-exchange amplitudes from two calculations

i) from the new phase shift analysis "Karlsruhe-Helsinki 78"

ii) from our fit to the data of Brown et al.⁶ which is described above. The quantities $\Sigma(\pm)$, eq. (6.2) have been taken from our fits to $d\sigma/d\Omega$ and to $P(d\sigma/d\Omega)/\sin \theta$. Our fit to $d\sigma/d\Omega$ was used together with the polarization data in the 2nd case. $\Sigma(\pm)$ is a polynomial in z and its zeros were determined by standard methods.

The second method does not lead to a unique result. Since $\Sigma(\pm)$ does not change if a zero z_1 of $F(\pm)$ is replaced by z_1^* (or w_1 by $1/w_1^*$), there remains a discrete ambiguity if zeros are determined from data alone.

We shall present and discuss 3 kinds of plots:

i) Zeros in the complex w -plane¹¹

Since

$$w = \exp(i\theta), \quad z = \frac{1}{2} \left(w + \frac{1}{w} \right); \quad w = z \pm \sqrt{z^2 - 1} \quad (6.3)$$

The unit circle corresponds to the physical region $-1 < z < +1$. The upper half of the figure belongs to $F(+)$, the lower half to $F(-)$. If a trajectory $w=w_1(k)$ crosses the unit circle, we have a zero in the real s, t -plane, i.e. either $P=1$ or $d\sigma/d\Omega = 0$. See also the "Collection of Pion-Nucleon Scattering Formulas" p. II.8 in chapter 2 of Ref.³⁵.

A zero trajectory can pass a resonance surface $s=s_{\text{res}} \equiv M^2 \equiv (M_{\text{res}} - i\Gamma_{\text{res}}/2)^2$ only at a Legendre zero or a double pole. The double poles are rather far away from the physical region. For instance the $N\Delta$ -double poles lie at $w = -10.7 - 2.6i$ and $w = -0.11 + 0.09i$. Therefore we are mainly interested in Legendre zeros.

The position of these zeros for some important resonances is given in Ref.³⁵.

Since we calculate the zeros for real k and s , the trajectory is expected to pass near the position of the Legendre zero at a k -value corresponding to $\text{Re } s_{\text{res}}$. The "causality condition" $\text{Im } s_{\text{res}} < 0$ demands that the Legendre zero must lie on the right hand side if we follow the trajectory in the direction of increasing k . (Ref.¹¹). An example is seen in Fig. 12.

ii) Zeros in the complex z -plane

For some applications it is more suitable to consider the zeros in the complex z -plane (Fig.13), because of the strong distortion caused by the mapping (6.3). The z -plane has two sheets z^\pm which are connected along the cuts from ± 1 to $\pm\infty$. z^+ is mapped onto the upper half of the w -plane and z^- onto the lower half. The upper half of the z^- -plane and the lower half of the z^+ -plane are mapped onto the interior of the unit circle in the w -plane respectively. (See page II.8 of chapter 2 in Ref.³⁵.) Fig. 13 shows trajectories A and B in the z -plane.

iii) Projections of the trajectories onto the $s, \text{Re } t$ -plane

In our calculation s is real and $\geq (m+\mu)^2$. We calculate the t -values of the zeros ($t = -2q^2(1-z)$, $q^2 = \text{c.m. momentum}$) and plot $\text{Re } t$ vs. s (Figs. 14 and 15).

The relation between the different figures is not simple because of distortions caused by the mapping (6.3). In particular zeros which appear near $t=0$ in the $s, \text{Re } t$ -plot are usually not related to dips of $\Sigma(\pm)$ in the forward direction. For discussions of this type it is useful to look at the lines $\text{Re } t = \text{const}$ and $\text{Im } t = \text{const}$ in the w -plane (Fig. II.2 in chapter 2 of Ref.³⁵).

6.2 Discussion of the results

6.2.1 Zeros in the lower half of the w-plane

These zeros correspond to those in the z^- -plane and to dips in $\Sigma(-) = (1-P)d\sigma/d\Omega$. From 0.8 to 2.2 GeV/c the $\Sigma(-)$ -plots show a pronounced dip structure and therefore the location of the zeros is well-defined (Fig. 16 a). The agreement between the results derived from phase shifts and from Legendre fits is good. However, $\Sigma(-)$ is almost flat in the central angular region at 600-800 MeV/c. This makes the results for zeros less reliable (Fig. 16 b). In the following we shall describe the well-established trajectories, in each case starting with the result derived from phase shift analysis.

Trajectory A starts at infinity in the w-plane. It enters the physical region of the s, Re-t-plot for $F(-)$ from the forward direction at $k \approx 125$ MeV/c, crosses the circle $|w|=1$ at almost the same momentum and passes the $\Delta(1232)$ Legendre zero in the expected way. Above 0.6 GeV/c it remains near the real z-axis around $z = 0.6$, i.e. near the circle, and can be followed up to 2.2 GeV/c. It crosses the real z-axis at 0.12, 0.54, 0.975 and 1.88 GeV/c.

Above 1.7 GeV/c the $\Sigma(-)$ -values calculated from phase shifts show increasing deviations from the data. This is related to a strange behaviour of the trajectory. We prefer to take the trajectory from the Legendre fit in this region which remains parallel to trajectory C' in the s, Re-t-plane. The agreement with D. Chew's trajectory A is reasonable.

It is remarkable that the strong $P_{11}(1410)$ resonance, which has no Legendre zero, is passed by the trajectory without a structure. The Legendre zeros of $D_{13}(1519)$ and $F_{37}(1913)$ are passed in the expected way but, in the first case, at a rather large distance.

Trajectory B starts in sheet z^+ (see Fig. 13). It enters sheet z^- at the deep minimum of the backward cross section at 0.53 GeV/c and is clearly seen up to 2.5 GeV/c. Above 0.7 GeV/c the trajectory remains near the real z-axis around $z = -0.2$.

The rapid movement at the energy of the $P_{11}(1410)$ resonance is probably due to the fact that this resonance has no Legendre zero. It is strange that both trajectories, A and B, pass the $D_{13}(1519)$ resonance without a structure, although there is only one Legendre zero. Trajectory B passes the Legendre zeros of $F_{37}(1913)$ in the expected way but at a rather large distance.

According to the phase shift solution trajectory B touches the circle from the inside at 0.53 GeV/c, goes to the outside at 0.60 GeV/c and enters again at 1.26 GeV/c. The results from our Legendre fits and from D. Chew's calculation (trajectory C) are similar. Small details are different, for instance a zero is slightly outside the circle instead of slightly inside. We think that small differences of this kind have no further consequences and are therefore not of interest.

Trajectory C' is the next trajectory which is clearly seen in the $s, \text{Re } t$ -plane belonging to sheet z^- . It enters this sheet at the deep forward dip at 1.36 GeV/c. The notation follows from the fact that, according to phase shift analysis, it is the continuation of trajectory C in sheet z^+ . However the connection is not certain, because the phase shift solution does not fit well the near-forward data.

The trajectory remains near the forward direction and near the real z -axis. It is seen up to 3.6 GeV/c and moves along $t \approx -0.5 \text{ GeV}^2$. It agrees essentially with the high energy part of D. Chew's trajectory G.

Trajectory D' is the last well-established trajectory in sheet z^- . According to phase shift analysis it is the continuation of trajectory D in sheet z^+ . But from our Legendre fits the connection is not obvious, although not excluded.

In sheet z^- trajectory D' is seen from the second dip of the backward cross section (0.85 GeV/c) to 3.6 GeV/c. It remains near the real z -axis around $z = -0.9$.

The result from our Legendre fit does not differ significantly. D. Chew chose the zero at 1.5 GeV/c inside the circle in order to have it nearer the Legendre zero of F37(1913). However, the shift is small because the zero is near the circle, and in our opinion, there is no reason to prefer a slightly smaller distance to the Legendre zero. One should notice that even in the case of P33(1233), where the background is small, the trajectory at $s = \text{Re } s_{\text{res}}$ has an appreciable distance from the Legendre zero in the z -Plane (Fig. 13).

Finally we discuss further nearby zeros which follow from phase shift analysis or from our Legendre fits.

i) Trajectory Z is seen from 0.614 to 2.0 GeV. It remains near the line from $z=1$ to $z=1-i$. Therefore it does not lead to a dip but follows essentially from the shape of the near-forward peak. As mentioned above it has not been possible to adjust the phase shift solution accurately to the experimental shape and to fulfill all the other conditions simultaneously. For this reason trajectory Z is doubtful.

Some of the zeros of trajectory Z follow also from our Legendre fit. Again there is a difficulty because at momenta below 1 GeV/c, the fit has the tendency to remain below the prediction from the forward dispersion relation although this prediction was used as part of the input. We conclude that at present trajectory Z is not yet established. There is a chance that improved near-forward data lead to a modification of trajectory Z which connects it with trajectory C'. It could be a trajectory which comes from the Δ_1 -double pole.

ii) Trajectory J(?) is a string of zeros which enters at the dip at 2.15 GeV/c and can be followed up to 3.6 GeV/c, where its imaginary part is fairly small.

In addition to the above mentioned zeros the phase shift solution shows pieces of zero trajectories in the vicinity of the backward point $z = -1$. Some of the zeros follow also from our Legendre fits.

We think that the complicated zero structure in this region is related to the fact that we have used backward data from Debenham et al.¹⁷ together with the data of Brown et al.⁶, although these two sets of data do not join smoothly. Furthermore near backward zeros are doubtful in the region 1.0 to 1.8 GeV/c because there are not data within the rapidly varying backward peaks or dips.

The Legendre fits show additional zeros around 90° which are essentially a doubling of the above mentioned trajectories in the limited range 616 to 825 MeV/c. If one looks at $\Sigma(-)$ in this region it is seen to be almost flat and small, the structures being comparable with the errors (Fig. 17). In this situation all methods for the determination of zeros are not reliable.

Some of our doubtful zeros correspond to trajectory I and to the low energy parts of trajectories E and G of D. Chew.

D. Chew:	A	C	E	G	I
<hr/>					
our notation:	A	B	D'+?	C'+?	?

6.22 Zeros in the upper half of the w-plane

These zeros correspond to those in the z^+ -plane and to dips in $\Sigma(+)$. In general the structure is less pronounced than in $\Sigma(-)$ and this makes the study of zeros more difficult.

Trajectory B starts at threshold at the center of the circle and moves towards the vicinity of the P33(1233) Legendre zero, leaving it on the right hand side

as expected. It passes at a rather large distance and runs towards the backward point which is almost reached at the deep minimum of the backward cross section at 530 MeV/c. Then the trajectory enters sheet z^- as described above. The path in the z -plane is shown in Fig. 13.

Trajectory C is the only trajectory in sheet z^+ which is seen in addition to B at momenta below those of the data of Brown et al.⁶. It comes from outside of the circle and enters the physical region from the backward direction. $\text{Im } z^+$ remains fairly large, presumably because of difficulties in passing the P11(1410) resonance. It remains at a large distance from the real z -plane, because it aims towards the Legendre zero of D13 (1519).

According to phase shift analysis this trajectory reaches $\text{Re } z=0$ at 850 MeV/c and moves towards the forward hemisphere. The connection between 1.11 and 1.15 GeV/c is disturbed by a nearby disconnected piece of another trajectory which is probably related to the difficulties with the near-forward data mentioned above. At the deep dip of the forward cross section at 1.36 GeV/c the trajectory almost reaches $z=+1$ and passes into sheet z^- where it is denoted as C', because the connection at 1.1 GeV/c is not well-established and the fit to the data at 1.17 and 1.27 GeV/c is bad.

Because of appreciable deviations of the phase shift fit from the data the zero structure derived from our Legendre fit is considerably different. Instead of trajectory C we have 2 pieces of trajectories C_1 and C_2 , which are fairly close together in the range 0.614 - 1.171 GeV/c and describe the broad dip of $\Sigma(+)$ in the region $-0.5 < z < 0$. At $k = 1.17$ GeV/c the two trajectories separate. C_1 moves to the backward direction and goes over into trajectory F which is known from the phase shift solution (see below). C_2 moves to the forward direction and goes over into trajectory E of the phase shift solution.

Trajectory D comes from the inside of the circle and aims towards the backward point which is almost reached at the minimum of the backward cross section at 0.85 GeV/c. In the w -plane the backward point is passed at the outside of the circle and the trajectory goes to the lower half-plane, corresponding to sheet z^- . According to our Legendre fit the connection is not well established. Therefore the continuation is called D'.

Our trajectory D corresponds to the low energy part of D. Chew's trajectory J ($k < 0.9$ GeV/c), but in our case the trajectory moves across the circle at 0.75 GeV/c.

Trajectory F starts inside the circle. In the lower half of the z^+ -plane it is first seen at 614 GeV/c and $z = 1-0.7i$. It moves rapidly towards the origin of the z^+ -plane and makes a loop in the upper half-plane (i.e. to the outside of the unit circle) between 1.0 and 1.2 GeV/c. Then it remains in the lower half z^+ -plane at $z \approx -0.8 - 0.2i$, near one of the F37(1913) Legendre zeros.

As mentioned above this trajectory is confirmed from our Legendre fits above 1.0 GeV/c but the continuation to lower momenta is not well-established, one reason being the large gap in the $\Sigma(\pm)$ data between 824 and 974 MeV/c.

Below 1.0 GeV/c in the region of the F-dip in $\Sigma(+)$ our Legendre fits give two trajectories which are called F_1 and F_2 . They approach each other at 1.17 GeV/c and then separate, F_1 moving to larger angles, whereas F_2 seems to jump towards the forward point $z = +1$ which is almost reached at the deep dip of the forward cross section at 1.36 GeV/c.

At larger momenta F_2 and F_1 go over into trajectories C' and G respectively.

D. Chew's trajectory F is similar to ours, if trajectory C_1 is chosen for the low-energy part.

Trajectory E is clearly seen in the phase shift solution above 1.0 GeV/c up to at least 2.5 GeV/c. It comes from large positive imaginary parts and $\text{Re } z \approx 0$ in the z^+ -plane. Since it starts at an intersection with trajectory F, the continuation to lower momenta is not clear. The Legendre fit suggests that it has the continuation C_2 or C_1 . A similar behaviour was obtained by D. Chew (trajectory B).

Trajectory E is the candidate for the Legendre zero of F37(1913) at 90° , but it is still rather far from it at $s = \text{Re } s_{\text{res}}$, coming nearer at higher momenta.

Trajectory G is the last well-established trajectory. In phase shift analysis it starts inside the circle, the first indication being seen at 923 MeV/c at $z=1-0.8i$. It remains in the forward hemisphere ($\text{Re } z \gtrsim 0.5$) and, above 1.5 GeV/c, near the real z^+ -axis. It crosses the circle at 1.60 GeV/c, going to the outside. At the momentum of the F37(1913) resonance it is near one of the Legendre zeros.

As mentioned above our Legendre fit suggests that trajectory G corresponds to F_1 below 1.1 GeV/c. This essentially agrees with D. Chew's trajectory H. However our G-trajectory starts inside the unit circle.

Trajectory H (?) denotes a string of zeros which is first seen at 1.5 GeV/c from phase shifts and also from our Legendre fits. It enters from the backward

direction and produces only a small structure in $\Sigma(+)$.

Trajectory I (?) is an indication for a trajectory which is seen above 1.4 GeV/c in the unphysical region beyond $z = -1$. It is not well determined, because accurate data for the shape of the backward peak or dip are not available. It comes from the inside of the circle and reaches the neighborhood of $z = -1$ at 2.0 GeV/c. The high energy part of D. Chew's trajectory J corresponds to this trajectory.

Further pieces of zero trajectories from phase shifts in sheet z^+ :

i) Zeros around $z = -0.5 - 0.6i$ are in the range 0.6 - 0.9 GeV/c just reflections of trajectory C.

ii) A string of zeros around $z = 1 + 0.4i$ is essentially a reflection of trajectory F. As mentioned above it is not reliable because of uncertainties in the shape of the forward peak.

A comparison with the trajectories of D. Chew shows the following correspondence:

D. Chew	B	D	F	H	J
our notation	$C_2 + E$	$F_2 + H$	$C_1 + F$	$F_1 + G$	D + I

The strange behaviour of Chew's trajectory D is hard to accept.

6.3 Zeros of invariant amplitudes

The zero structure of the transversity amplitudes is complicated and not yet well resolved. One could think that this is an indication for rather bad properties of the "Karlsruhe-Helsinki 78" phase shift solution. However the zero structure of the isospin odd invariant amplitudes A^- and B^- looks much better. (Fig. 18) and represents a beautiful example for the simplicity of zero trajectories in the presence of a large number of resonances.

Trajectory $A^-(1)$ comes from the P33(1233) Legendre zero and trajectory $A^-(2)$ from the $\Delta\rho$ -double pole. It is remarkable that the B^- -amplitude has almost the same zero trajectories although this is quite unexpected from Odorico's work¹⁴. $B^-(1)$ comes from the $N\Delta$ -double pole.

The zero structure of C^- is more complicated, because there exists a trajectory $C^-(1)$ which starts in the unphysical low-energy region where the Adler-Weisberger predictions from current algebra and PCAC is valid. Together with the

nucleon Born term it determines trajectory $C^-(1)$ which enters the physical region at the dip of the forward cross section at 120 MeV/c and aims towards the P33(1233) Legendre zero.

In addition we have trajectories $C^-(2)$, $C^-(3)$ which come from the $N\Delta$ and $\Delta\varrho$ double poles respectively. Furthermore $C^-(4)$ enters at the deep dip of the forward cross section at 1.36 GeV/c. It comes probably from the combined ϱ D15(1679) ϱ F15(1882) double poles.

This figure shows two bad features: a short piece of a zero trajectory between 614 and 851 MeV/c and a splitting of trajectory $C^-(1)$ above 1.68 GeV/c. We think that both difficulties are due to systematic experimental errors. The first one is clearly connected with our problem with the zeros of $F(\pm)$ in this region.

We learn from the invariant amplitudes that one can expect the following trajectories in $F(\pm)$:

i) Two trajectories come from threshold, where the flip term is suppressed and $F(\pm) \sim C^-$. These trajectories have been found: A and B.

ii) Two trajectories come from the $N\Delta$ double pole. The situation is complicated by the fact that trajectory B (as well as $C^-(1)$) moves to the backward point at 530 MeV/c, where the two trajectories are expected to enter. We conclude that 3 $F(\pm)$ -trajectories should emerge from this unusual intersection. According to phase shift analysis two of them are B and D, both being also seen in our Legendre fits. The third one is not clear, C being a candidate.

iii) Two trajectories come from the $\Delta\varrho$ -double pole. They enter around 850 MeV/c where the forward cross section has a dip.

The phase shift solution suggests trajectory F and possibly Z, whereas the Legendre fit has 3 candidates: F_1 , F_2 and Z.

Further points where new trajectories can be expected to enter are 1.36 GeV/c in the forward direction and 2.15 GeV/c in the backward direction..

We add a table of the dips of forward and backward amplitudes as derived from phase shifts

0°	110	822	1360	2460	k MeV/c
	1111	1570	1862	2350	W MeV
180°	532	851	2150		k MeV/c
	1390	1587	2223		W MeV

Table VII. Dips of the forward and backward charge exchange amplitude $|C^-|$.

7. Summary and Conclusions

i) Since a phase shift analysis based on analyticity constraints had difficulties with the charge-exchange data of the Rutherford group⁶, we have analysed these and other charge-exchange data up to 6 GeV/c directly, using Legendre expansions and studying zero trajectories.

ii) The Legendre coefficients A_n of $d\sigma/d\Omega$ are fairly well determined up to $n=10$, but a good fit requires a remarkably large number of coefficients already around 1 GeV/c. A_{10} is apparently well determined and has a peak at the position of the D15(1679) and F15(1684) (at about 1.0 GeV/c) which is difficult to accept. Legendre coefficients of $P(d\sigma/d\Omega)/\sin \theta$ show large uncertainties already for $n > 6$.

iii) As expected from the above mentioned difficulty there are some large discrepancies between Legendre coefficients determined from data and from phase shifts, for instance in A_4 , where the peaks at 1.0 GeV/c differ by a factor of two, and in B_3 , at 0.7 - 0.8 GeV/c.

The "CMU-LBL 76" phase shifts (which were determined without the Rutherford charge-exchange data) show larger deviations. Furthermore, they lead to coefficients which do not have a smooth momentum dependence above 1.5 GeV/c.

iv) Although data are available in a large angular interval ($-0.95 \leq \cos \theta \leq 0.95$), the extrapolations to 0° and 180° have considerable uncertainties because of strong variations of the data beyond this region. The situation is improved by adding the prediction from the forward dispersion relation and backward cross sections from other experiments. But this introduces an unknown error in our fit because of a fairly large discrepancy between the data of Brown et al.⁶ and of Debenham et al.¹⁷.

Since the structures at $|\cos \theta| \geq 0.90$ contain an important information on higher partial waves and therefore also on resonances, it will be important to carry out new accurate experiments especially designed for these intervals. The results will also help to exploit the information on the absolute phases which follows from the forward and backward dispersion relations.

v) It was pointed out in Ref.⁶ that, at some energies, the extrapolation to 0° disagrees strongly from the prediction derived from the forward dispersion relation. However, there is no serious problem, since reasonable fits are obtained if the prediction is added to the input. A systematic deviation below 1.0 GeV/c

deserves further attention. The CMU-LBL 76-prediction for the forward cross section shows large fluctuations above 1.5 GeV/c.

At some energies there are fairly large discrepancies between the slopes at 0° and 180° derived from phase shifts and those determined directly from our fit. Even larger discrepancies exist for the extrapolations of $P(d\sigma/d\Omega)/\sin\theta$ to 0° and 180° which are proportional to $\text{Im}(C^- B^-)$. This quantity is not yet well determined from the data, because accurate polarization data are not available in the near-forward and near-backward directions. As a consequence the B^- amplitudes at 0° and 180° have appreciable uncertainties.

vi) Contrary to earlier statements in the literature we find no evidence for a violation of the isospin bound at 180° or for a near-saturation of this bound in a large energy interval (see Fig. 8).

vii) The zeros of transversity amplitudes show a simple behaviour above 1.1 GeV/c (Figs. 14,15). Unexpected complications in the range 0.6 - 1.1 GeV/c are possibly due to experimental errors. At some energies fluctuations of the numbers of nearby zeros indicate that the phase shift solution should be improved.

The results for the zero trajectories are the basis for further studies of discrete ambiguities and for a representation of the amplitudes in terms of zeros and poles as it is suggested by dual models.

Acknowledgment: We are grateful to R. Koch and I. Sabba-Stefanescu for discussions.

Appendix A

Calculation of Clebsch-Gordan Coefficients *)

In order to calculate the coefficients A_n and B_n of the Legendre expansions eqs. (2.1), (3.2) from phase shifts, one needs the values of the Clebsch-Gordan coefficients a_n and b_n in eqs. (2.2) and (3.3). For small l they have been given in tables² but the recent phase shift analyses go to much higher angular momenta and furthermore it is more convenient to calculate the coefficients instead of using tables.

We start from the partial wave expansion

$$qG = \sum_{l=0}^{\infty} \alpha_l P_l(z); \quad qH = \sum_{l=1}^{\infty} \beta_l \sin \theta P'_l(z) \quad (A1)$$

where $l \pm$ belongs to $J = l \pm 1/2$ and

$$\alpha_l = (l+1)T_{l+} + lT_{l-}, \quad \beta_l = T_{l+} - T_{l-}. \quad (A2)$$

The cross sections and $P \frac{d\sigma}{d\Omega}$ can be expanded in terms of Legendre functions, eqs. (2.1), (3.2) and also in terms of partial waves, using (A1) and (A2).

$$\frac{d\sigma}{d\Omega} = \frac{1}{q^2} \sum_n A_n P_n(z) = |G|^2 + |H|^2 = \frac{1}{q^2} \sum_{l,m} \{ \alpha_l \alpha_m^* P_l(z) P_m(z) + \beta_l \beta_m^* P_l(z) P_m^1(z) \}, \quad (A3)$$

$$P \frac{d\sigma}{d\Omega} = -\frac{1}{q^2} \sum_n B_n P_n^1(z) = 2 \operatorname{Im}(GH^*) = -\frac{1}{q^2} 2 \operatorname{Im} \sum_{l,m} \alpha_l \beta_m^* P_l(z) P_m^1(z), \quad (A4)$$

where $P_n^1(z) = -\sin \theta P'_n(z)$. We solve for A_n , B_n , using the orthogonality properties

$$A_n = \frac{2n+1}{2} \int_{-1}^1 q^2 \frac{d\sigma}{d\Omega} P_n(z) dz, \quad (A5)$$

$$B_n = -\frac{2n+1}{2n(n+1)} \int_{-1}^1 q^2 P \frac{d\sigma}{d\Omega} P_n^1(z) dz. \quad (A6)$$

Inserting formulas (A3) and (A4) gives

*) After the completion of this work we received a preprint in which a different method was proposed by Oyanagi.³⁶

$$A_n = \operatorname{Re} \sum_{\ell, m} [\rho_{n\ell m} \alpha_\ell \alpha_m^* + \sigma_{n\ell m} \beta_\ell \beta_m^*] \quad (\text{A7})$$

$$B_n = 2 \sum_{\ell, m} \tau_{n\ell m} \cdot \operatorname{Im}(\alpha_\ell \beta_m^*) \quad (\text{A8})$$

where

$$\rho_{n\ell m} = \frac{2n+1}{2} \int_{-1}^1 P_n(z) P_\ell(z) P_m(z) dz, \quad (\text{A9})$$

$$\sigma_{n\ell m} = \frac{2n+1}{2} \int_{-1}^1 P_n(z) P_\ell^1(z) P_m^1(z) dz, \quad (\text{A10})$$

$$\tau_{n\ell m} = \frac{2n+1}{2n(n+1)} \int_{-1}^1 P_n^1(z) P_\ell(z) P_m^1(z) dz. \quad (\text{A11})$$

From the recurrence-relations of Legendre Polynomials it is possible to derive relations for the integrals $\rho_{n\ell m}$, $\sigma_{n\ell m}$, $\tau_{n\ell m}$. For fixed n they read

$$\rho_{n, \ell+1, m} = \frac{2\ell+1}{\ell+1} \frac{1}{2m+1} [(m+1) \rho_{n, \ell, m+1} + m \rho_{n, \ell, m-1}] - \frac{\ell}{\ell+1} \rho_{n, \ell-1, m} \quad (\text{A12})$$

$$\sigma_{n, \ell+1, m} = \frac{2\ell+1}{\ell} \frac{1}{2m+1} [m \sigma_{n, \ell, m+1} + (m+1) \sigma_{n, \ell, m-1}] - \frac{\ell+1}{\ell} \sigma_{n, \ell-1, m} \quad (\text{A13})$$

$$\tau_{n, \ell+1, m} = \frac{2\ell+1}{\ell+1} \frac{1}{2m+1} [m \tau_{n, \ell, m+1} + (m+1) \tau_{n, \ell, m-1}] - \frac{\ell}{\ell+1} \tau_{n, \ell-1, m}, \quad (\text{A14})$$

where starting-values ($\ell=0$ and $\ell=1$) are

$$\rho_{n, 0, m} = \delta_{nm} \quad \rho_{n, 1, m} = \frac{n+1}{2n+3} \delta_{n, m-1} + \frac{n}{2n-1} \delta_{n, m+1} \quad (\text{A15})$$

$$\sigma_{n, 0, m} = 0 \quad \sigma_{n, 1, m} = \frac{(n+1)(n+2)}{2n+3} \delta_{n, m-1} - \frac{n(n-1)}{2n-1} \delta_{n, m+1} \quad (\text{A16})$$

$$\tau_{n, 0, m} = \delta_{nm} \quad \tau_{n, 1, m} = \frac{n+2}{2n+3} \delta_{n, m-1} + \frac{n-1}{2n-1} \delta_{n, m+1} \quad (\text{A17})$$

Furthermore one obtains from the symmetries of the Legendre functions and the coefficients $\rho_{n\ell m}$, $\sigma_{n\ell m}$ and $\tau_{n\ell m}$:

$$\rho_{n\ell m} = \sigma_{n\ell m} = \tau_{n\ell m} = 0 \quad \text{if } n+\ell+m \text{ is odd,}$$

$$\rho_{n\ell m} = \sigma_{n\ell m} = \tau_{n\ell m} = 0 \quad \text{for } m > n+\ell \text{ and for } m < |n-\ell|.$$

References

1. S. Almeded and C. Lovelace, Nucl.Phys. 40B (1972) 157
2. R. Ayed, thesis, Paris 1976
3. E. Pietarinen, Nucl.Phys. B107 (1976) 21, Phys.Lett 61B (1976) 461,
Proceedings of the Topical Conference on Baryon Resonances. Oxford (July 1976). Paper submitted to the European Conference on Particle Physics, Budapest 1977.
4. R.E. Cutkosky, R.E. Hendrick, Y.A. Chao, R.G. Lipes, J.G. Sandusky, R.L. Kelly, J.W. Allcock, Proceedings of the Topical Conference on Baryon Resonances, Oxford (July 1976) and private communication from R.L. Kelly (August 1977), Phys.Rev.Lett 37 (1976) 645
5. K.H. Augenstein, G. Höhler, E. Pietarinen, H.M. Staudenmaier, Survey Index of Pion-Nucleon Scattering Data, ZAED Physics Data 1-2 (1977) Vols. I, II, III. Available from ZAED, Kernforschungszentrum D-7514 Leopoldshafen, Germany. Updated versions (Jan. 1978, Jan. 1979)
6. R.M. Brown et al., Nucl.Phys. B117 (1976) 12 and B144(1978)287
Erratum Nucl.Phys.B137(1978)542
7. G. Höhler, F. Kaiser and H.M. Staudenmaier, to be published
8. F. Bulos et al., Phys.Rev. 187 (1969) 1827
9. V. Kistiakowsky et al., preprint submitted to the International Conference on High Energy Physics at Tbilisi (1976). An earlier version was submitted to the Batavia Conference (Yamamoto et al., 1972)
10. G. Höhler, H.P. Jakob and F. Kaiser, Table of Pion-Nucleon Forward Amplitudes KFK-report 2457 (April 1977).
11. E. Barrelet, Nuovo Cim. 8A (1972) 331 and thesis (Paris 1970)
See also R.D. Baker, Rutherford Laboratory Report RL-76-013
12. D. Chew et al., Berkeley Report LBL-4644, 4856, 4851, 6102, 6406
E. Barrelet et al., Berkeley Report LBL-5386
G. Höhler, F. Kaiser and I. Sabba-Stefanescu, Karlsruhe preprint TKP 76-15 (October 1976)
- 12a. D. Chew, Berkeley preprint LBL-6472
13. A. Gersten, Nucl.Phys. B12 (1969) 537
14. R. Odorico, Nucl.Phys. B37 (1972) 509, Phys.Rev. D8 (1973) 3952
F. Fukugita and K. Igi, Phenomenological Duality, Phys. Reports 31C (1977) 237.

- M. Fukugita, preprint KEK-TH 6, National Lab. for High Energy Physics, Japan.
15. E. Borie, W. Gampp, G. Höhler, R. Koch and I. Sabba-Stefanescu, preprint TKP 78-18, to be published
 16. P.R. Bevington, Data Reduction and Error Analysis for the Physical Sciences McGraw Hill Book Co. 1969
 17. N.C. Debenham et al., Phys.Rev. D12 (1975) 2545
 18. V. Kistiakowsky et al., Phys.Rev. D6 (1972) 1882
 19. G. Höhler et al., Phys.Lett. 20 (1966) 79, 22 (1966) 203
N. Navelet and P.R. Stevens, Nucl.Phys. B118 (1977) 475
 20. P. Borgeaud et al., Phys.Lett. 10 (1964) 134
 21. J.E. Nelson et al., Phys.Lett 47B (1973) 281
 22. J. Feltesse, thesis Paris (1975), Note CEA-N-1838
 23. C.B. Chiu et al., Phys.Rev. 156 (1967) 1415
 24. S.R. Shannon et al., Phys.Rev.Lett. 33 (1974) 237
 25. O. Guisan and M. Yvert, private communications (Saclay group) ,see Ref.⁵
A.V. Stirling et al., Phys.Rev.Lett. 14 (1965) 763
P. Sonderegger et al., Phys.Lett. 20 (1966) 75
 26. W.S. Brockert et al., Phys.Lett. 51B (1974) 390
C. De Marzo et al., Phys.Lett. 56B (1975) 487
J.P. Boright, Phys.Lett. 33B (1970) 615
P. Rehak, Thesis (Pisa, 1972)
J. Schneider, Thesis (Paris, 1971)
 27. P. Borgeaud et al., Phys.Lett. 10 (1964) 134
 28. H.P. Jakob and P. Kroll, Nucl.Phys. B58 (1973) 269
 29. J. Dronkers and P. Kroll, Nucl.Phys. B47 (1972) 291
 30. N.A. Törnquist, Phys.Rev.D13 (1976) 1947
Earlier papers are cited there
 31. G. Höhler and W. Schmidt, Phys.Lett 38B (1972) 237
 32. M.R. Sogard, Phys.Rev. D9 (1974) 1486
 33. E.Pietarinen, University of Helsinki preprint No. HU-TPT-78-13 (April 78)
 34. G.Höhler and I.Sabba-Stefanescu, Singularities of Zero Trajectories of Scattering Amplitudes, Karlsruhe preprint TKP 78-7

35. G. Höhler, F. Kaiser, R. Koch and E. Pietarinen, "Handbook of Pion-Nucleon Scattering", to appear in ZAED Physics Data 1978. The tables are based on the "Karlsruhe-Helsinki 78" phase shift solution. Chapter 1 and 9 are available as Karlsruhe preprint TKP 78-11 (June 1978), Chapter 2 as preprint TKP 78-12. TKP 78-22 is a preprint of the sections on $\pi\pi NN$ amplitudes and Low Energy Parameters.

36. Y.Oyanagi, KEK preprint-78-2, to be published

Figure Captions

Fig. 1 χ_{DF}^2 as a function of N, eq. (2.1), for different momenta (MeV/c).

Fig. 2 Legendre coefficients A_n for differential cross sections.

i) Phase shift solutions: — Karlsruhe-Helsinki 78, —+— CMU-LBL 76
At some peaks we have given the most important interference terms.

ii) Legendre fits: \star Nelson et al. (from Ref.²¹), \ast Brown et al.⁶ and Υ Feltesse²²: our fit with N=11, including the prediction at 0° (Ref.¹⁰) and backward data.^{17,18}

iii) $A_n(k)$ from Υ -distributions: \uparrow Bulos et al.⁸, \diamond Kistiakowsky et al.⁹

iv) $A_n(k)$ from spline fits and eq. (4.1), data of Refs.^{6,25,26}: \square . Abscissa: k =lab.momentum in GeV/c, W =total energy in GeV.

Fig. 3 Legendre coefficients $B_n(k)$ for $P(d\sigma/d\Omega)/\sin\theta$. Notation: the same as in Fig. 2

Fig. 4 Experimental discrepancies at 2.7 GeV/c.

\ast Brown et al.⁶, \uparrow Saclay group²⁵, — \diamond — Kistiakowsky et al.⁹,
Kistiakowsky et al.¹⁸, \square : prediction from Ref.¹⁰. solid line:
from "Karlsruhe-Helsinki 78" phase shifts. Notice the region near $\cos\theta = 0.6$.

Fig.5a,b Discrepancies between the data of Brown et al.⁶ and the "Karlsruhe-Helsinki 78" phase shift fit.

$\Delta\sigma \equiv d\sigma/d\Omega$ from data (\ast) or from the fit (N=11) minus the prediction from the phase shift analysis. The area under the curve is proportional to the discrepancies in A_4 and A_{10} respectively. The deviation of the experimental points from the abscissa shows that the difficulty comes from the region of the near-backward peak of $d\sigma/d\Omega$ and from the first point at small angles. Our fit (solid line) tries to follow the data and this leads to the peak in A_{10} .

Fig. 6 Forward charge-exchange cross sections.

Dispersion predictions¹⁰: for two high energy assumptions. HJK 1 was adjusted to the NAL total cross sections and HJK 2 to the NAL charge-exchange forward cross sections.

◇ calculated from CMU-LBL 76 phase shifts. We have not yet evaluated the errors.

+ from our Legendre fit to the data of Brown et al.⁶, including the dispersion prediction (HJK 1) with the error estimated in Ref.¹⁰.

◊ Saclay data²⁵, (extrapolation of Grein and Kroll), † Nelson et al.²¹

◆ Borgeaud et al.²⁰, ‡ Kistiakowsky et al.⁹.

Fig. 7 Slope B_0 at 0° , eq. (5.1). $B = (d/d \cos \theta) d\sigma/d\Omega$

From "Karlsruhe-Helsinki 78" phase shifts: solid line, from CMU-LBL 76 phase shifts: □, from our Legendre fit: * from Legendre fit of Kistiakowsky et al.⁹: ◇, from a fit to the Saclay data²⁵ (Grein and Kroll): X, from data of Borgeaud et al.²⁰: †. W =total c.m. energy.

Fig. 8 Isospin bounds for the charge-exchange backward cross section. Solid lines: bounds and charge-exchange cross section from "Karlsruhe-Helsinki 78" phase shifts.

Charge exchange cross sections: the dashed line connects the prediction from CMU-LBL 76 phase shifts, + from our Legendre fit, † Debenham et al.¹⁷, ◆ Kistiakowsky et al.⁹, ◆ De Marzo et al.²⁶.

Fig. 9 Slope B_{180} at $\theta=180^\circ$, eq. (5.5). $B = (d/d \cos \theta) d\sigma/d\Omega$

Notation: see Fig. 7, ■ Boright et al.²⁶

Fig. 10 $P(d\sigma/d\Omega)/\sin \theta$ at $\theta=0^\circ$.

From the "Karlsruhe-Helsinki 78" solution: + from phase shifts, solid-line: from the fixed-t solution. ◇ from CMU-LBL 76 phase shifts, * from our Legendre fit.

Fig. 11 $P(d\sigma/d\Omega)/\sin \theta$ at $\theta=180^\circ$.

Notation: the same as in Fig. 10, but there is no result from the fixed-t amplitude. The line connects the points calculated from phase shifts.

Fig. 12 Zero trajectories A and B in the w-plane.

Fig. 13a,b,c Zero trajectories in the z-plane.

Fig. 14a,b Projection of zero trajectories at real s onto the physical s,t-plane. The arrows indicate the location of dips of forward and backward

cross sections. The zeros have been calculated from our Legendre fit.

Fig. 15a,b The same as Fig. 14, but the zeros have been calculated from "Karlsruhe-Helsinki 78" phase shifts.

Fig. 16a,b Plots of $(1 \pm P)d\sigma/d\Omega$. At the dips we have written the name of the nearby zero trajectory.

Fig. 17a,b,c Projection of zero trajectories of invariant amplitudes at real s onto the physical s, t -plane.

Table Caption

Table I Legendre coefficients $A_n(k)$, eq.(2.1), and χ_{DF}^2 from our fit to the data of Brown et al.⁶, including the prediction from the forward dispersion relation¹⁰ and backward data^{17,18}. The diagonal error is also listed.

Table II Legendre coefficients $A_n(k)$ calculated from "Karlsruhe-Helsinki 78" phase shifts. Only coefficients up to A_{12} have been listed.

Table III Legendre coefficients $B_n(k)$, eq.(3.2) and χ_{DF}^2 from our fit to the data of Brown et al.⁶ The diagonal error is also listed.

Table IV Legendre coefficients $B_n(k)$ from "Karlsruhe-Helsinki 78" phase shifts

Table V see page 9

Table VI Values of differential cross sections, their slopes and of $P(d\sigma/d\Omega)/\sin \theta$ at 0° and 180° as calculated from "Karlsruhe-Helsinki 78" phase shifts.

Table VII see page 23.

PLAB	A 0	A 1	A 2	A 3	A 4	A 5	A 6	A 7	A 8	A 9	A10	A11	χ^2_{DF}
518.	0.269	0.453	0.364	0.171	0.102	0.051	0.071	0.052	0.044	-0.010	0.002	0.009	1.844
	± 0.003	0.005	0.006	0.007	0.008	0.009	0.010	0.010	0.011	0.011	0.012	0.011	
675.	0.320	0.511	0.494	0.154	0.116	0.037	0.043	0.014	0.034	-0.021	0.022	0.015	7.004
	0.002	0.003	0.004	0.005	0.006	0.006	0.007	0.007	0.008	0.008	0.008	0.007	
724.	0.295	0.387	0.433	0.084	0.055	0.091	0.051	0.031	0.046	-0.046	0.037	0.063	4.431
	0.003	0.005	0.006	0.007	0.008	0.009	0.010	0.010	0.011	0.011	0.012	0.012	
776.	0.253	0.126	0.271	0.084	-0.044	0.193	0.023	0.008	0.051	-0.019	0.044	0.025	4.606
	0.001	0.003	0.003	0.004	0.005	0.005	0.006	0.006	0.006	0.006	0.007	0.007	
825.	0.236	-0.045	0.269	0.138	-0.082	0.272	-0.019	0.007	0.057	-0.021	0.036	0.027	3.995
	0.002	0.004	0.004	0.005	0.006	0.007	0.007	0.007	0.008	0.007	0.008	0.008	
974.	0.472	-0.131	0.777	0.382	0.042	0.893	-0.109	0.034	0.086	-0.050	0.113	-0.007	7.716
	0.003	0.007	0.008	0.008	0.010	0.012	0.013	0.011	0.012	0.011	0.011	0.012	
997.	0.471	-0.111	0.751	0.364	0.069	0.890	-0.062	-0.023	0.091	-0.051	0.136	0.063	5.581
	0.005	0.012	0.016	0.019	0.021	0.023	0.023	0.022	0.021	0.019	0.018	0.018	
1027.	0.455	-0.082	0.640	0.265	0.067	0.862	-0.032	-0.018	0.056	-0.052	0.158	0.007	2.122
	0.005	0.012	0.018	0.021	0.023	0.025	0.025	0.022	0.021	0.019	0.018	0.019	
1077.	0.314	-0.053	0.328	0.025	0.088	0.544	0.133	-0.075	0.037	-0.056	0.123	0.038	1.241
	0.004	0.010	0.013	0.017	0.019	0.020	0.020	0.019	0.019	0.018	0.018	0.019	
1171.	0.222	-0.024	0.164	-0.082	0.026	0.200	0.155	-0.141	-0.005	-0.038	0.049	0.010	2.333
	0.003	0.006	0.008	0.010	0.011	0.011	0.012	0.013	0.013	0.012	0.012	0.013	
1275.	0.218	0.004	0.182	-0.078	0.008	0.028	0.131	-0.212	-0.055	-0.077	0.029	-0.012	1.540
	0.003	0.007	0.009	0.011	0.012	0.013	0.013	0.014	0.016	0.014	0.014	0.016	
1356.	0.253	0.014	0.217	-0.017	0.042	-0.034	0.052	-0.270	-0.068	-0.097	-0.010	-0.020	1.831
	0.004	0.009	0.012	0.014	0.014	0.014	0.015	0.016	0.018	0.017	0.017	0.018	
1438.	0.254	0.022	0.180	0.027	0.106	-0.008	-0.025	-0.247	-0.071	-0.080	-0.014	0.010	2.019
	0.003	0.006	0.009	0.010	0.012	0.011	0.011	0.012	0.013	0.013	0.013	0.013	
1505.	0.243	0.048	0.127	0.092	0.162	0.020	-0.049	-0.208	-0.034	-0.037	0.002	0.014	2.227
	0.003	0.007	0.010	0.011	0.011	0.011	0.011	0.011	0.013	0.014	0.014	0.013	
1601.	0.243	0.119	0.130	0.188	0.235	0.090	-0.054	-0.161	-0.007	-0.047	-0.049	0.009	1.197
	0.004	0.008	0.012	0.013	0.013	0.011	0.011	0.012	0.014	0.015	0.015	0.014	
1688.	0.199	0.131	0.105	0.196	0.254	0.125	-0.005	-0.097	0.040	0.014	-0.017	0.006	2.142
	0.003	0.008	0.011	0.012	0.013	0.012	0.011	0.011	0.013	0.014	0.014	0.012	
1767.	0.195	0.148	0.100	0.210	0.292	0.184	0.003	-0.092	0.061	0.014	-0.013	-0.000	1.445
	0.003	0.008	0.011	0.013	0.014	0.013	0.013	0.013	0.014	0.014	0.014	0.012	
1872.	0.180	0.167	0.125	0.189	0.312	0.202	0.040	-0.049	0.043	0.035	0.007	0.011	1.442
	0.003	0.008	0.011	0.013	0.014	0.014	0.014	0.014	0.014	0.014	0.015	0.012	
1975.	0.170	0.164	0.138	0.179	0.293	0.204	0.053	-0.010	0.056	0.066	-0.032	-0.022	0.807
	0.004	0.008	0.012	0.014	0.015	0.015	0.014	0.015	0.016	0.016	0.016	0.013	
2056.	0.154	0.160	0.131	0.150	0.282	0.193	0.070	0.001	0.042	0.075	-0.053	-0.018	1.249
	0.003	0.008	0.011	0.013	0.014	0.014	0.014	0.014	0.014	0.014	0.014	0.011	
2267.	0.137	0.131	0.124	0.072	0.169	0.105	0.056	-0.023	-0.018	0.026	-0.066	-0.033	1.061
	0.003	0.006	0.009	0.010	0.010	0.010	0.010	0.010	0.011	0.013	0.013	0.011	
2724.	0.105	0.139	0.150	0.055	0.106	0.131	0.152	0.021	-0.040	-0.095	-0.077	-0.060	2.250
	0.003	0.007	0.009	0.011	0.011	0.010	0.009	0.010	0.012	0.014	0.013	0.010	

Table I

FLAB	A 0	A 1	A 2	A 3	A 4	A 5	A 6	A 7	A 8	A 9	A10	A11	A12
0.573	0.313	0.544	0.376	0.183	0.064	0.005	-0.082	0.001	0.000	0.000	0.000	0.000	0.000
0.614	0.314	0.525	0.408	0.198	0.111	0.038	0.035	0.019	0.007	0.000	0.001	0.000	0.000
0.653	0.336	0.561	0.523	0.233	0.161	0.062	0.050	0.028	0.021	0.003	0.001	0.001	0.001
0.675	0.339	0.542	0.526	0.189	0.137	0.045	0.047	0.029	0.021	0.003	0.001	0.001	0.001
0.705	0.349	0.513	0.551	0.179	0.144	0.090	0.041	0.024	0.014	0.005	0.003	0.002	0.001
0.725	0.331	0.433	0.487	0.131	0.109	0.103	0.024	0.040	0.019	0.007	0.006	0.001	0.002
0.750	0.304	0.311	0.413	0.115	0.082	0.127	0.013	0.036	0.010	0.013	0.004	0.002	0.001
0.777	0.265	0.166	0.308	0.107	0.004	0.174	0.026	0.021	0.020	0.011	0.004	0.004	0.002
0.800	0.248	0.084	0.298	0.123	-0.003	0.190	0.006	0.035	0.005	0.018	0.003	0.003	0.002
0.822	0.233	0.007	0.274	0.144	-0.044	0.244	0.001	0.023	0.047	0.007	0.004	0.013	0.003
0.851	0.237	-0.034	0.330	0.192	-0.021	0.291	-0.014	0.032	0.025	0.010	0.008	0.004	0.003
0.875	0.260	-0.059	0.414	0.246	0.002	0.374	-0.038	0.030	0.033	0.006	0.005	0.005	0.002
0.895	0.293	-0.072	0.492	0.302	0.028	0.450	-0.046	0.030	0.031	0.012	0.009	0.004	0.002
0.923	0.353	-0.075	0.614	0.379	0.081	0.599	-0.050	0.034	0.048	0.018	0.020	0.008	0.002
0.954	0.420	-0.068	0.735	0.411	0.149	0.744	-0.065	0.054	0.043	0.024	0.034	0.013	0.003
0.975	0.457	-0.079	0.775	0.394	0.149	0.842	-0.064	0.076	0.048	0.017	0.078	0.007	0.002
1.000	0.476	-0.046	0.814	0.390	0.232	0.863	-0.020	0.053	0.021	0.011	0.021	0.013	-0.000
1.030	0.448	-0.052	0.703	0.256	0.208	0.773	0.004	0.016	0.007	0.016	0.048	0.029	-0.001
1.055	0.405	-0.049	0.605	0.140	0.211	0.645	0.041	0.002	-0.017	0.009	0.023	0.034	-0.004
1.080	0.349	-0.049	0.461	0.050	0.171	0.522	0.066	-0.038	-0.025	-0.016	0.027	0.031	-0.006
1.113	0.291	-0.054	0.334	-0.037	0.137	0.348	0.103	-0.069	-0.014	-0.018	0.009	0.018	-0.005
1.154	0.238	-0.049	0.229	-0.087	0.096	0.184	0.134	-0.105	-0.015	-0.013	-0.002	0.014	-0.003
1.174	0.222	-0.036	0.198	-0.086	0.075	0.144	0.141	-0.124	-0.017	-0.009	0.010	-0.001	-0.003
1.210	0.210	-0.026	0.195	-0.096	0.071	0.054	0.152	-0.146	-0.033	-0.011	-0.005	0.005	-0.003
1.235	0.210	-0.017	0.199	-0.100	0.066	0.012	0.159	-0.171	-0.044	-0.018	-0.005	0.005	-0.003
1.280	0.216	-0.007	0.209	-0.087	0.053	-0.057	0.130	-0.222	-0.047	-0.028	-0.003	-0.008	0.002
1.324	0.223	-0.012	0.228	-0.080	0.066	-0.123	0.087	-0.250	-0.057	-0.028	0.005	0.000	0.005
1.360	0.232	-0.016	0.212	-0.053	0.059	-0.125	0.056	-0.269	-0.043	-0.039	0.013	0.005	0.007
1.400	0.233	-0.021	0.206	-0.035	0.101	-0.136	0.030	-0.258	-0.038	-0.027	0.009	0.012	0.005
1.430	0.236	-0.014	0.187	-0.007	0.113	-0.099	0.003	-0.261	-0.031	-0.031	0.009	0.020	0.007
1.473	0.241	0.003	0.178	0.038	0.173	-0.084	-0.007	-0.249	-0.027	-0.015	0.005	0.017	-0.006
1.505	0.240	0.031	0.175	0.086	0.208	-0.035	-0.017	-0.223	-0.017	-0.032	0.004	0.005	-0.008
1.550	0.233	0.055	0.154	0.116	0.242	-0.001	-0.037	-0.221	-0.026	-0.017	-0.003	0.011	-0.011
1.590	0.228	0.069	0.131	0.152	0.238	0.028	-0.048	-0.197	-0.014	-0.028	-0.015	0.012	-0.012
1.640	0.209	0.100	0.127	0.186	0.278	0.070	-0.031	-0.151	-0.014	-0.006	-0.018	0.019	-0.003
1.680	0.205	0.117	0.122	0.205	0.298	0.110	-0.036	-0.127	0.012	0.012	-0.023	0.009	-0.004
1.720	0.196	0.124	0.121	0.218	0.303	0.122	-0.030	-0.103	0.023	0.004	-0.030	0.020	-0.004
1.760	0.191	0.143	0.124	0.222	0.313	0.151	-0.010	-0.097	0.019	0.012	-0.022	0.011	-0.012
1.800	0.188	0.145	0.135	0.233	0.328	0.152	-0.001	-0.076	0.013	0.010	-0.033	0.006	-0.018
1.840	0.181	0.158	0.152	0.233	0.349	0.175	0.010	-0.055	0.025	0.022	-0.033	0.007	-0.009
1.890	0.176	0.166	0.164	0.226	0.341	0.185	0.029	-0.056	0.009	0.022	-0.038	-0.003	-0.016
1.920	0.169	0.159	0.161	0.225	0.344	0.189	0.039	-0.027	0.024	0.019	-0.042	0.007	-0.008
1.980	0.158	0.152	0.152	0.200	0.308	0.181	0.047	-0.026	0.016	0.023	-0.052	-0.004	-0.011
2.030	0.149	0.149	0.154	0.182	0.285	0.179	0.064	0.002	0.011	0.018	-0.050	0.008	-0.001

FLAB	A 0	A 1	A 2	A 3	A 4	A 5	A 6	A 7	A 8	A 9	A10	A11	A12
2.070	0.143	0.144	0.145	0.157	0.259	0.172	0.074	-0.009	-0.004	0.021	-0.057	-0.000	-0.003
2.150	0.130	0.128	0.143	0.126	0.206	0.141	0.083	0.006	-0.019	0.004	-0.057	0.008	-0.005
2.200	0.124	0.118	0.130	0.107	0.187	0.127	0.078	-0.008	-0.034	-0.005	-0.059	0.004	-0.003
2.260	0.117	0.114	0.142	0.087	0.164	0.108	0.098	-0.010	-0.051	-0.034	-0.087	-0.009	-0.005
2.340	0.112	0.110	0.146	0.083	0.156	0.106	0.092	-0.033	-0.064	-0.061	-0.097	-0.025	-0.015
2.460	0.105	0.120	0.185	0.079	0.154	0.106	0.138	-0.021	-0.088	-0.114	-0.138	-0.052	-0.041
2.560	0.102	0.147	0.197	0.121	0.150	0.145	0.158	-0.003	-0.072	-0.153	-0.145	-0.093	-0.053
2.750	0.104	0.167	0.224	0.161	0.191	0.199	0.202	0.045	-0.048	-0.133	-0.142	-0.120	-0.068
3.000	0.087	0.172	0.228	0.212	0.230	0.231	0.223	0.103	0.019	-0.071	-0.084	-0.107	-0.086
3.400	0.071	0.150	0.227	0.211	0.229	0.213	0.210	0.150	0.098	0.010	-0.047	-0.083	-0.077
3.650	0.066	0.148	0.224	0.222	0.238	0.224	0.229	0.179	0.137	0.044	-0.015	-0.067	-0.087
4.000	0.062	0.150	0.225	0.240	0.253	0.237	0.229	0.196	0.160	0.079	0.019	-0.047	-0.075
5.000	0.056	0.147	0.228	0.260	0.285	0.284	0.285	0.264	0.241	0.185	0.131	0.054	-0.000
6.000	0.053	0.143	0.228	0.271	0.309	0.314	0.317	0.300	0.281	0.238	0.197	0.128	0.073
10.000	0.049	0.135	0.215	0.286	0.352	0.386	0.414	0.434	0.448	0.430	0.404	0.377	0.344

Table II

PLAB	B 1	B 2	B 3	B 4	B 5	B 6	B 7	B 8	B 9	B 10	χ^2_{DF}
617.	.139	.101	.026	-.004	-.008	.004	-.001	.000	-.004	-.003	.680
	.007	.008	.008	.009	.008	.009	.007	.008	.004	.004	
675.	.161	.115	.053	-.007	-.007	-.001	.000	.006	.003	.004	.869
	.005	.005	.005	.004	.004	.004	.004	.004	.003	.002	
723.	.130	.131	.018	.005	-.024	.003	.002	.003	.001	-.001	.516
	.005	.005	.004	.004	.003	.003	.003	.003	.002	.002	
776.	.047	.140	-.034	.027	-.014	-.007	.013	-.003	-.002	.001	.855
	.005	.005	.004	.003	.003	.003	.002	.002	.002	.002	
827.	.052	.087	-.024	.044	-.017	.004	.011	-.004	.004	.001	.951
	.006	.005	.004	.004	.003	.003	.003	.003	.002	.002	
974.	.019	-.051	.080	.031	-.010	-.012	.004	.008	.008	-.001	1.607
	.006	.005	.005	.005	.004	.004	.003	.003	.003	.003	
1027.	-.057	-.059	.066	.016	-.015	-.040	-.000	.007	.010	.001	2.564
	.006	.004	.004	.004	.003	.003	.003	.003	.002	.002	
1076.	-.055	-.009	.023	-.008	.003	-.033	.004	.000	.005	-.004	2.439
	.004	.003	.002	.002	.002	.002	.002	.002	.002	.001	
1170.	-.056	.034	-.001	-.034	.021	-.046	.009	.003	.007	-.003	1.515
	.004	.003	.002	.002	.002	.002	.002	.002	.002	.002	
1274.	-.067	.002	-.031	-.059	.009	-.066	.010	-.007	.006	-.000	.905
	.004	.004	.004	.004	.004	.004	.003	.003	.002	.002	
1355.	-.065	-.026	-.037	-.055	-.000	-.082	.009	-.013	-.002	-.005	1.046
	.005	.004	.004	.004	.004	.004	.004	.003	.002	.002	
1437.	-.055	-.033	.010	-.006	.012	-.055	.027	.004	.002	-.003	1.086
	.006	.004	.004	.004	.004	.004	.003	.003	.003	.003	
1505.	-.051	-.039	.022	.024	.014	-.040	.030	.014	-.001	-.003	1.295
	.005	.004	.004	.004	.004	.004	.003	.003	.002	.002	
1600.	-.041	-.024	.041	.057	.030	-.012	.040	.022	.005	.000	1.128
	.007	.005	.006	.006	.006	.005	.004	.004	.003	.003	
1687.	-.021	-.011	.042	.056	.028	.004	.036	.022	.005	.000	.938
	.006	.005	.005	.006	.005	.005	.004	.003	.003	.002	
1767.	-.017	-.004	.044	.058	.023	.007	.033	.020	.004	.000	1.088
	.004	.003	.003	.003	.003	.003	.002	.002	.002	.001	
1871.	-.017	.006	.045	.049	.026	.015	.034	.023	.009	.000	.805
	.006	.004	.005	.005	.005	.004	.004	.003	.003	.002	
1975.	-.012	-.001	.034	.035	.013	.008	.023	.014	-.003	.001	1.043
	.004	.003	.003	.003	.003	.003	.002	.002	.002	.001	
2055.	.002	.018	.041	.033	.014	.012	.029	.022	.003	.002	1.091
	.005	.005	.004	.004	.004	.004	.003	.003	.002	.002	
2267.	-.004	.013	.020	.010	-.004	-.004	.011	.003	-.010	-.007	1.109
	.005	.004	.004	.004	.003	.003	.003	.003	.002	.002	

Table III

FLAB	B 1	B 2	B 3	B 4	B 5	B 6	B 7	B 8	B 9	B10	B11	B12
0.573	0.217	0.141	0.055	0.005	-0.001	0.000	0.000	-0.000	0.000	0.000	0.000	0.000
0.614	0.208	0.134	0.060	0.005	-0.004	0.001	0.001	0.000	0.000	-0.000	0.000	-0.000
0.358	0.192	0.158	0.072	0.019	-0.004	0.004	0.004	0.002	-0.000	0.000	0.000	0.000
0.675	0.186	0.168	0.065	0.020	-0.009	0.005	0.004	0.002	-0.000	0.000	0.000	0.000
0.705	0.165	0.176	0.042	0.027	-0.015	0.006	0.004	0.004	0.000	0.000	0.000	0.000
0.725	0.143	0.173	0.021	0.030	-0.020	0.004	0.004	0.004	0.001	0.000	0.000	0.000
0.750	0.108	0.149	0.004	0.037	-0.023	0.004	0.003	0.005	0.001	0.000	0.000	0.000
0.777	0.091	0.111	-0.000	0.030	-0.020	0.003	0.005	0.005	0.000	-0.000	0.000	0.000
0.800	0.081	0.085	0.005	0.036	-0.014	0.004	0.002	0.005	-0.000	0.000	-0.000	0.000
0.822	0.071	0.057	0.012	0.029	-0.009	0.003	-0.000	0.005	0.000	0.001	0.001	0.000
0.851	0.064	0.025	0.032	0.029	-0.002	0.002	-0.001	0.006	-0.002	0.001	-0.000	0.000
0.875	0.056	0.004	0.045	0.031	-0.000	0.002	-0.002	0.004	-0.002	0.000	0.000	-0.000
0.895	0.045	-0.016	-0.063	0.030	0.003	-0.004	-0.003	0.004	-0.002	-0.000	0.000	-0.000
0.923	0.027	-0.041	0.080	0.028	-0.000	-0.012	-0.005	0.003	-0.000	-0.001	0.001	-0.000
0.954	0.001	-0.057	0.089	0.016	-0.006	-0.026	-0.009	0.001	-0.000	-0.001	0.001	-0.000
0.975	-0.014	-0.058	0.084	0.012	-0.013	-0.037	-0.009	0.000	0.001	0.000	-0.002	-0.000
1.000	-0.043	-0.052	0.081	-0.007	-0.007	-0.050	-0.009	-0.001	-0.002	-0.001	-0.002	-0.000
1.030	-0.061	-0.039	0.062	-0.018	-0.011	-0.059	-0.008	-0.004	0.001	-0.002	-0.004	-0.000
1.055	-0.074	-0.018	0.048	-0.033	-0.000	-0.068	-0.005	-0.004	-0.002	-0.001	-0.005	-0.000
1.080	-0.077	-0.006	0.030	-0.038	0.005	-0.068	-0.003	-0.003	-0.001	-0.001	-0.005	-0.000
1.113	-0.081	0.011	0.005	-0.041	0.007	-0.068	-0.003	-0.002	-0.001	-0.000	-0.003	-0.000
1.154	-0.074	0.016	-0.013	-0.043	0.011	-0.066	-0.002	-0.001	-0.001	0.000	-0.001	-0.000
1.174	-0.069	0.015	-0.016	-0.044	0.012	-0.064	-0.003	-0.001	-0.001	0.001	-0.001	-0.000
1.210	-0.063	0.005	-0.021	-0.045	0.010	-0.062	-0.002	-0.000	-0.001	-0.001	-0.001	-0.000
1.235	-0.063	-0.003	-0.020	-0.045	0.010	-0.061	-0.002	0.001	0.000	-0.001	-0.002	-0.000
1.280	-0.057	-0.012	-0.016	-0.044	0.010	-0.057	0.001	0.005	0.002	-0.002	-0.001	0.000
1.324	-0.049	-0.026	-0.008	-0.034	0.013	-0.054	0.004	0.010	0.004	0.000	-0.001	0.000
1.360	-0.046	-0.033	-0.001	-0.023	0.016	-0.050	0.009	0.015	0.005	0.001	-0.000	0.000
1.400	-0.035	-0.037	0.014	-0.004	0.027	-0.040	0.015	0.019	0.005	0.001	-0.001	-0.000
1.430	-0.037	-0.037	0.023	0.010	0.031	-0.037	0.020	0.020	0.006	0.001	-0.000	-0.000
1.473	-0.026	-0.039	0.035	0.030	0.039	-0.022	0.025	0.029	0.007	0.001	-0.001	-0.001
1.505	-0.021	-0.034	0.042	0.042	0.045	-0.013	0.031	0.032	0.009	0.003	-0.000	-0.002
1.550	-0.020	-0.029	0.044	0.053	0.043	-0.006	0.032	0.033	0.008	0.003	-0.000	-0.001
1.590	-0.017	-0.020	0.041	0.058	0.041	-0.000	0.035	0.030	0.006	0.003	0.001	-0.002
1.640	-0.007	-0.010	0.041	0.061	0.038	0.008	0.033	0.032	0.007	0.004	0.000	-0.000
1.680	-0.005	-0.006	0.041	0.061	0.037	0.012	0.036	0.033	0.007	0.004	-0.000	-0.000
1.720	-0.000	-0.000	0.038	0.060	0.033	0.013	0.032	0.032	0.006	0.003	-0.000	-0.000
1.760	-0.000	0.006	0.039	0.058	0.032	0.013	0.034	0.029	0.006	0.003	-0.000	-0.001
1.800	0.005	0.008	0.036	0.056	0.030	0.014	0.032	0.029	0.005	0.003	-0.001	-0.001
1.840	0.003	0.009	0.036	0.050	0.027	0.013	0.029	0.028	0.005	0.002	-0.000	-0.000
1.880	0.000	0.007	0.039	0.047	0.025	0.012	0.029	0.025	0.005	0.001	-0.002	-0.002
1.920	0.003	0.008	0.033	0.041	0.022	0.009	0.025	0.024	0.004	0.002	-0.001	-0.001
1.960	-0.001	0.007	0.033	0.036	0.015	0.003	0.020	0.018	0.002	0.000	-0.002	-0.002
2.030	0.003	0.004	0.029	0.026	0.014	-0.004	0.014	0.014	0.000	-0.001	-0.002	-0.001

FLAB	B 1	B 2	B 3	B 4	B 5	B 6	B 7	B 8	B 9	B10	B11	B12
2.070	0.003	0.003	0.028	0.021	0.009	-0.007	0.012	0.009	-0.002	-0.002	-0.003	-0.001
2.150	0.006	-0.002	0.023	0.010	0.008	-0.015	0.003	0.002	-0.004	-0.004	-0.003	-0.001
2.200	0.005	-0.004	0.022	0.006	0.008	-0.017	0.001	-0.001	-0.006	-0.006	-0.003	-0.002
2.280	-0.001	-0.007	0.020	-0.001	0.007	-0.017	-0.000	-0.008	-0.007	-0.007	-0.002	-0.002
2.340	-0.005	-0.008	0.020	0.001	0.009	-0.017	-0.002	-0.008	-0.008	-0.007	-0.003	-0.002
2.460	-0.007	-0.010	0.018	0.000	0.016	-0.011	0.003	-0.010	-0.003	-0.005	-0.001	-0.001
2.560	-0.007	-0.003	0.012	0.007	0.015	-0.000	0.003	-0.003	-0.002	-0.001	0.000	0.000
2.750	0.001	0.005	0.012	0.007	0.019	0.008	0.011	0.004	0.005	0.004	0.005	0.004
3.000	0.001	0.010	0.011	0.011	0.016	0.014	0.013	0.009	0.009	0.007	0.006	0.005
3.400	0.006	0.009	0.010	0.011	0.010	0.010	0.009	0.006	0.007	0.005	0.003	0.003
3.650	0.008	0.009	0.010	0.011	0.011	0.011	0.010	0.009	0.009	0.007	0.006	0.005
4.000	0.004	0.008	0.008	0.009	0.010	0.009	0.009	0.006	0.007	0.005	0.006	0.004
5.000	0.003	0.005	0.005	0.007	0.007	0.007	0.007	0.007	0.006	0.005	0.004	0.004
6.000	0.001	0.003	0.003	0.005	0.005	0.005	0.005	0.005	0.004	0.004	0.004	0.004
10.000	0.004	0.002	0.002	0.004	0.005	0.004	0.003	0.003	0.004	0.002	0.001	0.001

Table IV

Table V: see page 9.

k (GeV/c)	$d\sigma/d\Omega$ (mb/sr)		B (mb)		$P \cdot (d\sigma/d\Omega) / \sin\theta$ (mb)	
	0°	180°	0°	180°	0°	180°
.020	.307	.347	-.0	-.0	-.000	-.000
.040	.256	.411	-.1	-.1	-.000	-.000
.060	.184	.528	-.1	-.2	-.001	-.001
.080	.115	.770	-.2	-.5	-.002	-.002
.100	.044	1.020	-.2	-.8	.001	.002
.110	.019	1.179	-.2	-1.0	.005	.006
.120	.003	1.376	-.2	-1.3	.013	.014
.140	.026	1.903	-.1	-2.0	.043	.043
.160	.148	2.612	.2	-2.9	.105	.095
.180	.432	3.431	.7	-4.1	.219	.165
.200	.995	4.397	1.4	-5.7	.440	.236
.218	1.934	5.673	2.7	-7.7	.791	.353
.247	4.293	8.129	5.9	-11.3	1.903	.624
.267	6.200	8.571	8.7	-12.1	2.587	.612
.280	7.011	8.095	10.0	-11.7	2.782	.494
.290	7.239	7.586	10.4	-11.1	2.848	.494
.295	7.445	7.181	10.8	-10.6	3.041	.436
.301	7.575	6.678	11.1	-10.0	3.217	.319
.305	7.601	6.328	11.2	-9.5	3.251	.223
.310	7.675	5.859	11.5	-8.9	3.359	.043
.320	7.513	5.041	11.4	-7.8	3.310	-.125
.331	7.114	4.341	11.0	-6.7	3.010	-.045
.351	6.848	2.996	11.1	-4.7	3.065	-.196
.378	6.116	1.930	10.5	-3.2	2.806	-.387
.408	5.591	1.303	10.4	-2.4	2.724	-.582
.427	5.470	.925	10.9	-1.5	2.995	-.679
.456	5.107	.409	10.3	-.4	2.987	-.441
.490	4.671	.149	9.3	.1	3.055	-.366
.532	4.197	.002	8.3	.5	3.133	-.042
.573	4.025	.060	9.4	.1	2.722	.174
.614	4.043	.232	15.1	-1.3	2.512	.168
.658	4.375	.457	19.9	-2.8	3.295	-.371
.675	4.044	.515	18.0	-2.4	3.137	-.727
.705	3.833	.582	17.2	-1.5	2.750	-1.488
.725	3.264	.510	16.4	.1	2.278	-1.810
.750	2.627	.410	14.1	3.0	1.839	-2.171
.777	1.941	.252	12.9	3.8	1.452	-1.616
.800	1.696	.180	11.9	7.0	1.398	-1.564
.822	1.546	.130	15.0	6.2	1.350	-1.118
.851	1.633	.115	14.1	7.6	1.203	-.880
.875	1.898	.112	15.7	9.5	1.068	-.501
.895	2.205	.120	18.3	10.8	.863	.046
.923	2.800	.141	25.2	12.5	.486	.662
.954	3.291	.184	30.7	14.7	-.397	1.108
.975	3.460	.239	35.0	12.6	-1.146	1.011
1.000	3.496	.321	30.2	14.5	-1.886	1.513
1.030	2.920	.453	27.9	10.7	-2.547	1.722
1.055	2.353	.560	21.2	8.9	-2.773	1.960
1.080	1.720	.607	14.4	3.9	-2.565	1.934
1.113	1.118	.718	9.0	-1.0	-2.372	1.789
1.154	.636	.749	3.2	-4.0	-1.972	1.722
1.174	.519	.734	2.0	-6.0	-1.907	1.584
1.210	.355	.774	-1.1	-6.3	-1.933	1.574
1.235	.275	.812	-3.0	-7.4	-1.841	1.473
1.280	.137	.862	-6.1	-9.8	-1.371	1.440

Table VI (B = $(d/d\cos \theta) d\sigma/d\Omega$)

k (GeV/c)	$d\sigma/d\Omega$ (mb/sr)		B (mb)		$P \cdot (d\sigma/d\Omega) / \sin\theta$ (mb)	
	0°	180°	0°	180°	0°	180°
1.324	.059	.894	-7.1	-10.0	-.741	1.247
1.360	.041	.850	-6.7	-10.4	-.084	1.151
1.400	.066	.806	-6.3	-9.1	.582	1.051
1.450	.104	.710	-5.5	-8.0	1.055	1.093
1.473	.200	.637	-5.0	-6.6	1.636	.691
1.505	.297	.554	-5.0	-6.6	2.428	.692
1.550	.353	.434	-3.2	-4.5	2.586	.415
1.590	.371	.327	-3.3	-3.4	2.583	.341
1.640	.510	.222	.7	-1.8	2.310	.001
1.680	.576	.162	1.6	-1.1	2.764	-.049
1.720	.597	.125	2.3	-.4	2.578	-.182
1.760	.631	.102	2.8	-.2	2.439	-.082
1.800	.633	.090	2.1	.3	2.239	-.161
1.840	.693	.080	3.9	.6	2.094	-.170
1.880	.665	.073	2.6	.7	1.792	-.070
1.920	.679	.064	4.0	1.0	1.597	-.135
1.980	.587	.048	1.9	1.5	1.002	-.104
2.030	.579	.036	3.5	1.6	.661	-.020
2.070	.512	.033	2.3	2.0	.281	.016
2.150	.415	.032	1.1	1.8	-.187	.161
2.200	.345	.037	-.1	1.5	-.498	.229
2.280	.263	.053	-3.0	1.3	-.672	.321
2.340	.199	.066	-5.4	.6	-.733	.291
2.460	.143	.084	-9.8	.5	-.342	.432
2.560	.152	.080	-12.0	-1.5	.019	.114
2.750	.224	.066	-11.8	-1.5	.680	.153
3.000	.296	.041	-11.1	-1.4	1.005	.010
3.400	.285	.025	-9.9	-.4	.644	-.005
3.650	.304	.022	-8.9	-.4	.781	-.060
4.000	.287	.018	-11.2	-1.2	.781	.106
5.000	.308	.014	-13.5	-1.5	.384	.018
6.000	.280	.009	-20.0	-.4	.490	-.075
10.000	.305	.002	-32.4	.3	.541	.058

Table VI (continued)

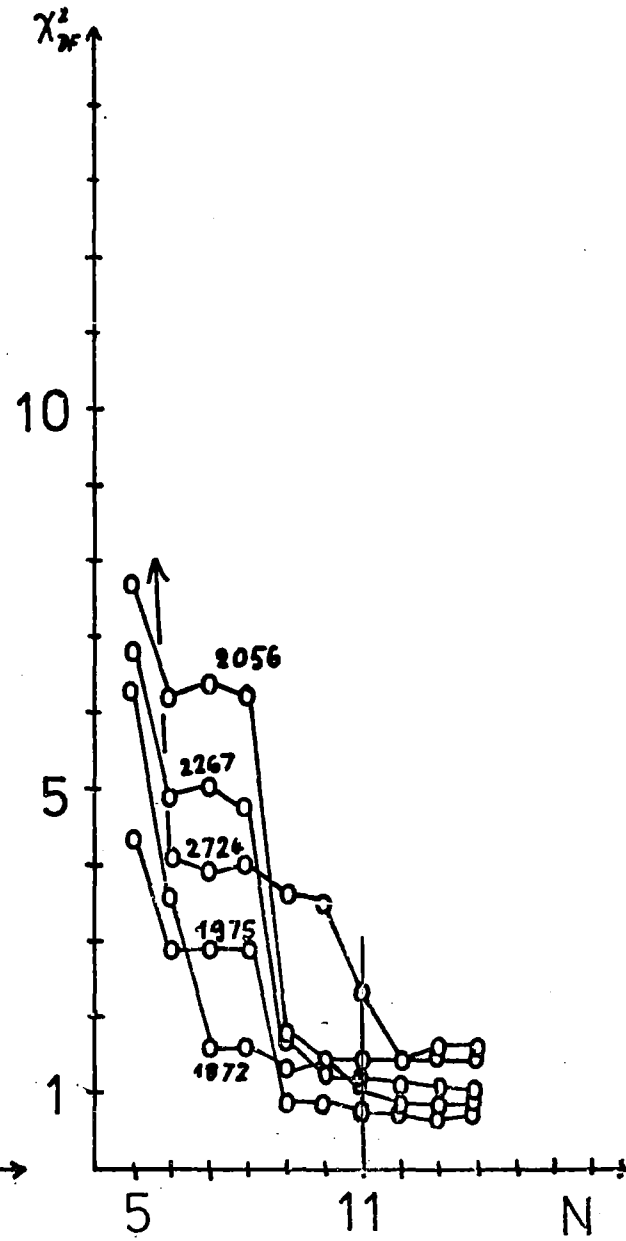
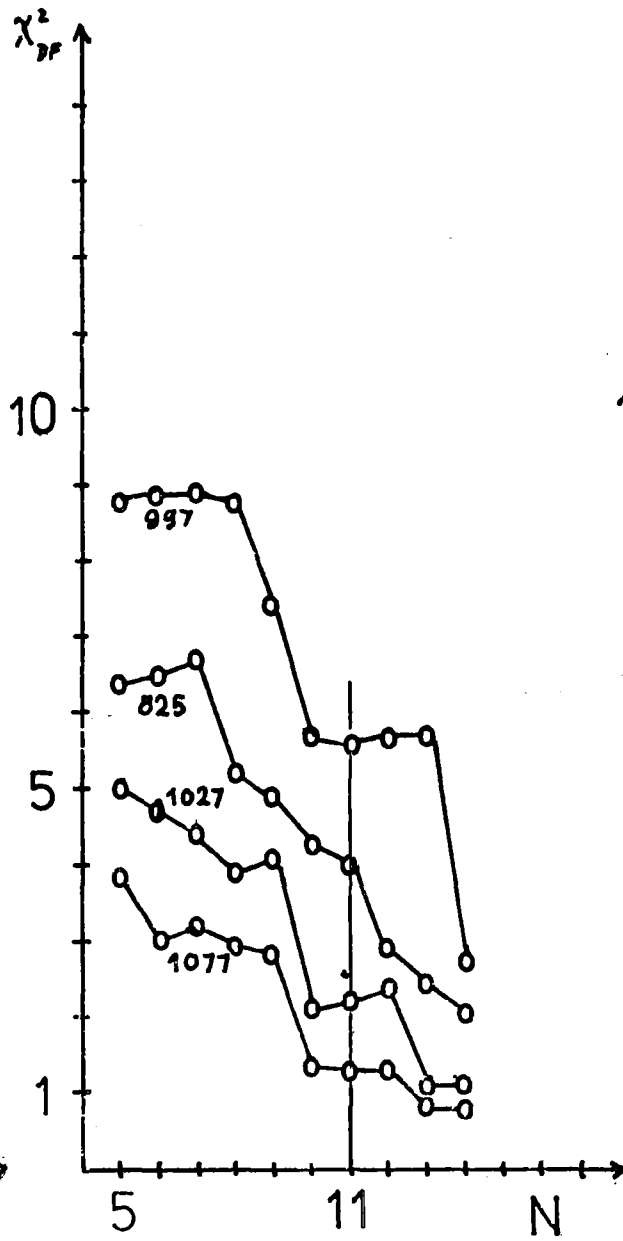
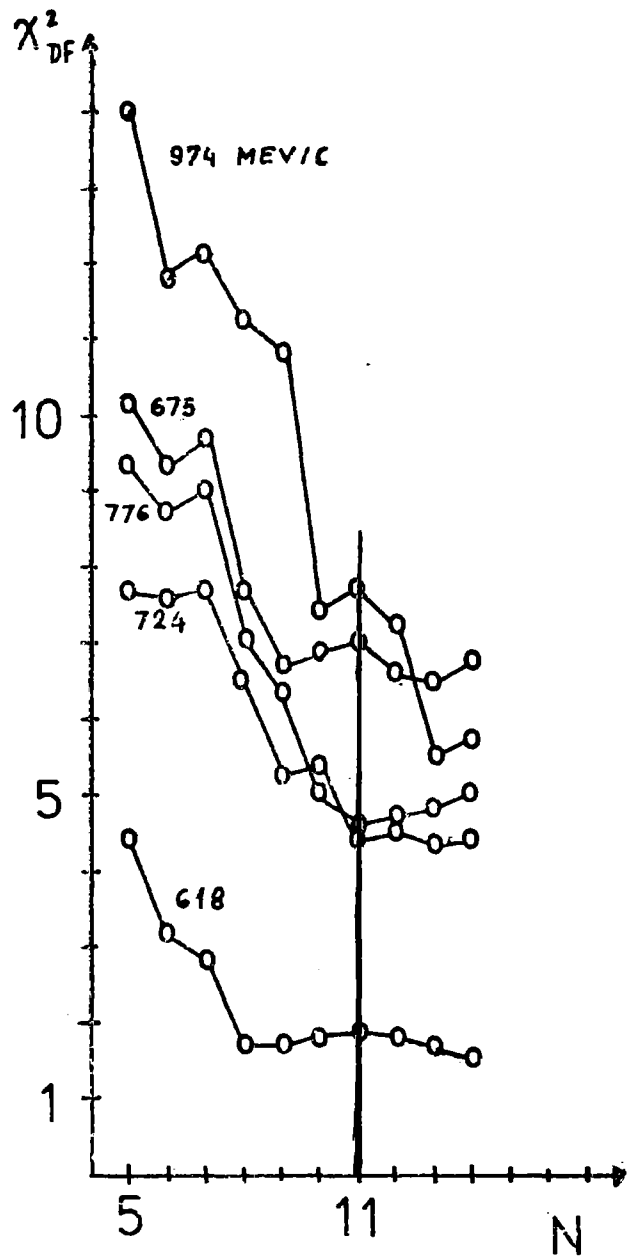


Fig. 1

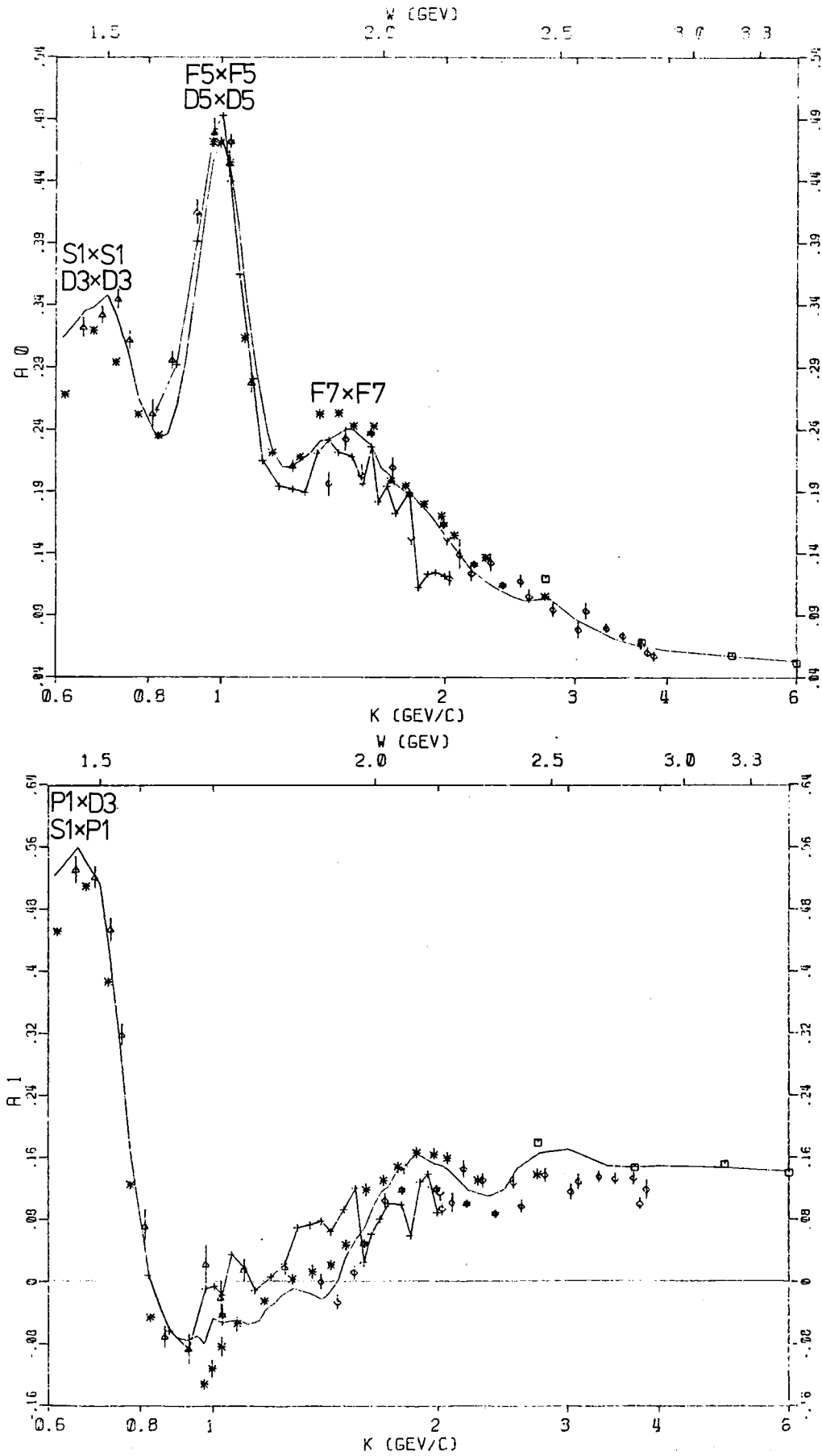


Fig. 2 A_0, A_1

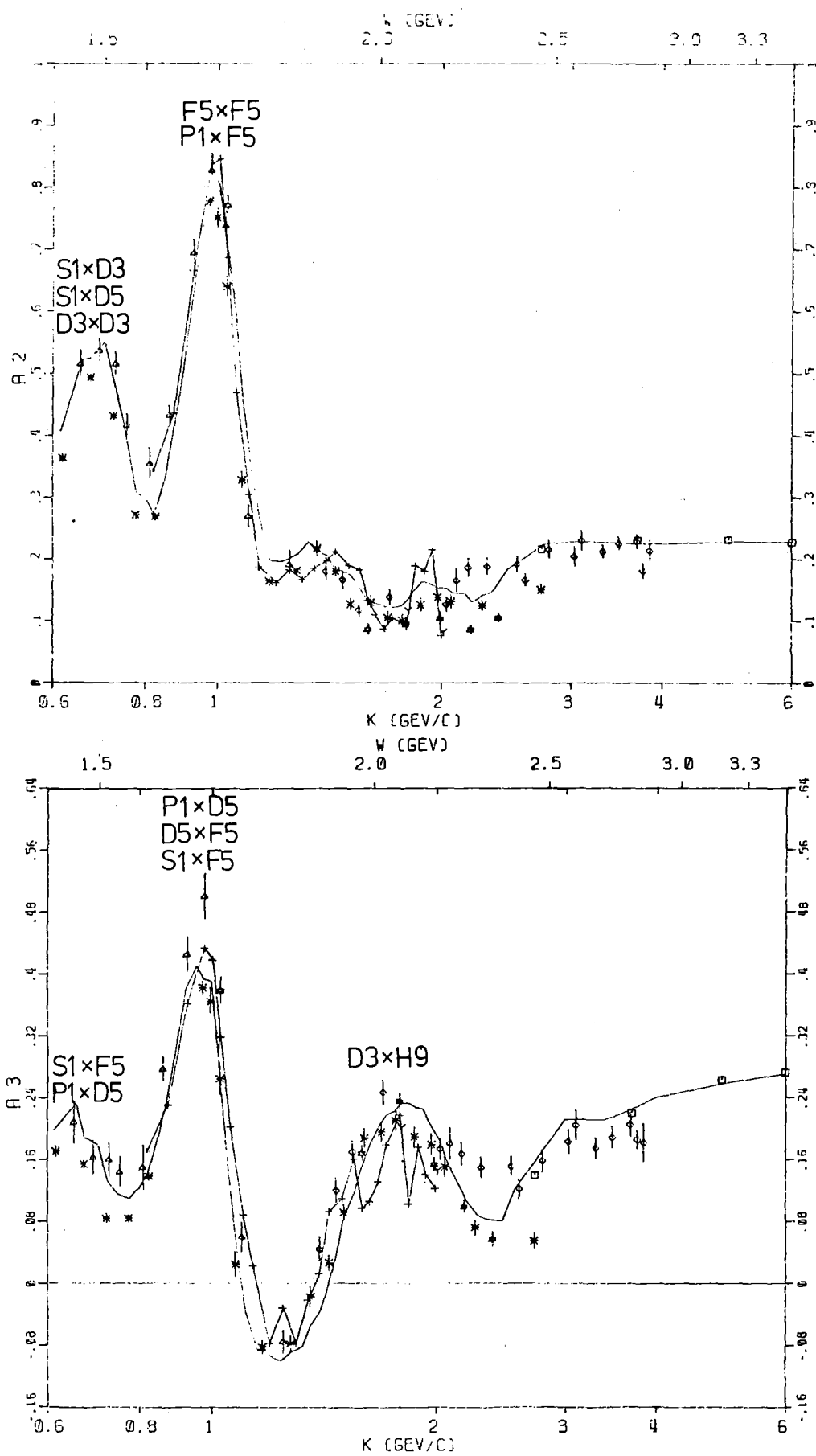


Fig. 2 A_2 , A_3

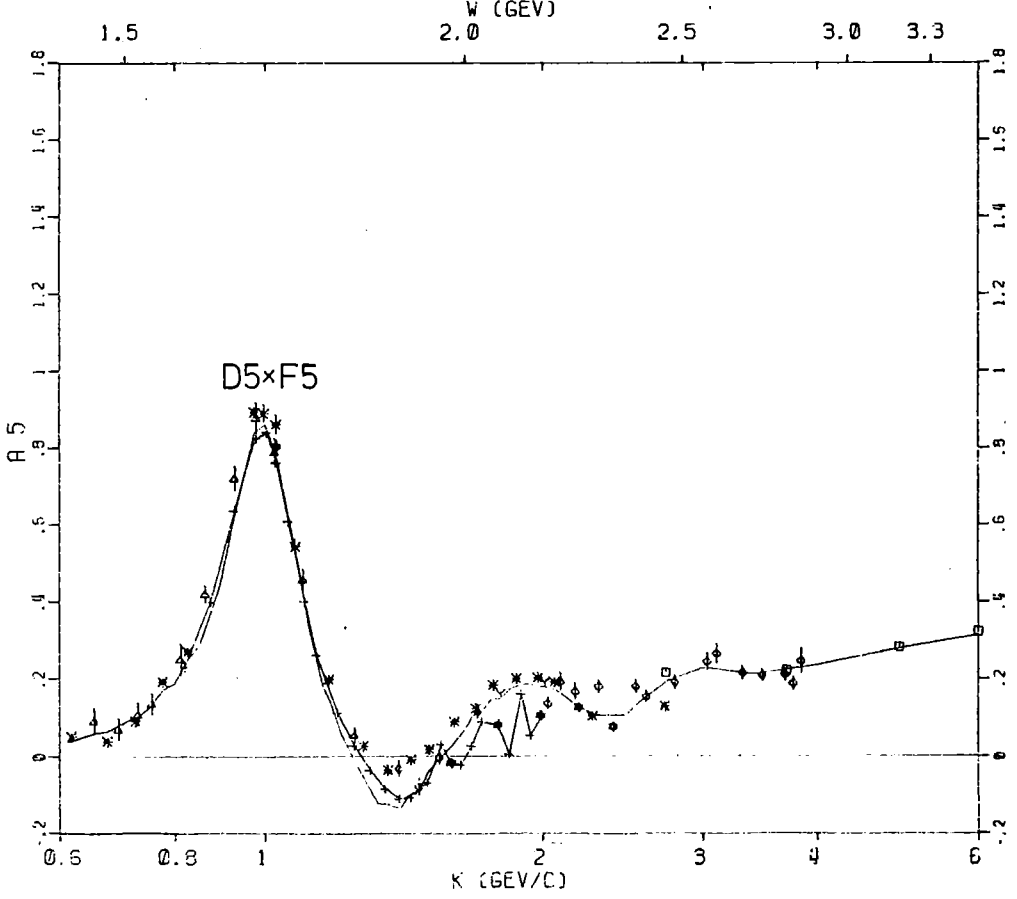
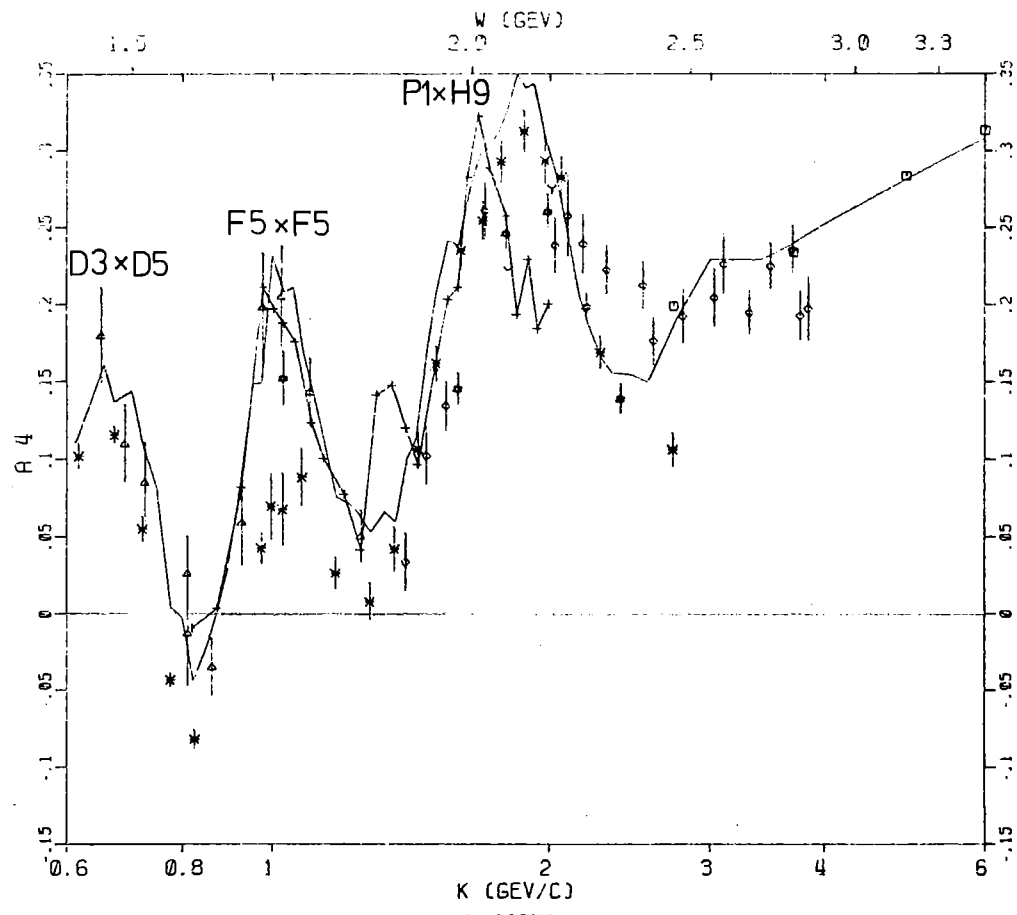


Fig. 2 A_4, A_5

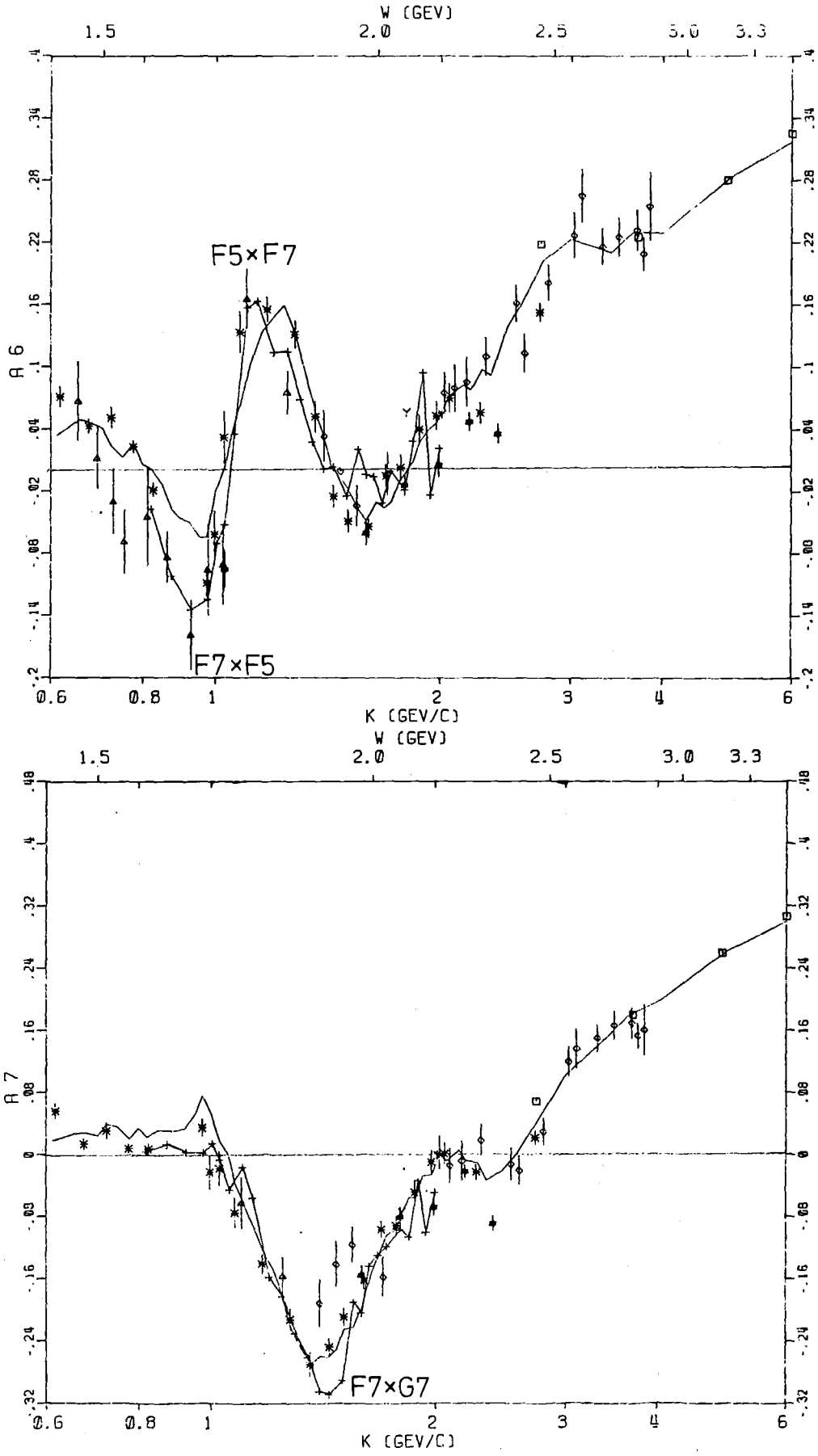


Fig. 2 A_6, A_7

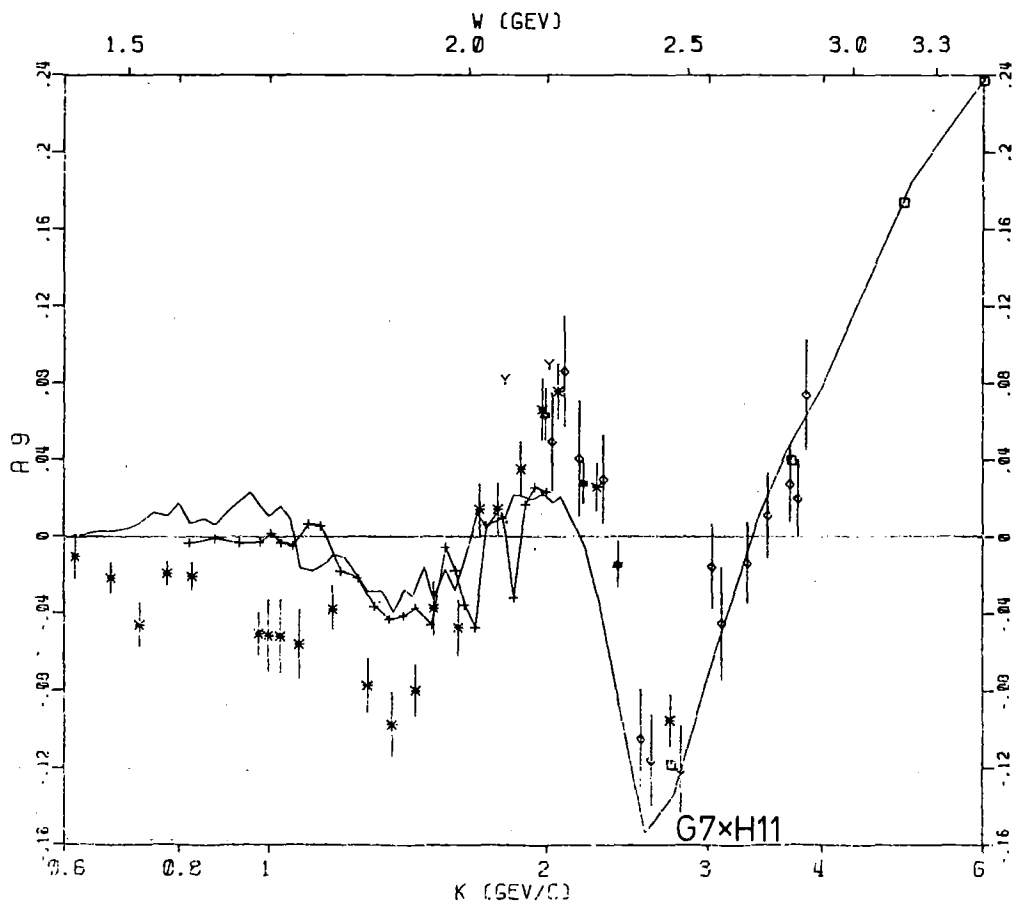
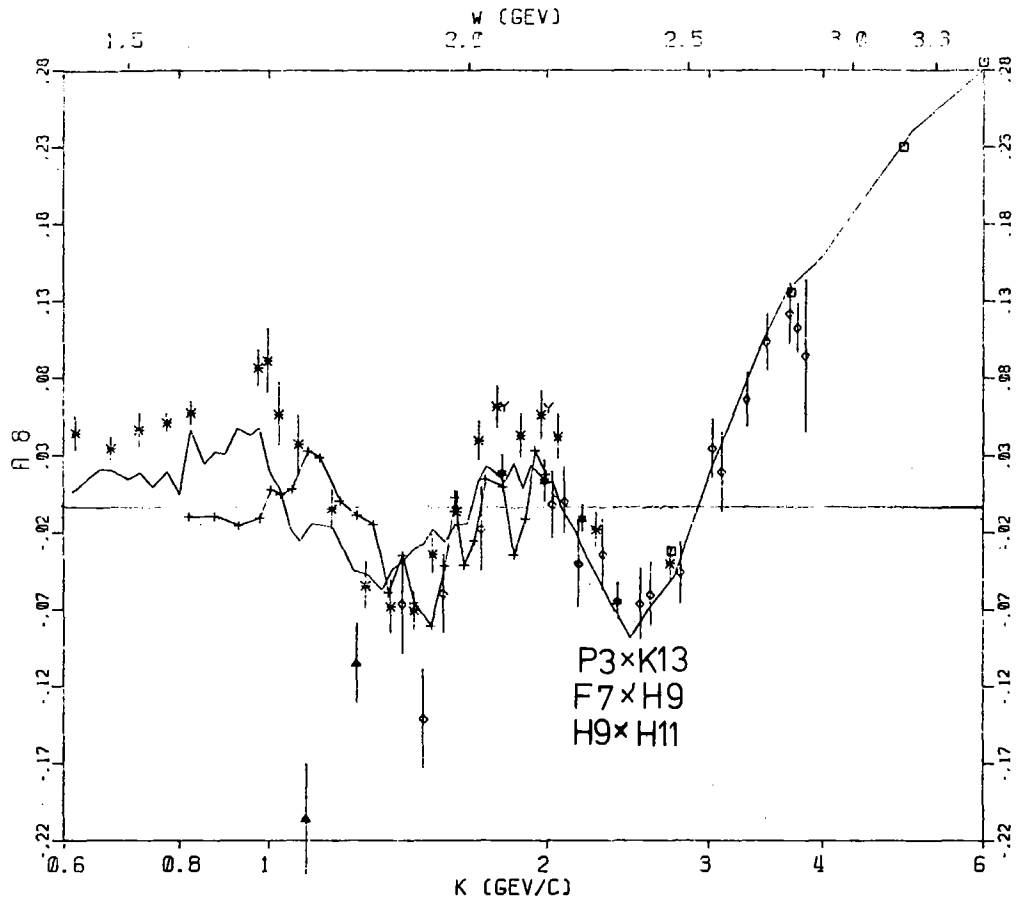


Fig. 2 A_8, A_9

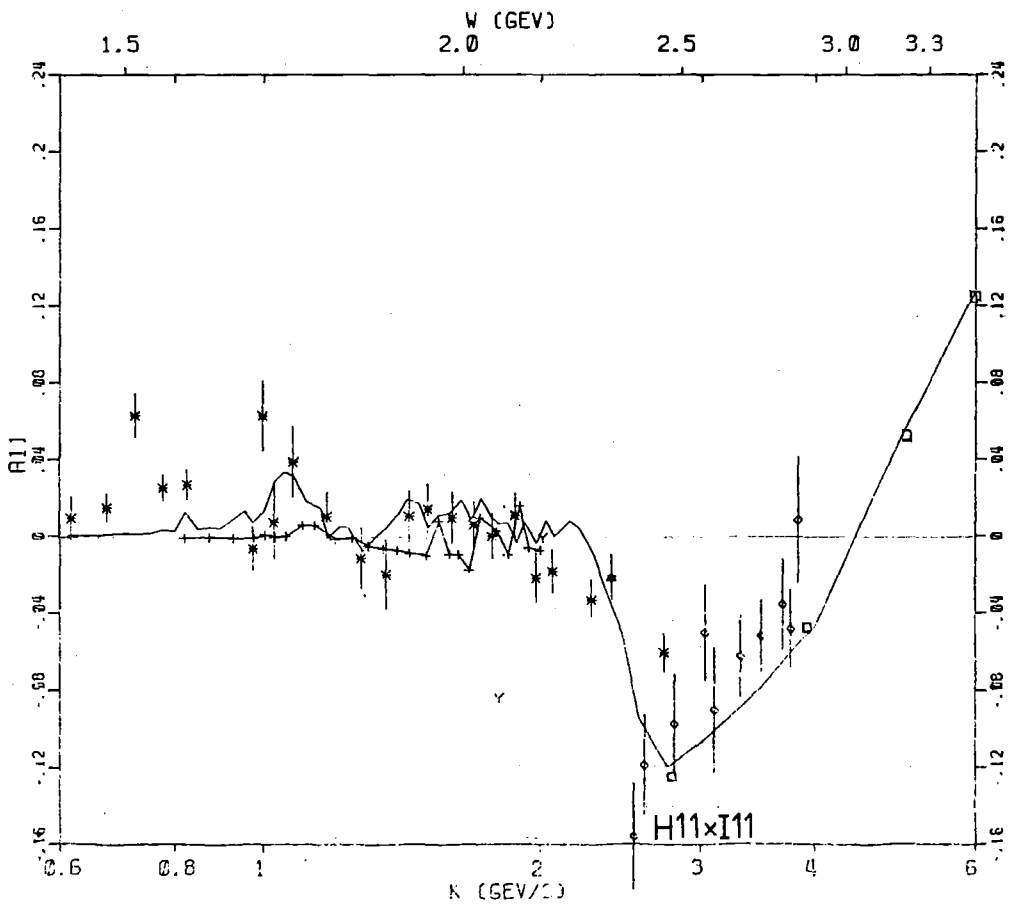
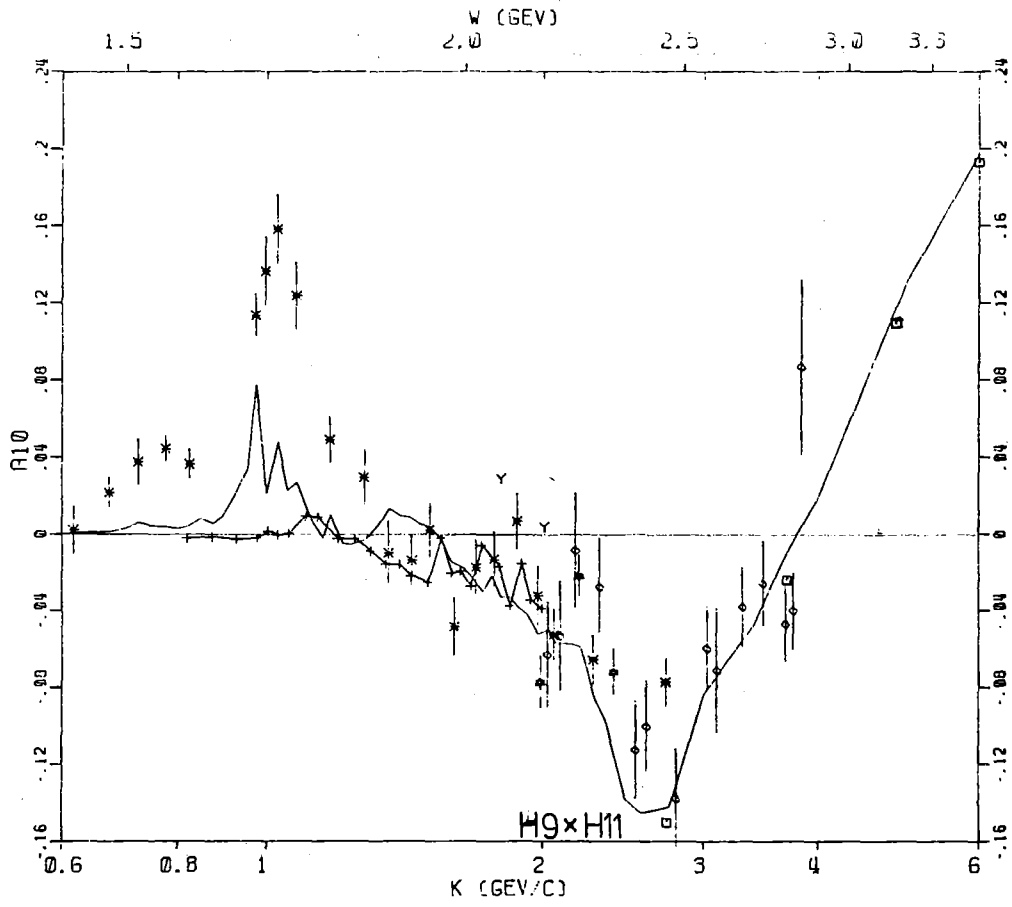


Fig. 2 A_{10}, A_{11}

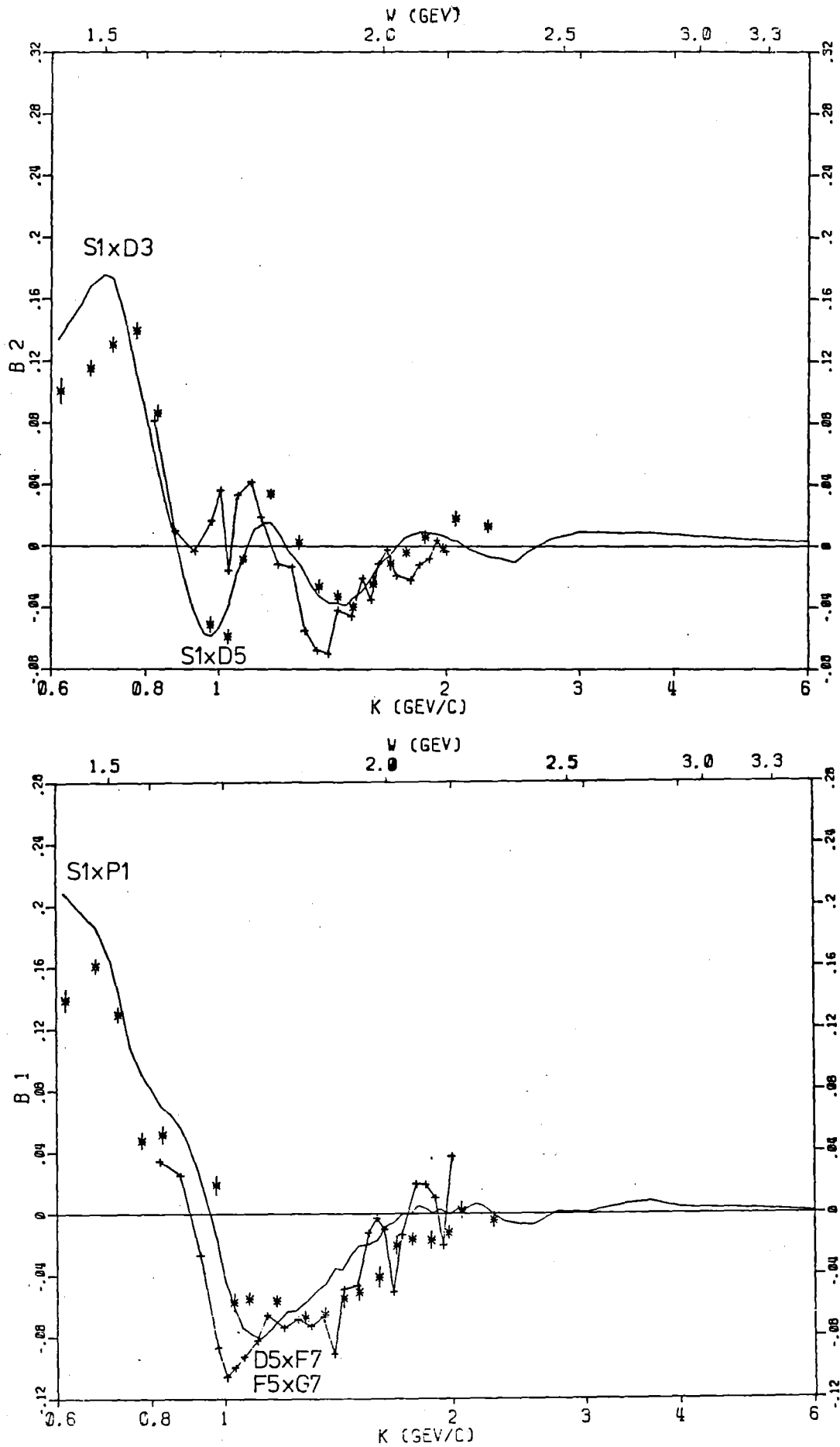


Fig. 3 B_1, B_2

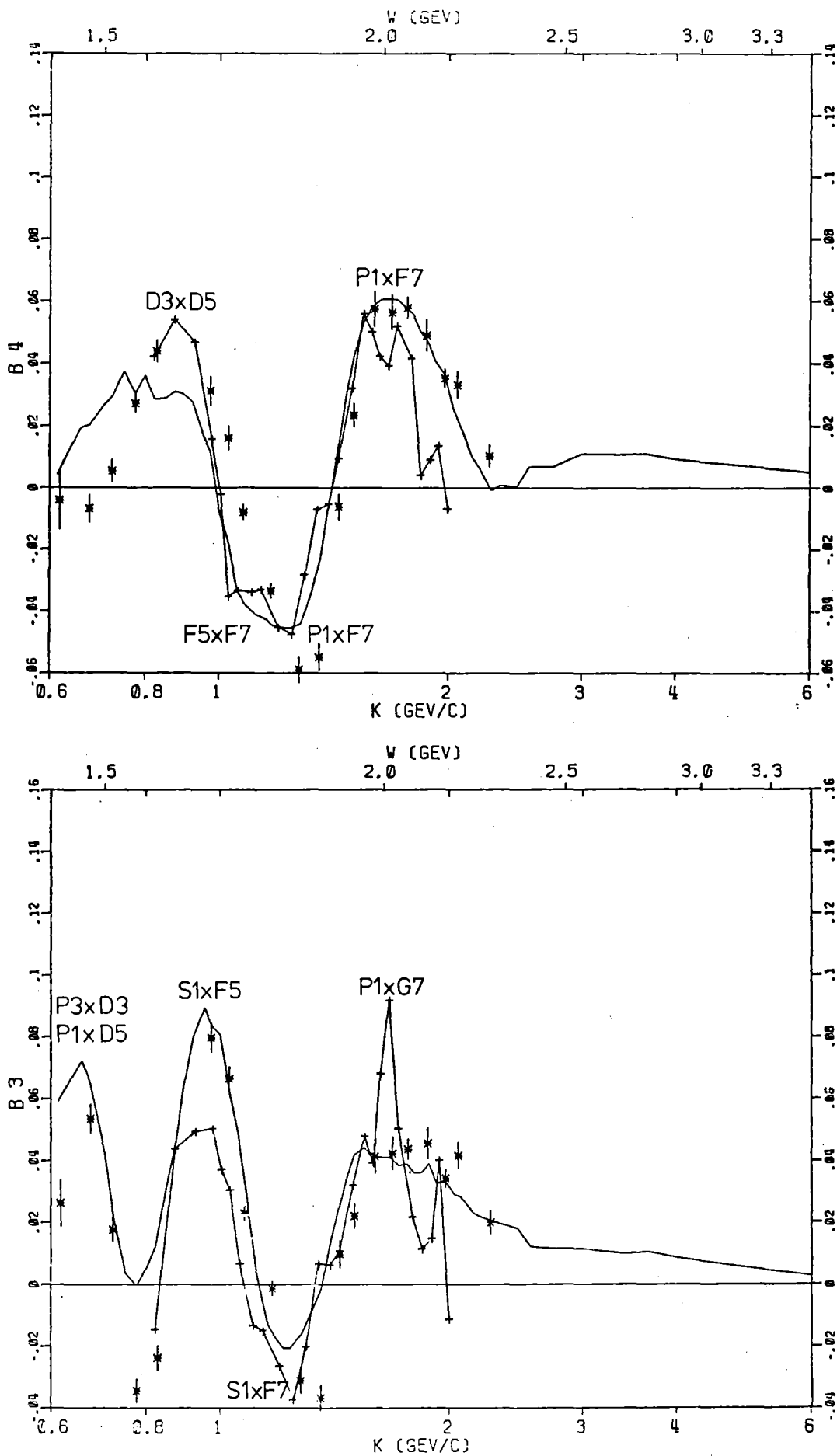


Fig. 3 B_3, B_4

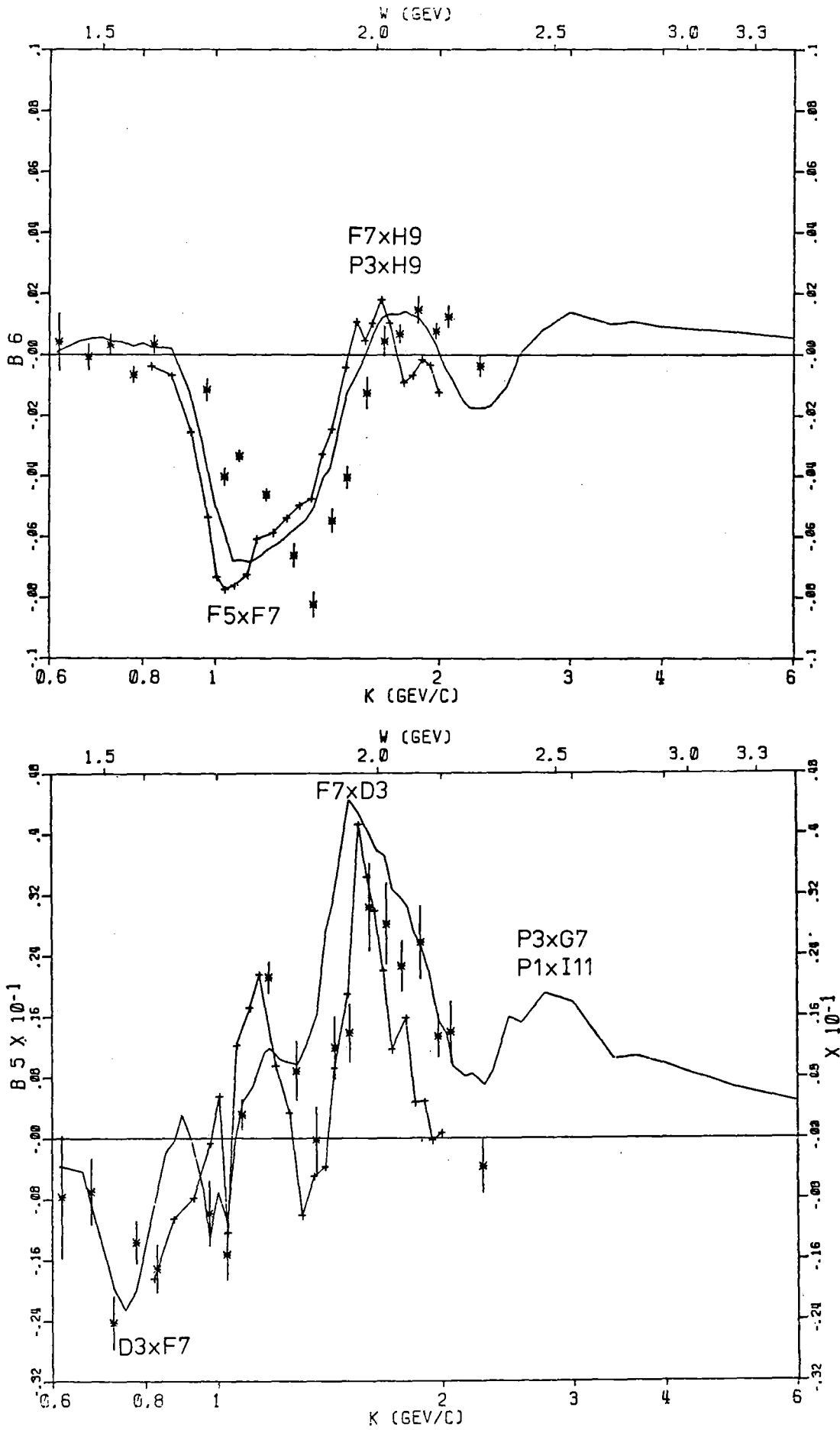


Fig. 3 B_5, B_6

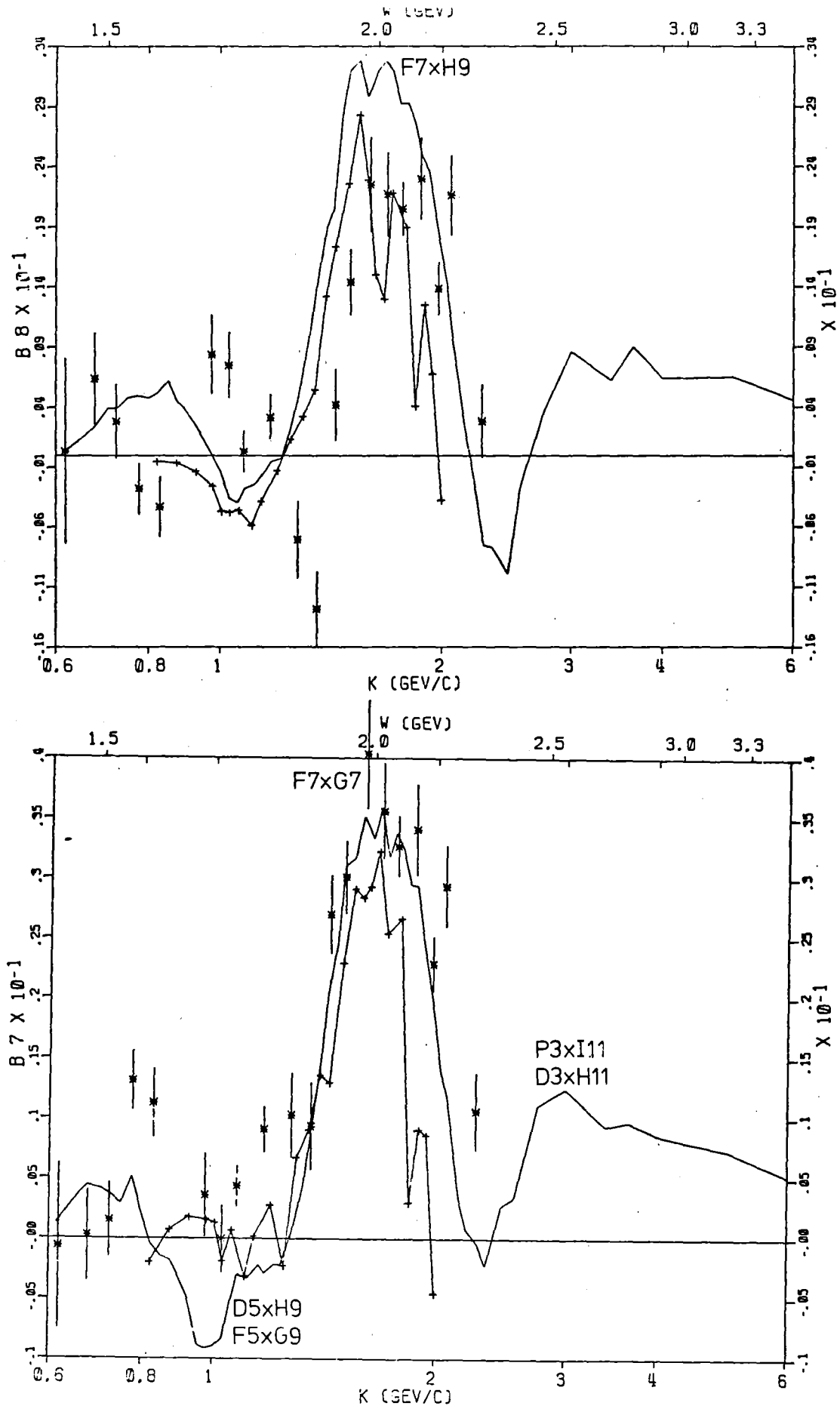


Fig. 3 B_7, B_8

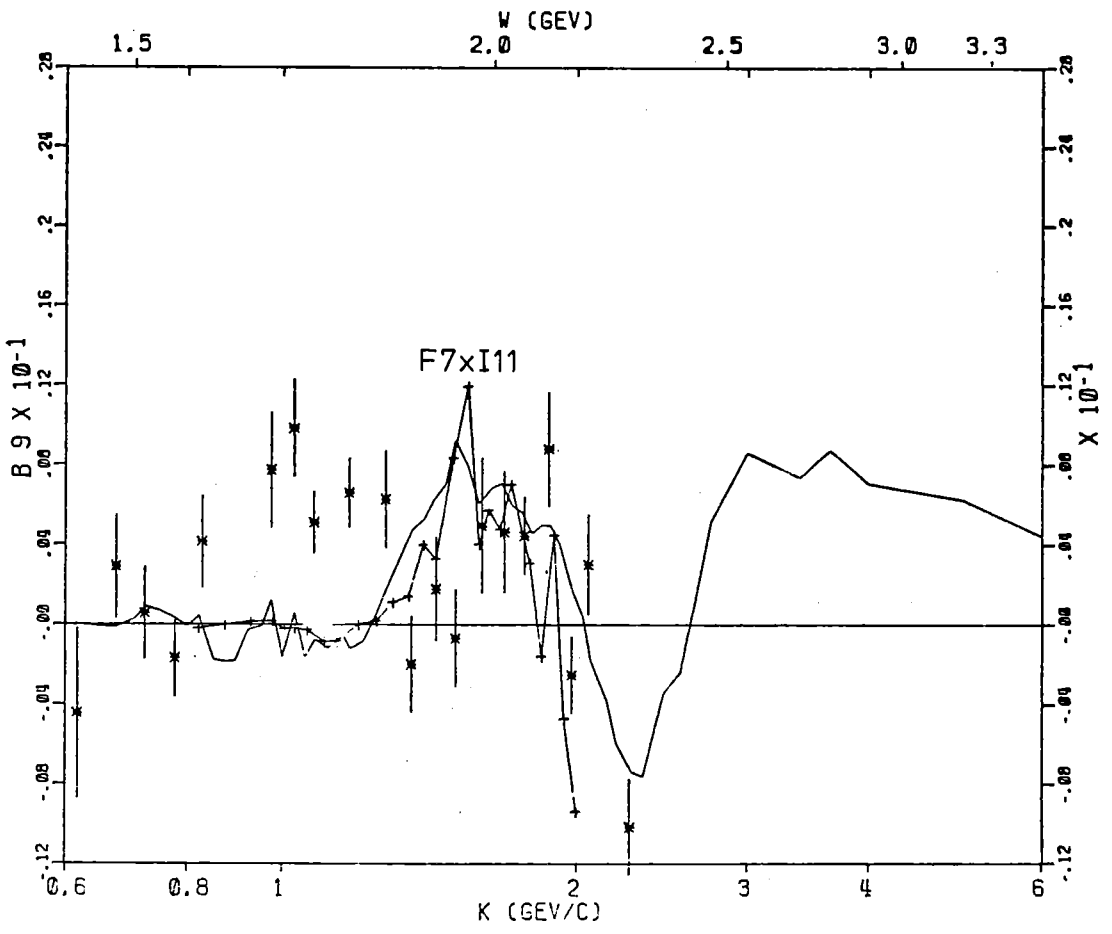
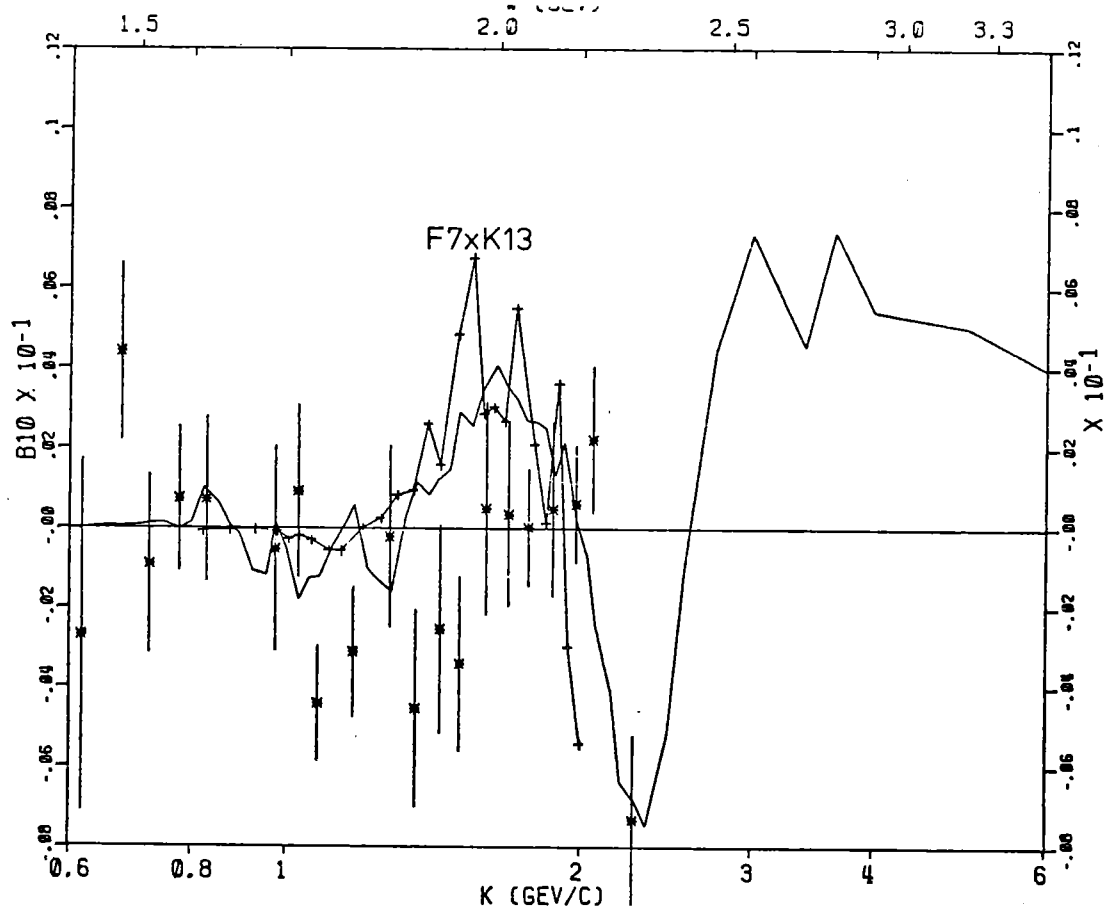


Fig. 3 B_9, B_{10}

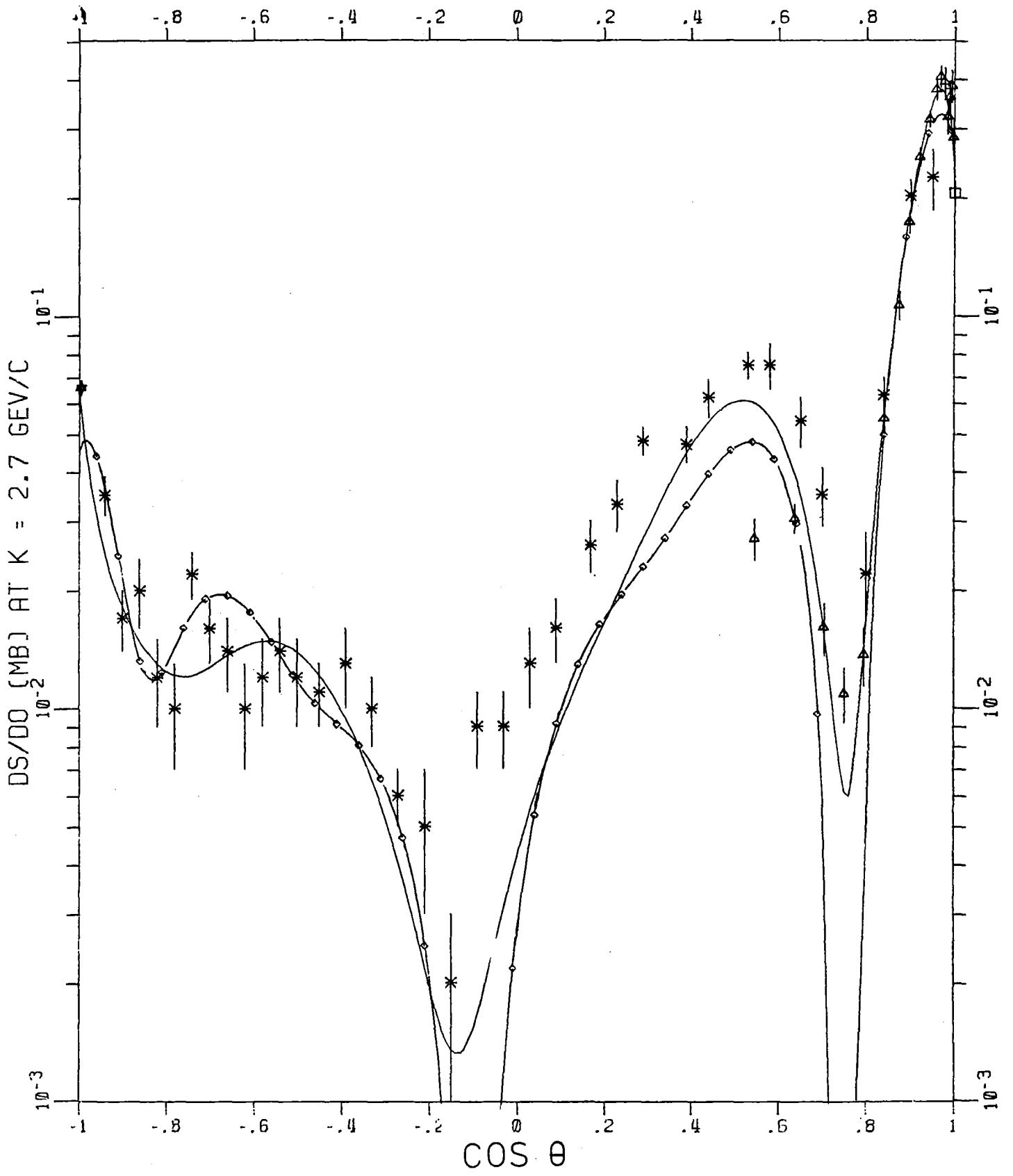


Fig. 4

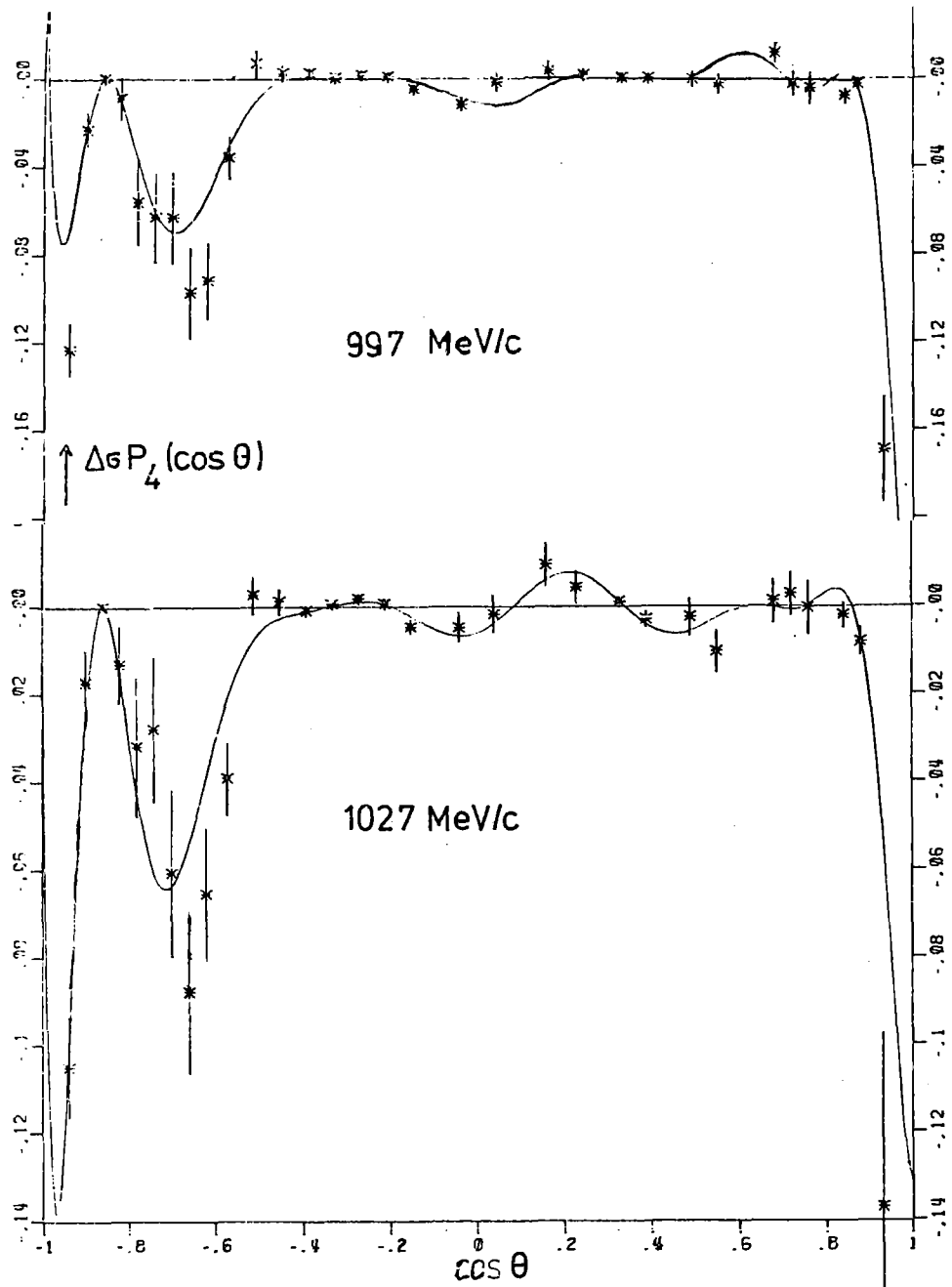


FIG 5a

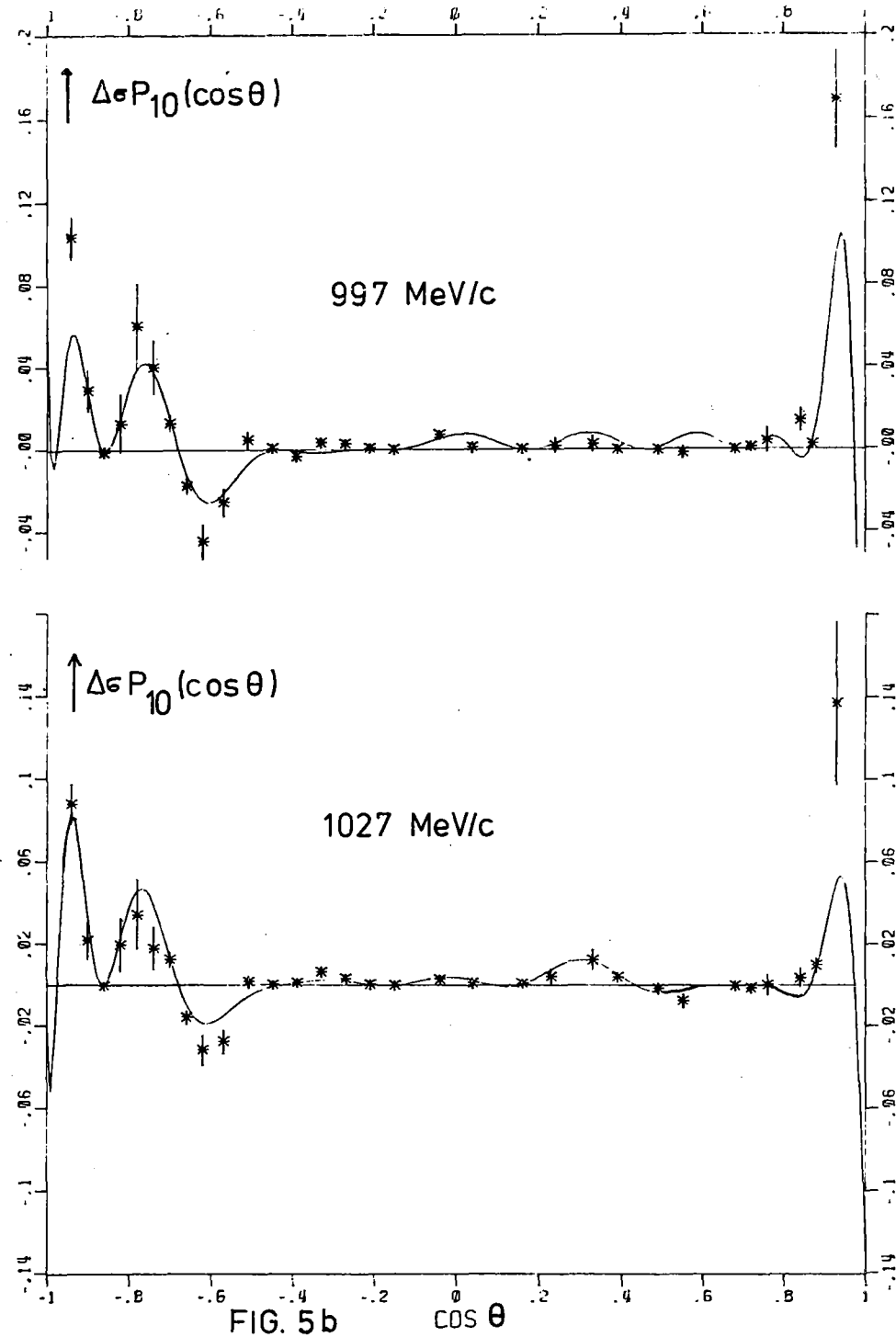


FIG. 5b

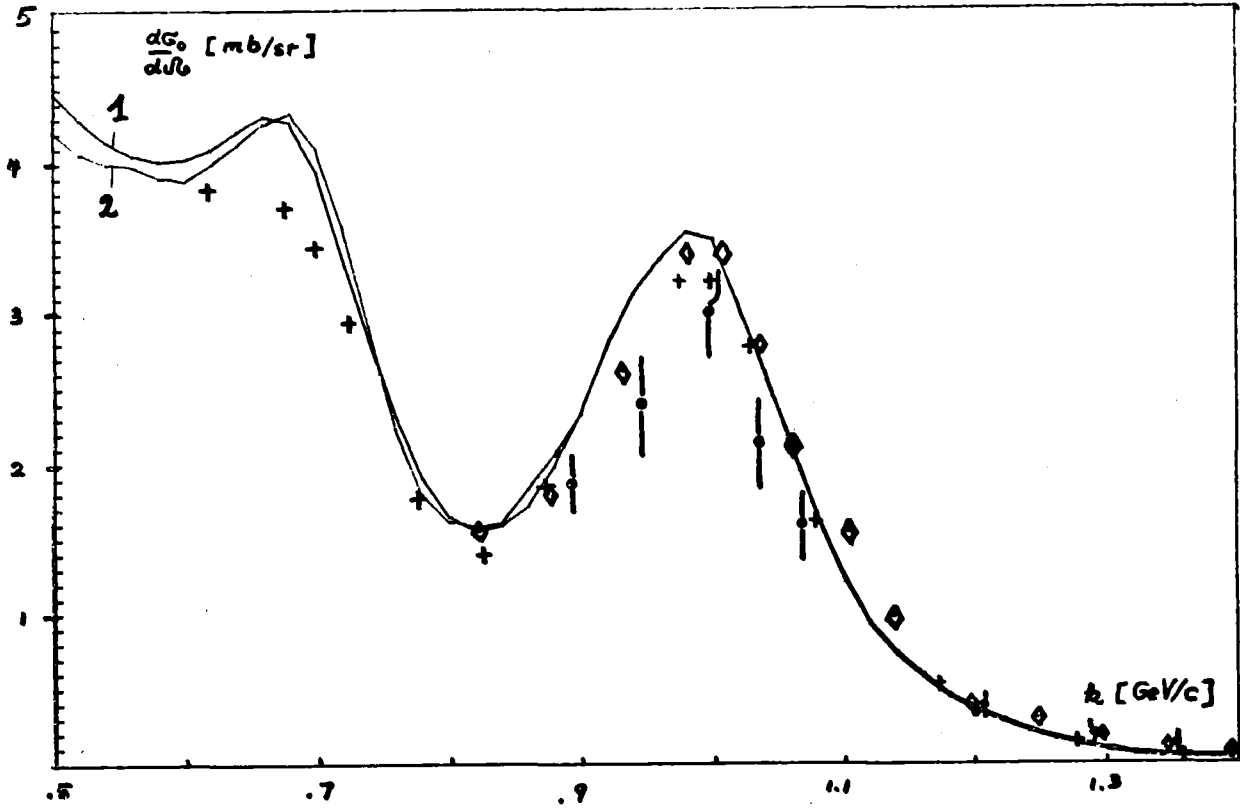


Fig. 6a

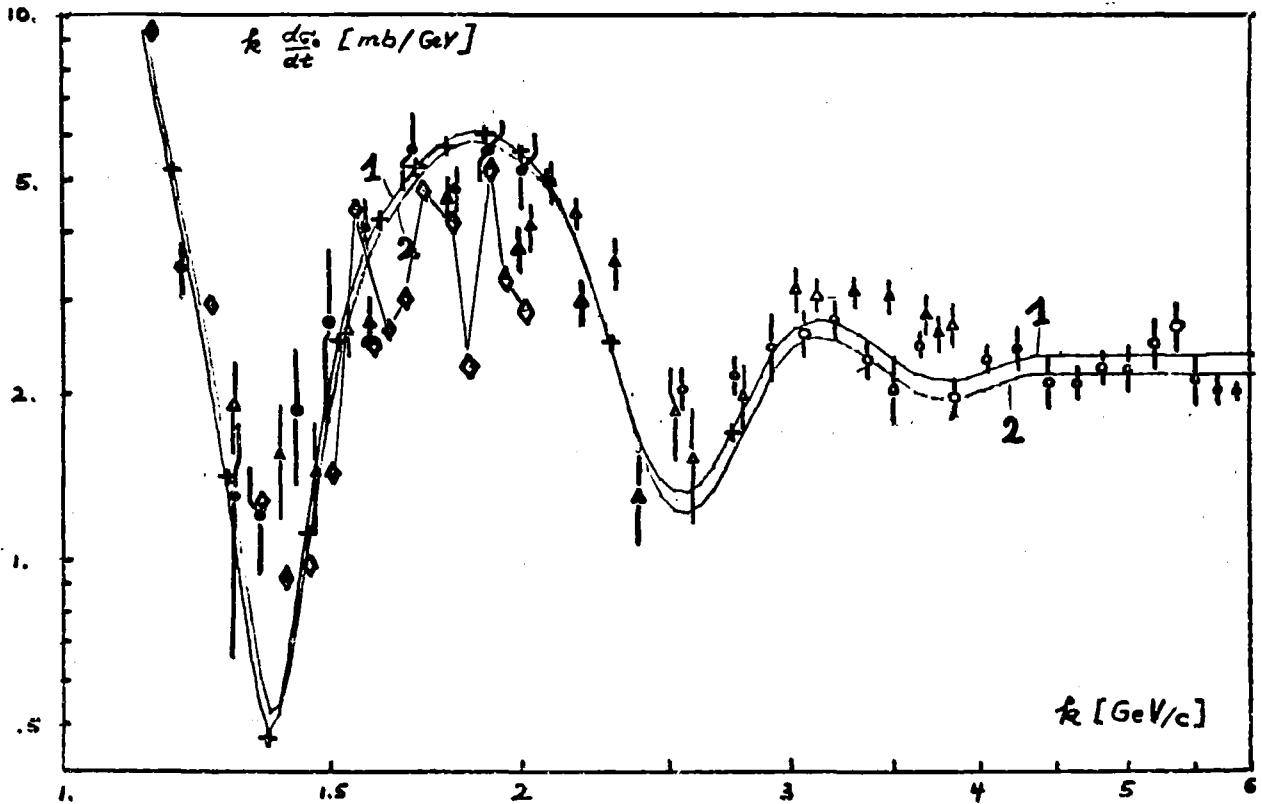


Fig. 6b

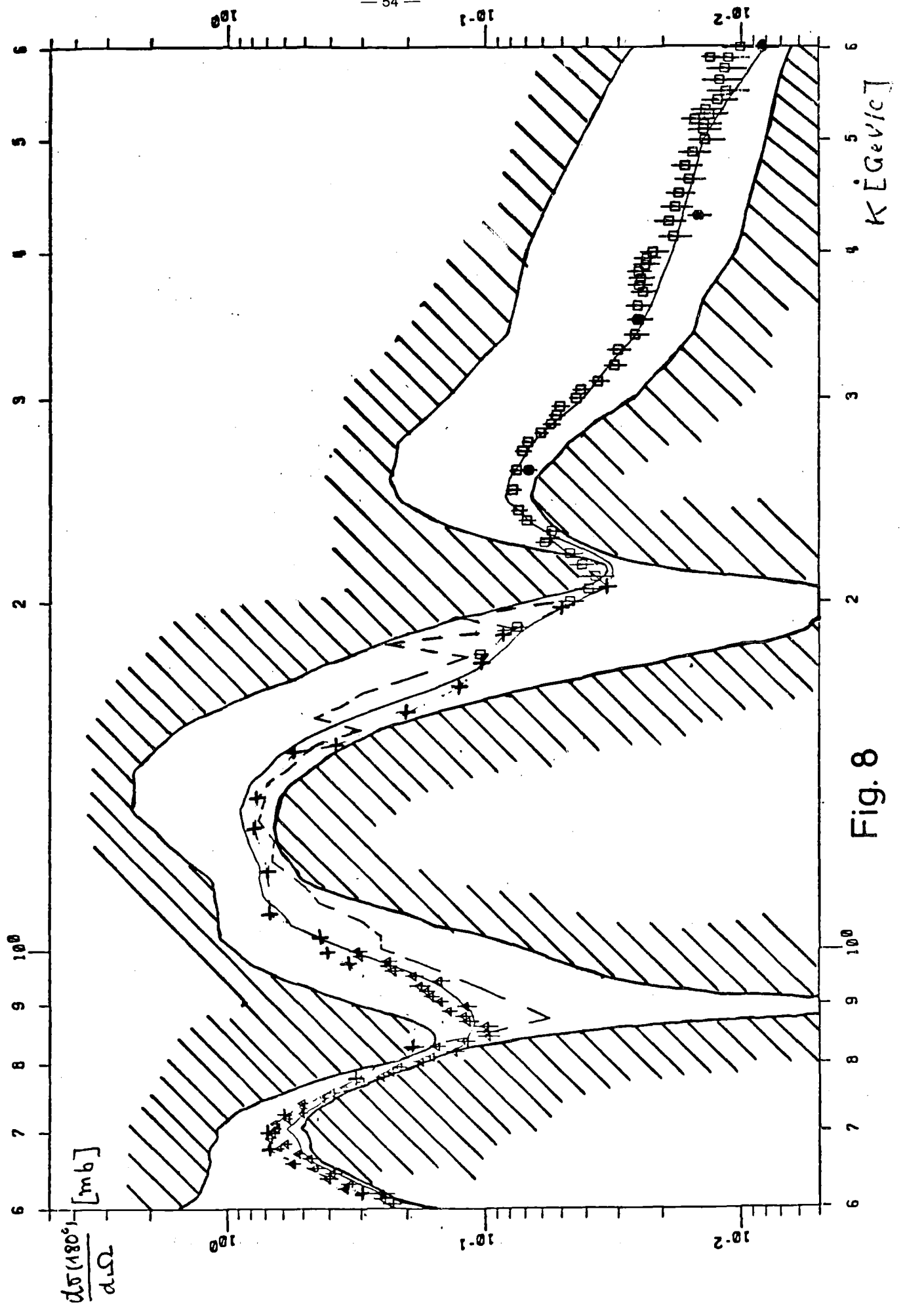


Fig. 8

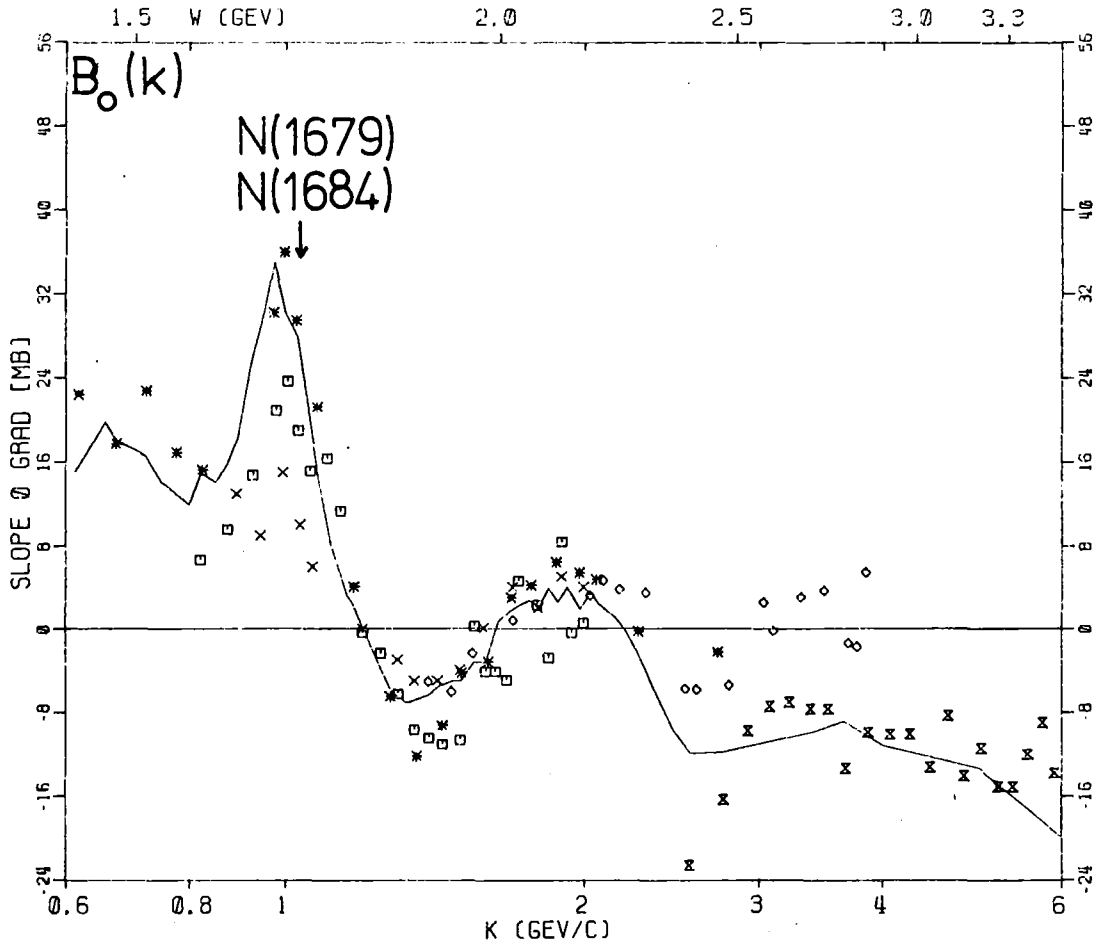


Fig. 7 $B = (d/d\cos\theta) d\sigma/d\Omega$

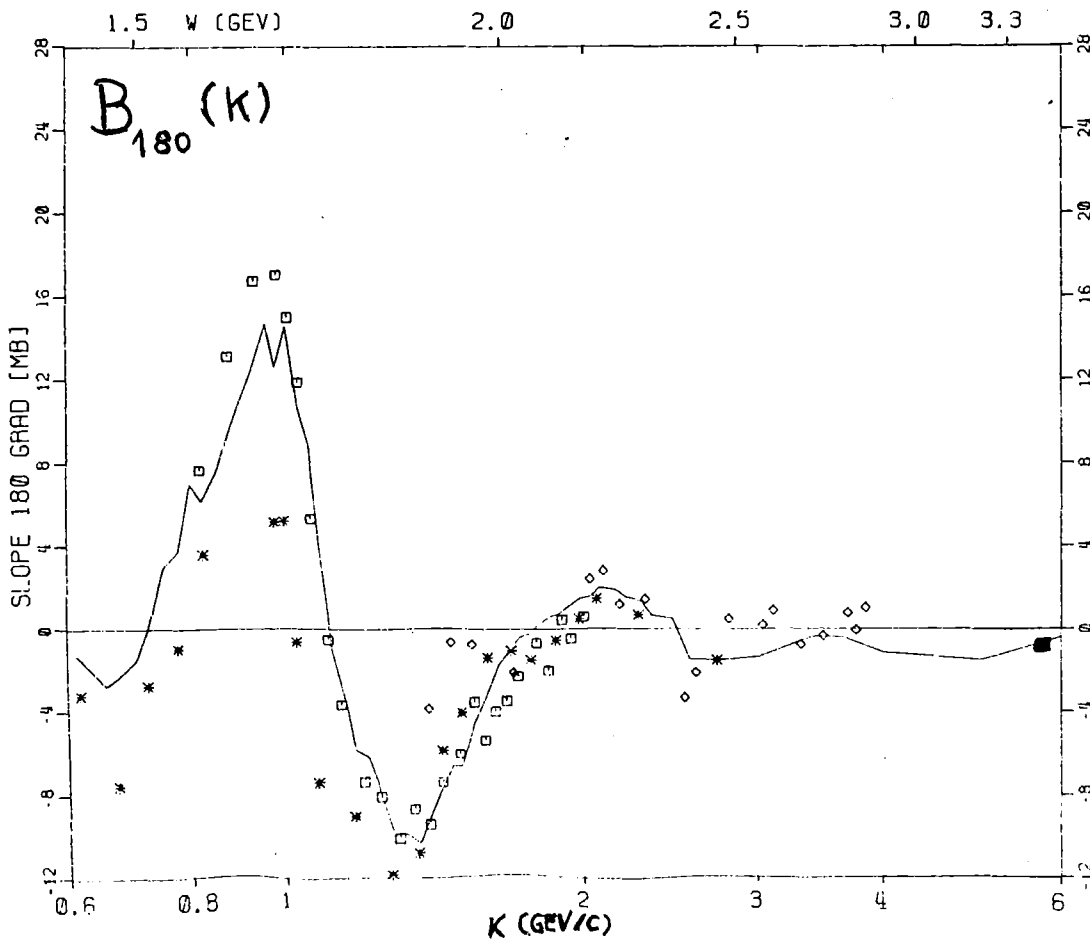


Fig. 9

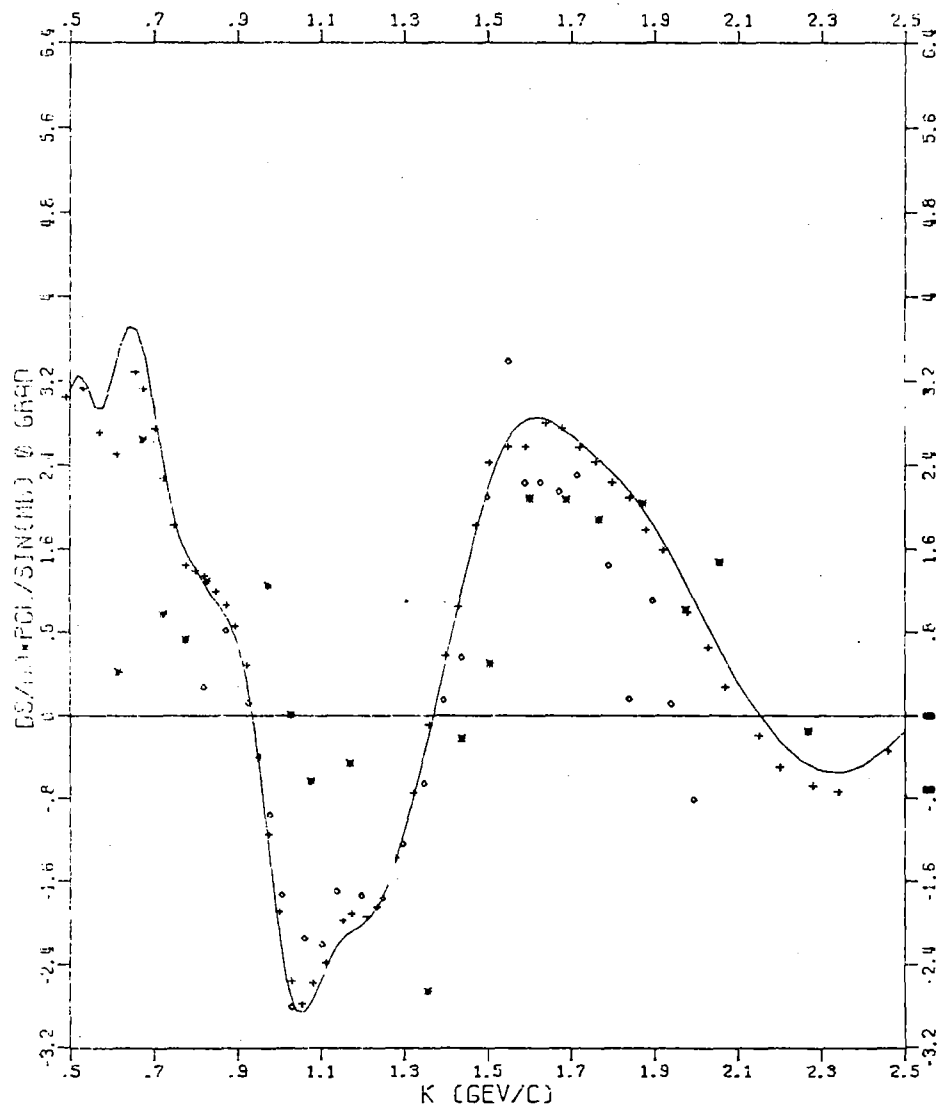


Fig. 10

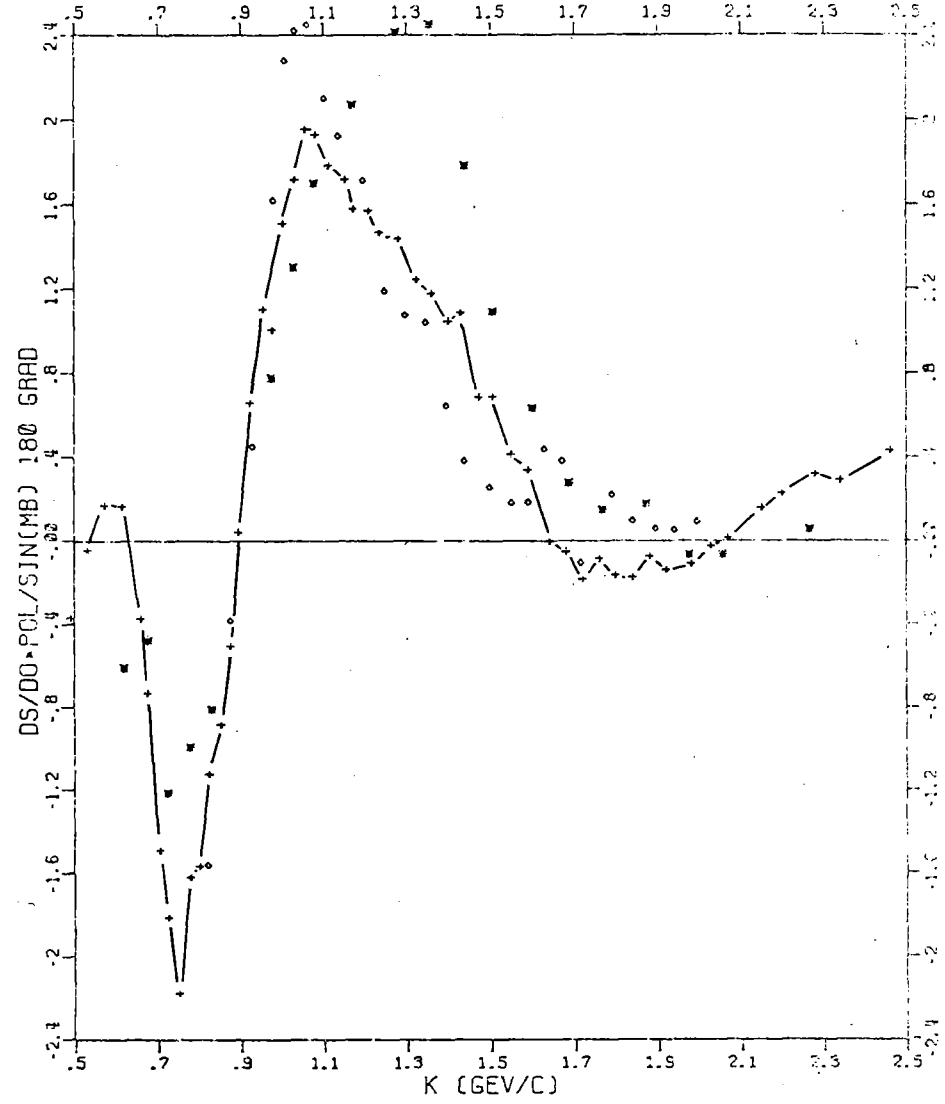


Fig. 11

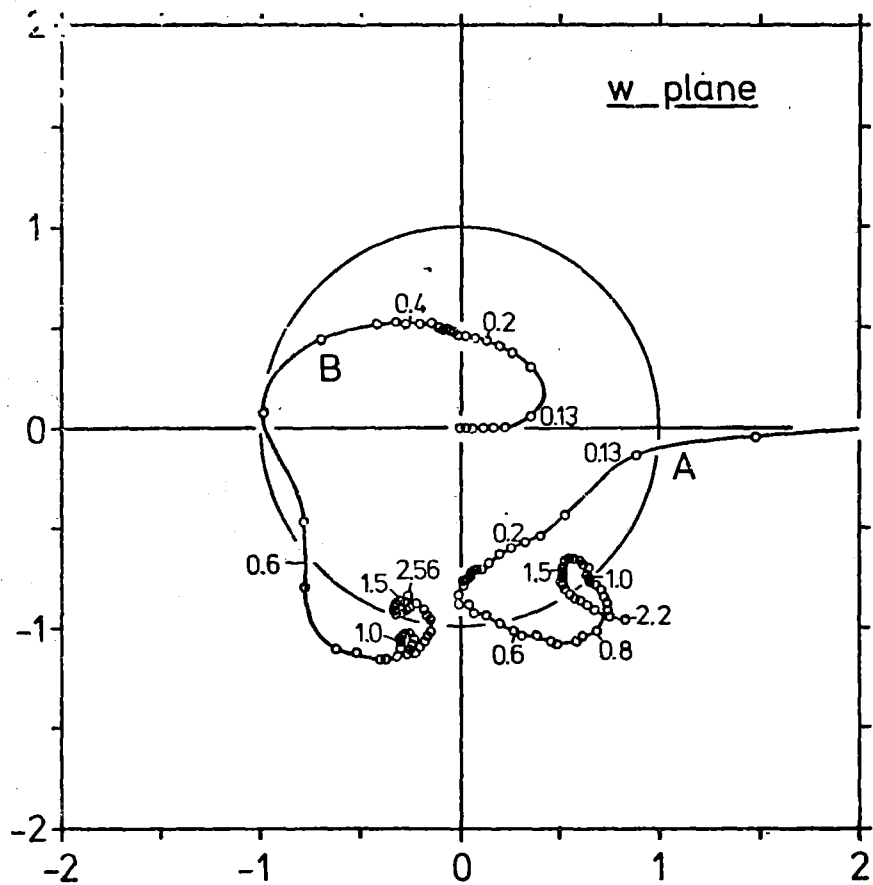


Fig. 12

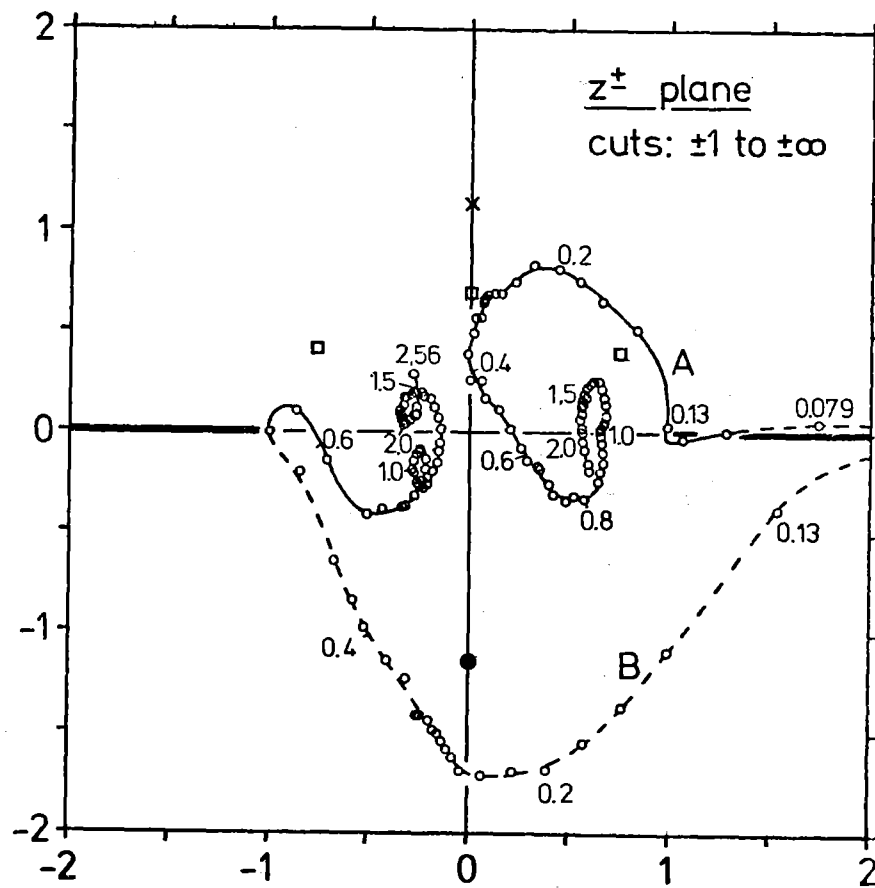


Fig. 13a

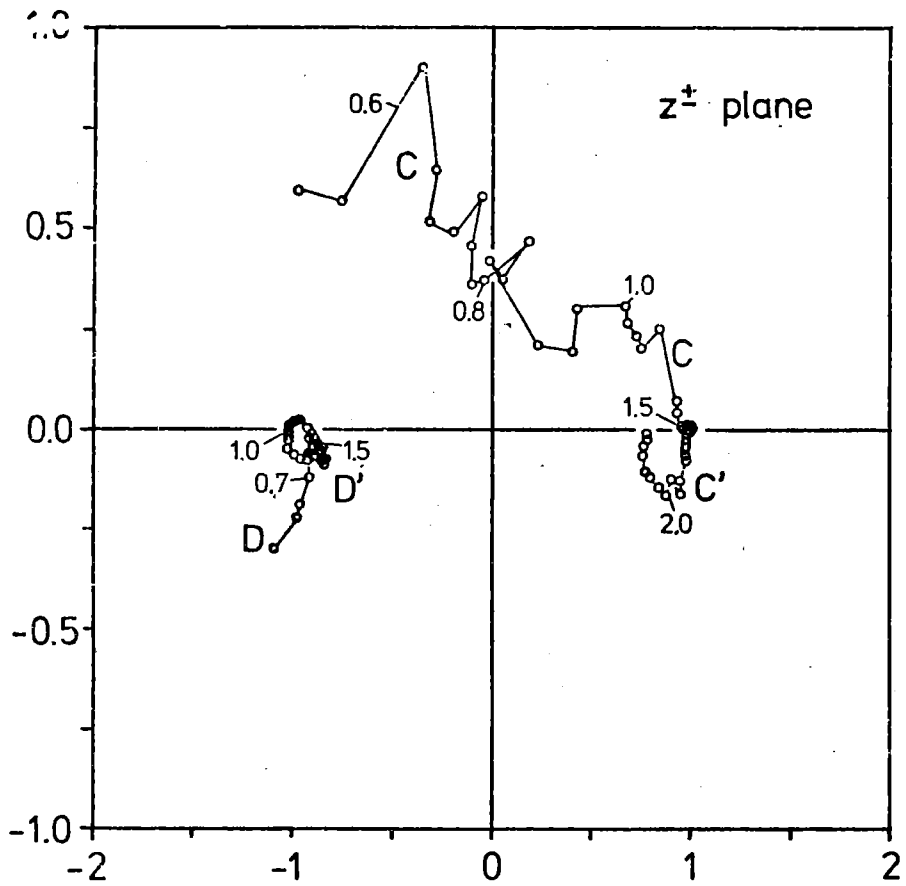


Fig. 13b

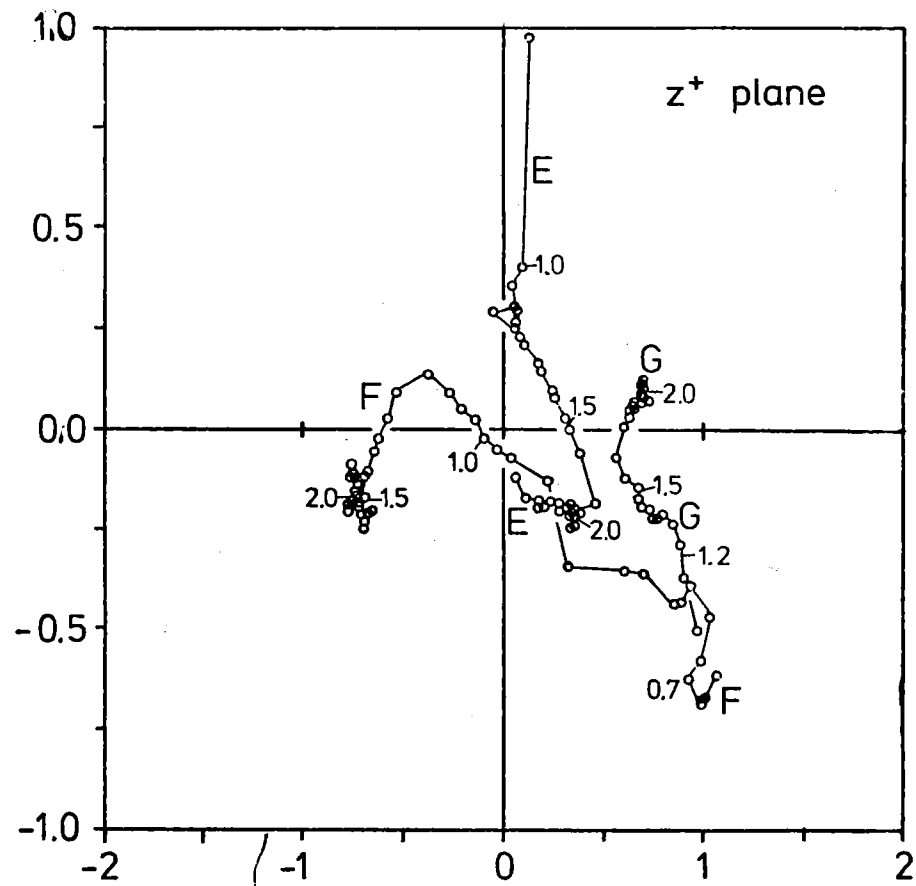
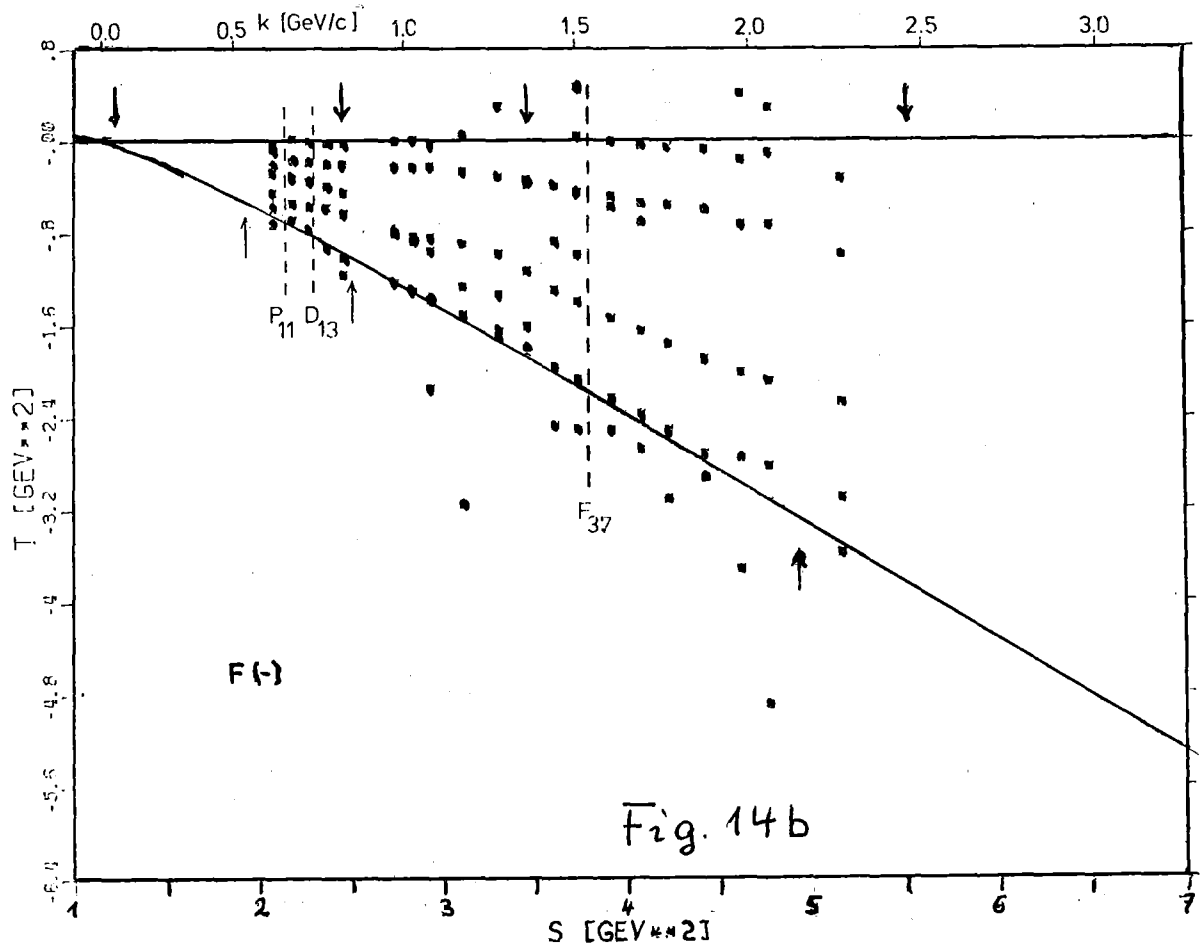
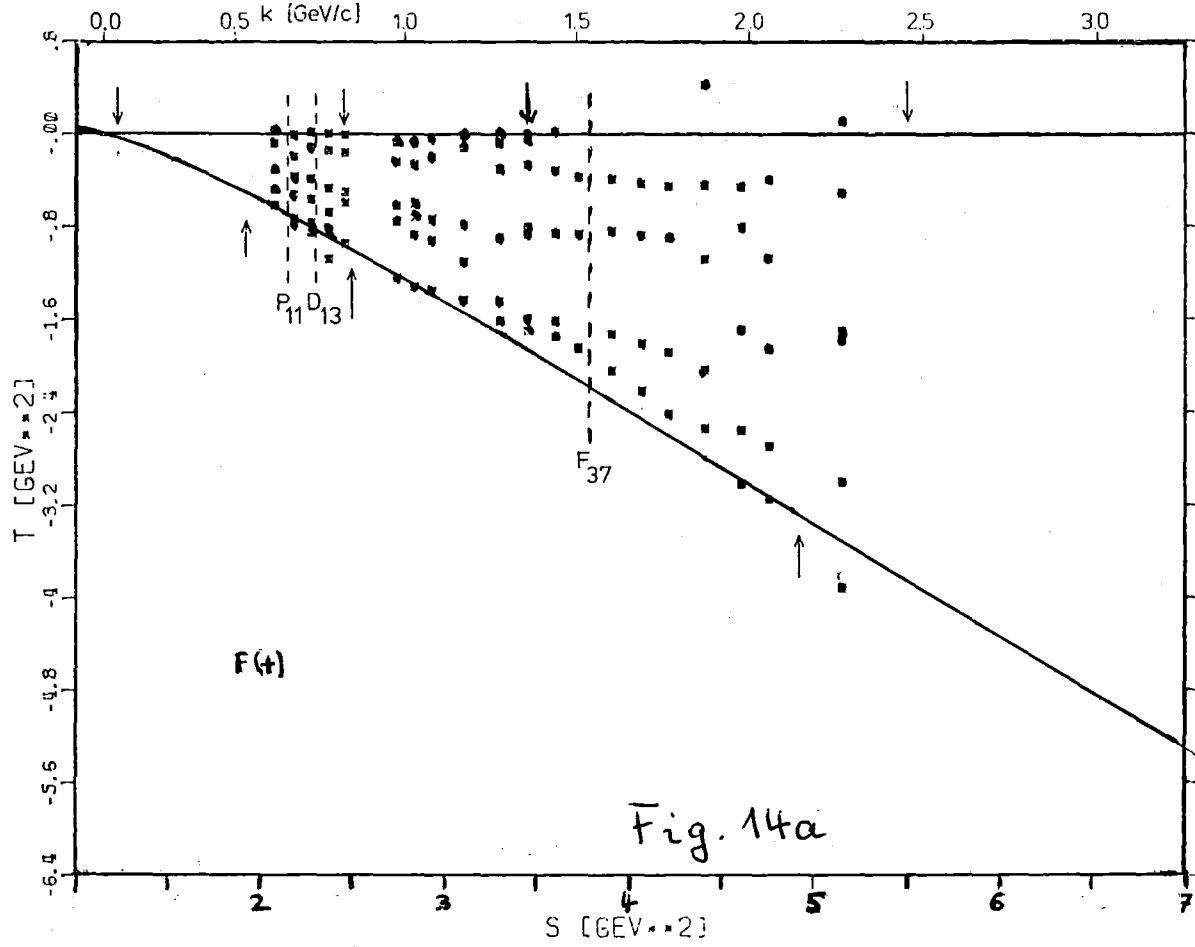


Fig. 13c



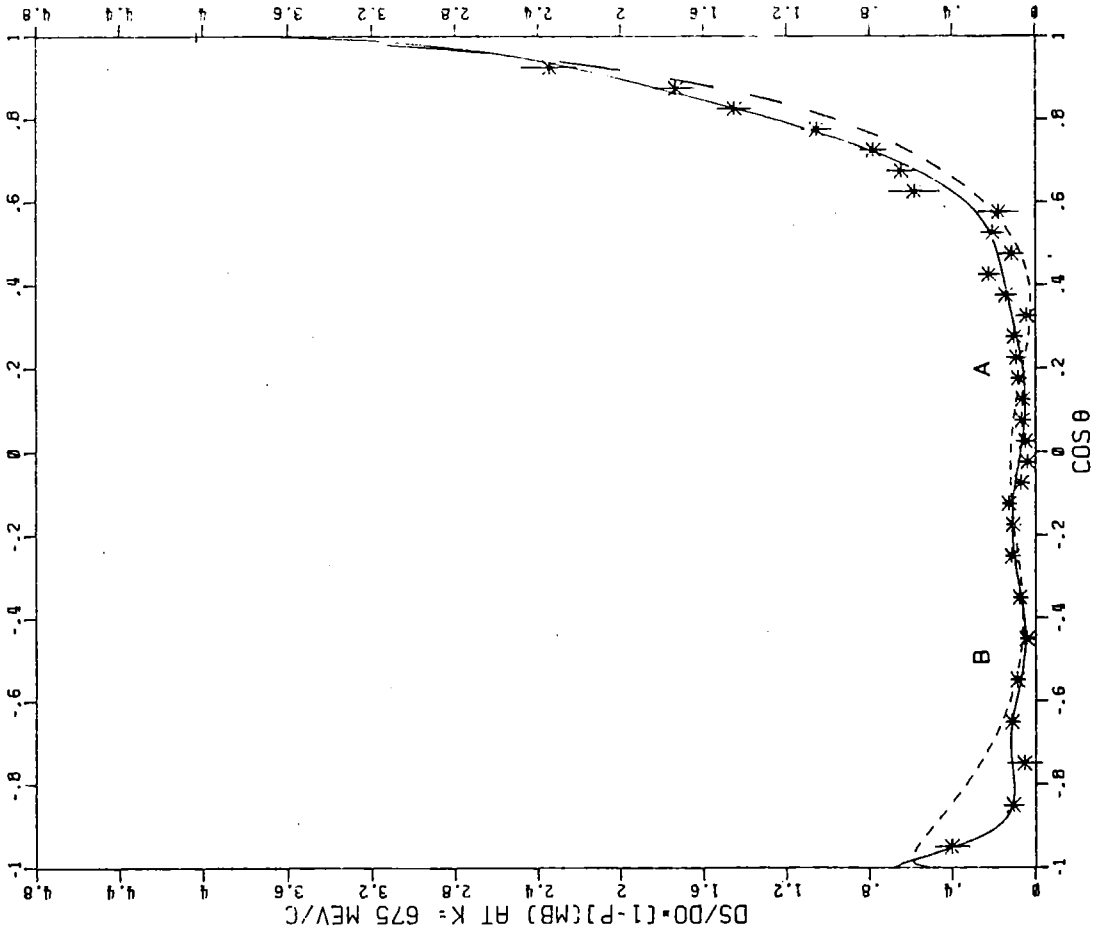


Fig. 16b

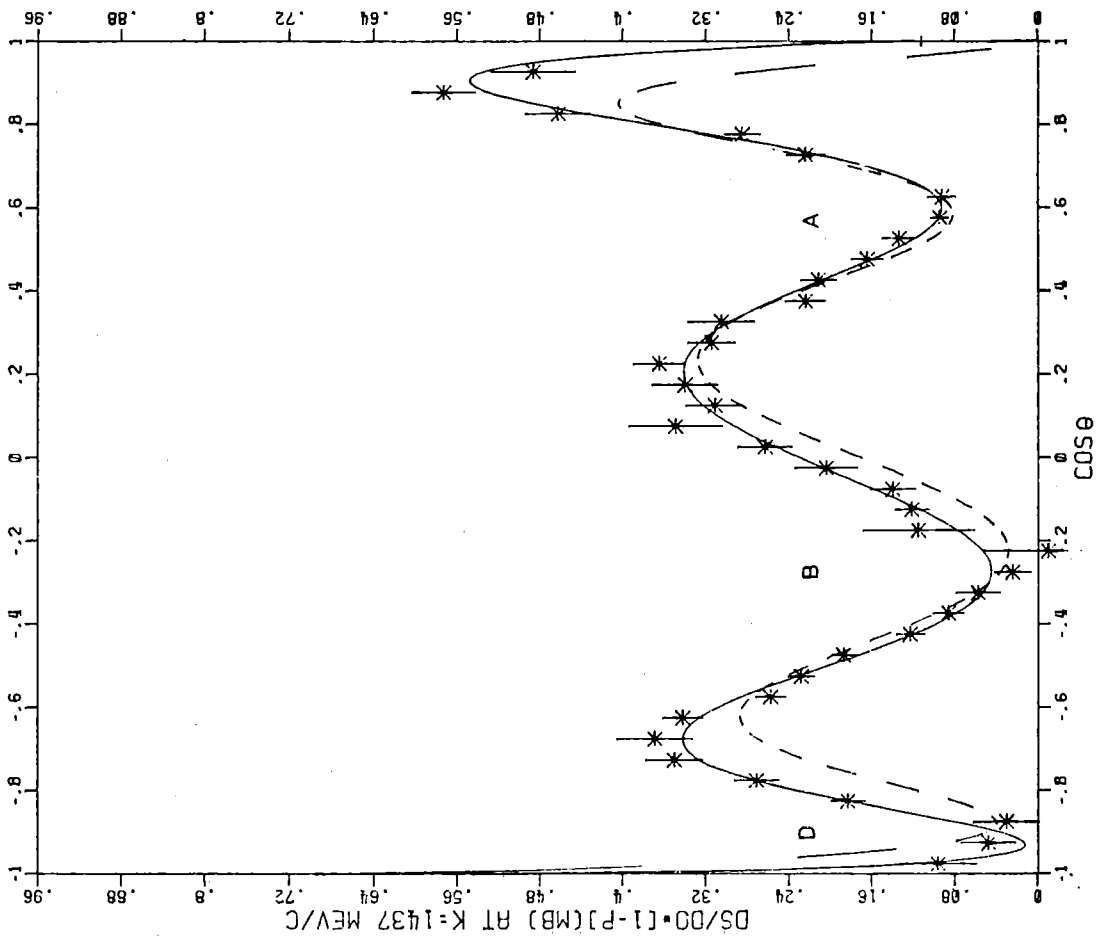


Fig. 16a

